



UNIVERSITÀ DEGLI STUDI DI SALERNO



UNIVERSITÀ DEGLI STUDI DI SALERNO  
Dipartimento di Farmacia

Dottorato di ricerca  
in **Scienze Farmaceutiche**  
Ciclo **XIV**- Anno di discussione 2016

Coordinatore: Chiar.mo Prof. *Gianluca Sbardella*

***DESIGN AND SYNTHESIS OF  
MODULATORS OF APOPTOTIC  
ACTIVITY***

settore scientifico disciplinare di afferenza: **CHIM/08**

**Dottorando**

**Dott. *Veronica Di Sarno***

**Tutore**

**Chiar.mo Prof. *Pietro Campiglia***



**Abstract**

<b>CHAPTER I:</b>	<b>1</b>
<i>'The cancer and p53 "guardian of the genome"'</i>	
<b>1.1 Introduction: Carcinogenesis, an overview</b>	<b>2</b>
<b>1.2 Cell cycle regulation</b>	<b>10</b>
<i>1.2.1 The cancer and the cell cycle</i>	
<b>1.3 Apoptosis</b>	<b>15</b>
<i>1.3.1 Connecting apoptosis and proliferation in cancer</i>	
<b>1.4 Molecular targeting of cell proliferation and apoptosis</b>	<b>21</b>
<b>1.5 p53: molecular target</b>	<b>23</b>
<i>1.5.1 The role of p53 in normal cells</i>	
<i>1.5.2 The role of p53 in cancer cells</i>	
<b>1.6 p53 network: co-activators and associated proteins</b>	<b>29</b>
<i>1.6.1 p53 and the DNA repair</i>	
<i>1.6.2 p53 and the growth arrest</i>	
<i>1.6.3 p53 and the apoptosis</i>	
<i>1.6.3.1 p53 role in trascription dependent apoptosis</i>	
<b>CHAPTER II:</b>	<b>37</b>
<i>'Search setting'</i>	
<b>2.1 Aim of the study</b>	<b>38</b>
<b>CHAPTER III:</b>	<b>43</b>
<i>'Design, synthesis, results and discussion of potential p53 modulators (SERIES 1 AND SERIES 2)'</i>	

<b>3.1 Background and design</b>	<b>44</b>
<b>3.2 Chemistry</b>	<b>46</b>
3.2.1 Chemistry of 1 <sup>st</sup> series	
3.2.2 Chemistry of 2 <sup>nd</sup> series	
<b>3.3 Biological effects</b>	<b>52</b>
3.3.1 Antiproliferative activity	
3.3.2 Modulating p53-MDM2 interaction in vitro	
3.3.3 Modulating p53-MDM2 interaction in cell	
3.3.4 Cell cycle progression	
3.3.5 Apoptotic cell death	
<b>3.4 Molecular modeling studies</b>	<b>63</b>
<b>CHAPTER IV:</b>	<b>65</b>
<i>'Experimental section for series 1 and 2'</i>	
<b>4.1 Chemistry</b>	<b>66</b>
<b>4.2 Biology</b>	<b>79</b>
<b>4.3 Molecular modeling methods</b>	<b>83</b>
<b>CHAPTER V:</b>	<b>85</b>
<i>'Design, synthesis, results and discussion of potential p53 modulators (SERIES 3 AND SERIES 4)'</i>	
<b>5.1 Background and design</b>	<b>86</b>
<b>5.2 Chemistry</b>	<b>87</b>
5.2.1 Chemistry of 3 <sup>rd</sup> series	
5.2.2 Chemistry of 4 <sup>th</sup> series	

<b>5.3 Biological effects</b>	<b>90</b>
<i>5.3.1 Antiproliferative activity</i>	
<b>Chapter VI:</b>	<b>93</b>
<i>'Experimental section for series 2 and 3'</i>	
<b>6.1 Chemistry</b>	<b>94</b>
<b>6.2 Biology</b>	<b>101</b>
<b>CHAPTER VII:</b>	<b>103</b>
<i>'Biological bases for SM13 tumour growth inhibition'</i>	
<b>7.1 Background</b>	<b>104</b>
<b>7.2 Effects of SM13 on KAT-4 cell proliferation in vitro</b>	<b>104</b>
<b>7.3 Effects of SM13 on FRO cell proliferation in vitro</b>	<b>107</b>
<b>7.4 Effects of SM13 on KAT-4 cell proliferation in vivo</b>	<b>108</b>
<i>7.4.1 Evaluation of side effects after treatment with SM13</i>	
<b>7.5 Discussion</b>	<b>111</b>
<b>Chapter VIII:</b>	<b>115</b>
<i>'Experimental section'</i>	
<b>CHAPTER IX:</b>	<b>119</b>
<i>'Design and synthesis of thiazolidine and diketopiperazine as potential p53 modulators'</i>	
<b>9.1 Background and design</b>	<b>120</b>
<b>9.2 Chemistry</b>	<b>121</b>

9.2.1 Chemistry of thiazolidine based derivatives	
9.2.2 Chemistry of diketopiperazine based derivatives	
<b>9.3 Biological effects</b>	<b>125</b>
<b>CHAPTER X:</b>	<b>127</b>
<i>'Experimental section for thiazolidine and diketopiperazine derivatives'</i>	
<b>10.1 Chemistry</b>	<b>128</b>
<b>CHAPTER XI:</b>	<b>135</b>
<i>'Dihydrithieno [2,3-b]naphto-4,9-dione analogues as anticancer agents: synthesis and in cell pharmacological studies'</i>	
<b>11.1 Introduction</b>	<b>136</b>
<b>11.2 Background and design</b>	<b>136</b>
<b>11.3 Chemistry</b>	<b>138</b>
11.3.1 Chemistry of series F	
11.3.2 Chemistry of series G	
<b>11.4 Biological effects</b>	<b>141</b>
11.4.1 In vitro cytotoxicity	
11.4.2 Cardiotoxicity	
11.4.3 Biological effects of compound 14 on LN299 cells	
<b>CHAPTER XII:</b>	<b>149</b>
<i>'Experimental section for series F and G'</i>	
<b>12.1 Chemistry</b>	<b>150</b>

<b>12.2 Biology</b>	<b>156</b>
<b>12.3 Statistical analysis</b>	<b>159</b>
<b>CHAPTER XIII:</b>	<b>161</b>
<i>Conclusions</i>	
<b><i>REFERENCES</i></b>	<b>165</b>



**ABSTRACT**

p53 is a transcription factor with tumour suppressor properties, which is able to induce mitochondrial apoptosis independently of its transcriptional activity. Analogues of the spiro[imidazo[1,5-c] thiazole-3,3'-indoline] -2',5,7(6H,7aH) -trione, previously synthesized from my research group, as p53 modulators were synthesized during my PhD, aiming to explore new structural requirements at the thiazolidine domain to increase the antiproliferative activity and improve p53 modulation. Derivative 5-bromo-3'-(cyclohexane carbonyl) -1-methyl-2oxospiro[indoline-3,2'-thiazolidine] (**SM13**) emerged as the most potent compound of all series, inhibiting, in vitro, 30% of p53–MDM2 interaction at 5  $\mu$ M and the cell growth of different human tumor cells at nanomolar concentrations. Docking studies confirmed the interactions of **SM13** with the well-known Trp23 and Phe19 clefts, explaining the reasons for its binding affinity to MDM2. **SM13** at 50 nM is capable of inducing the accumulation of p53 protein, inducing significant apoptotic cell death without affecting the cell cycle progression. Comparative studies using nutlin in the same cellular system confirmed the potential of **SM13** as a tool for increasing understanding of the process involved in the nontranscriptional proapoptotic activities of p53. Thus, the effectiveness of this compound in tumors carrying a mutated form of the p53 gene without transcriptional activity was verified. The effectiveness of **SM13** in cancer cell lines carrying WT, mutated and null p53 gene were evaluated *in vitro*. At the same time, *in vivo* studies were performed in BALB/c nude mice and the signal-dependent mitochondrial apoptosis was evaluated by western stain. **SM13** reduced cell proliferation and induced apoptosis in the *in vitro* studies, suggesting that its effect is independent of p53 transcriptional activity. On the contrary, **SM13** had no effect in a null p53 cell line. *In vivo*, **SM13** induced tumor cell death in a dose dependent manner through the activation of death mitochondrial-dependent signaling in cells mutated p53. Overall these studies highlights the efficacy of **SM13** as anticancer cancer to be used for the treatment of p53-dependent tumors, even in the absence of transcriptional activity of p53.

A second part of my PhD was, instead, dedicated, to the synthesis of a series of highly functionalized DNTQ-based derivatives. Most of the synthesized compounds exerted, in vitro, a cytotoxic effect against several tumour cell lines greater than doxorubicin. In particular N-(4-chlorobenzyl)-4,9-dioxo-3-(2-(piperidin-1-yl) acetamido)-2,3,4,9-tetrahydronaphtho[2,3-b]thiophene-3-carboxamide (compound **14**), showed a reduced cardiotoxicity, inducing, at the same time, cell differentiation and was distributed mainly in the cytoplasm in the human glioblastoma LN229 cell line. Moreover, compound **14** reduced both cellular glucose uptake and serine/threonine kinase AKT expression, and triggered cell apoptosis. These findings suggest that highly functionalized DTNQ-based derivatives are promising pharmacological tools for the study of human solid tumours.



**CHAPTER I:  
THE CANCER AND P53 “*GUARDIAN OF THE  
GENOME*”**

### ***1.1 Introduction: Carcinogenesis, an overview***

Cancer is the name given to a collection of related diseases, which have a common feature: their cells grow without stopping and spread into surrounding tissues. Cancer originates in our own cells, but several intrinsic and external factors can add to the cancer risk. Infections, diet, toxins, smoking, alcohol, obesity, environmental chemical pollutants, industrial effluents and some therapeutic drugs can act as a stimulus to induce and promote cancer development. Cancer research has generated a rich and complex body of knowledge crystallizing, so far, in two drastically different approaches to understanding the driving forces behind cancer onset and proliferation. These are the somatic mutation theory (SMT)<sup>1</sup> and the tissue organization field theory (TOFT).<sup>2</sup> The essence of SMT is that cancer is derived from a single somatic cell which has successively accumulated multiple DNA mutations, and that those mutations occur on gene controlling cell proliferation and cell cycle. Thus, according to SMT the neoplastic lesions that destroy normal tissue architecture are the results of DNA-level events. Conversely, according to TOFT, carcinogenesis is primarily a problem of tissue organization: carcinogenic agents (eg, environmental chemicals, inflammation, viruses) destroy the normal tissue architecture thus disrupting cell-to-cell signaling and compromising genomic integrity. Hence, in TOFT the DNA mutations are the effect, and not the cause, of the tissue-level events. However, a large grey zone of biological facts and clinical cases exists which poses the questions that are difficult to resolve from either of these view-points.<sup>3</sup> Essentially, for a long time the theories conceptually close to SMT and TOFT were considered as two different facets (along with many others) of the complex phenomenon of carcinogenesis. Indeed, the cornerstone of SMT is the notion that carcinogenesis is triggered by a single aberrant cell which happened to acquire multiple DNA mutations, and that these mutations predominantly damage the genes responsible for the cell cycle and apoptosis. Cancer cells develop the ability to defy the mechanisms of

apoptosis, to out trick the immune system responsible for their elimination, and as a result, to obtain exclusive capabilities to survive, to proliferate, and to transfer deleterious mutations to progeny. (Figure 1)

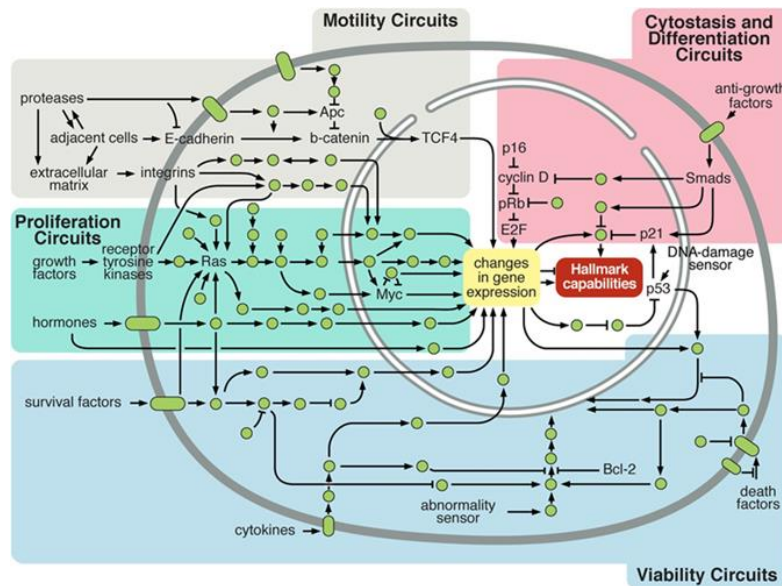


**Figure 1.** Intracellular Signaling Networks Regulate the Operations of the Cancer Cell: SMT theory. An elaborate integrated circuit operates within normal cells and is reprogrammed to regulate hallmark capabilities within cancer cells. Separate subcircuits, depicted here in differently colored fields, are specialized to orchestrate the various capabilities. At one level, this depiction is simplistic, as there is considerable crosstalk between such subcircuits. In addition, because each cancer cell is exposed to a complex mixture of signals from its microenvironment, each of these subcircuits is connected with signals originating from other cells in the tumor microenvironment

In direct opposition to these views, TOFT depicts carcinogenesis as general deterioration of the tissue microenvironment due to extracellular causes. This deterioration hinders normal cell-to-cell signaling thus making normal functioning of the intracellular machinery impossible and eventually leading it to the breaking point. In such a scenario, the deleterious mutations should be scattered all over the genome randomly and incoherently with little chance for clonal homogeneity. (Figure 2)

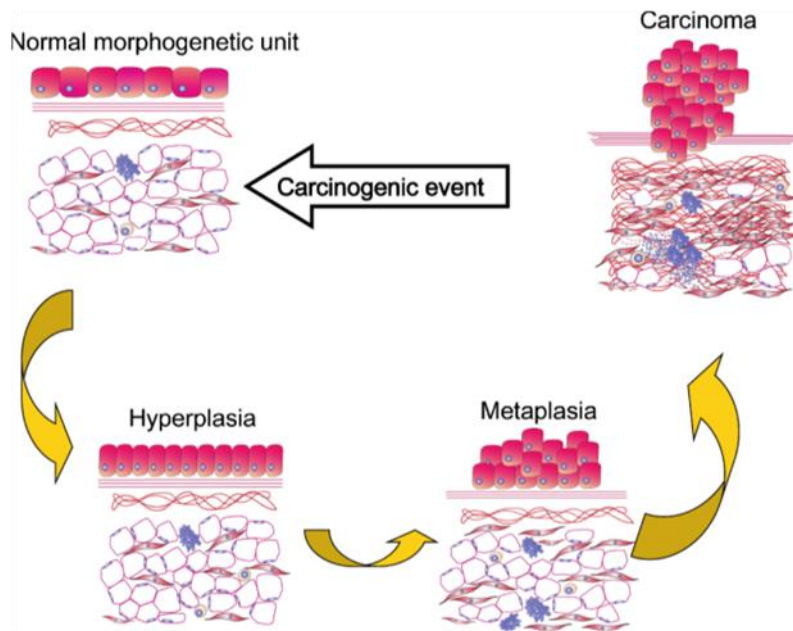


**Figure 2.** Carcinogenesis according to the TOFT. A single or multiple carcinogenic exposure acts disturbing the reciprocal biophysical and biomechanical communication between the parenchyma and the mesenchyme/stroma in a given morphogenic field. This results in miscues that manifest morphologically in both the stroma and the epithelium. The proliferation and motility restraints imposed by normal tissue architecture loosen and as a consequence, hyperplasia of the epithelium may occur. Further alteration of the reciprocal interactions between tissue compartments will induce metaplasia, dysplasia, and carcinoma. The stroma also may show alterations (desmoplasia, inflammatory cells)

According to SMT, cancer progression is a unidirectional and mostly irreversible process; the disease cannot be cured unless the entire tumor mass is surgically removed, radiationally killed, or deprived of its aggressive nature by carefully targeted chemotherapeutic agent. Paramount importance of TOFT for cancer biology, for the practice of clinical oncology and for cancer prevention, dwells in the fact that according to this view carcinogenesis is not a unidirectional process; rather, it is curable and reversible.<sup>4</sup>

Recently a new approach outlines a plausible scenery, in an attempted reconciling the two previous theories, in which a single event, insignificant on its own, may trigger a system-wide catastrophic restructuring. Such a scenery

may be envisioned and conceptualized within the framework of the so called self-organized criticality (SOC).<sup>5</sup> Genetic regulatory network in an individual cell is an excellent example of a system permanently existing on the edge of chaos. Each transcription event, i.e., synthesis of a single mRNA molecule, requires participation of a large number of transcription factors (TFs) which essentially are the proteins expressed by other genes. In turn, these supporting proteins cannot come into existence unless their parent genes have complete teams of their own TFs coming from yet another set of genes. This tight interdependence of genes (gene-to-gene interactions) creates the situation when each gene may be expressed only with the support of many other genes, essentially of the entire network. Ideally, the system can only work in a perfectly synchronized manner, with each of thousands of parts being produced and delivered where needed in a timely manner. If, however, at least one part fails to arrive in time to its destination, the corresponding assembly line then comes to a stop, thus triggering the domino effect of secondary failures and ultimately driving the entire system to a complete halt. Comparatively simple and universal forces driving the living systems towards critical conditions are always present behind the scenes in all SOC phenomena. In very general terms, a hallmark of living entities is their ability to replicate and proliferate themselves. In a community of such entities, unstoppable proliferation will inevitably drive the community towards exhaustion of common resources, whatever these resources are, thus bringing the populations to the verge of extinction. SOC plays an important role in DNA damage and transition of cellular machinery into chaotic state. The first cellular factor to sustain the damage is the RNA Polymerase II during the transcription of an active gene; this damage leads to a stalled transcription fork. The stalled fork triggers DNA repair mechanisms by attracting a large number of proteins which, in turn, allosterically modify binding affinities of many other proteins. It may happen that the damage occurs in the so called “hub” proteins (such as p53 protein) which are capable of

modifying a large number of vital cellular functions simultaneously.<sup>6</sup> A subtle balance always exists between the rates of damage and repair. Up to a certain level of mutagenic load, the repair mechanisms are capable of containing damage, thus maintaining a generally healthy cell population. However, the last straw effect may also occur when the cell, after an insult, remains unrepaired yet undestroyed, thus giving rise to a genetically aberrant sub-population. This last straw event is analogous to the last grain of sand in the sandpile avalanche because it fires up multiple, very complex, and mostly irreversible pathways. Such a massive complex response to a seemingly minor event is a hallmark of SOC. It would be an obvious misjudgment to regard any particular minor event as a cause of the system's collapse. Rather, one may expect that a mutationally overloaded system would collapse anyway, whatever a minor event actually happens to be the trigger. In this context both the self-organized criticality and the somatic mutation theories match. (Figure 3) In particular, as observed by Nowell,<sup>7</sup> cytogenetic studies have demonstrated that in many primary tumors all cells show the same abnormal karyotype; the immunoglobulin produced by plasma cell tumors has in almost every case the homogeneity characteristic of a single clone. As an ultimate manifestation of this paradigm, direct evidence of a single catastrophic event triggering carcinogenesis has been presented by Stephens et al.<sup>8</sup> The authors explain that the overwhelming majority of rearrangements leading the distinctive genomic structures, present in the different cancer types, occurs in a single catastrophic event. In this scenario, the chromosome or chromosomal region shatters into tens to hundreds of pieces, some (but not all) of which are then stitched together by the DNA repair machinery in a mosaic patchwork of genomic fragments. A cell suffering tens to hundreds of DNA breaks in a single cataclysmic event would be expected to undergo apoptosis.

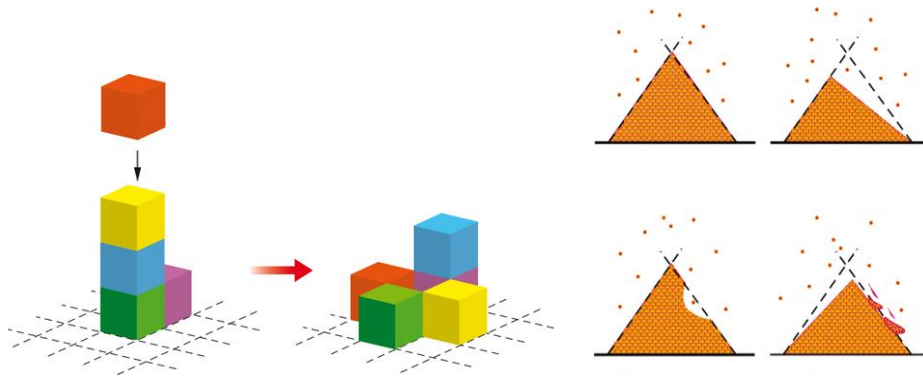


**Figure 3.** *Different representations of self-organized criticality theory. Sandpile paradigm: if additional sand grains are randomly added to a sand pile then inevitably an instance will occur when local steepness of the slope surpasses a certain critical threshold thus causing local failure of structural stability. The excess of material will cascade into adjacent areas of the pile causing their failure as well*

That a cell can survive such an insult and progress to become cancerous suggests that the extensive remodeling of the genome may confer significant selective advantage to that clone. Self-organized criticality confirms also one basilar point of the tissue organization field theory on the evolution of tissue, from a healthy state to a precancerous state and further to tumorigenesis, using some concepts of the somatic mutation theory. In particular, chronic systemic inflammation has been widely recognized to be among the leading factors in progression of healthy tissue towards precancerous and cancerous lesions. The specific mechanisms of such progression include sustained cell proliferation in an environment rich in inflammatory cells and molecular agents causing DNA damage.<sup>9</sup> Excessive and pathologic inflammation causes DNA damage, genomic instability, epigenetic dysregulation, and alteration of intracellular signaling, all of which are involved in neoplastic transformation.<sup>10</sup> It is important to realize that inflammation-triggered carcinogenesis cannot be reduced to just cell proliferation and conquering new tissue territories. A number of complex molecular mediators facilitate proliferation of genomic

damage, among which an important role belongs to inflammasomes, i.e., the multi-protein complexes that mediate immune response.<sup>11</sup>

Another fundamental aspect of carcinogenesis is the DNA methylation. In normal tissue, gene methylation is mostly localized in the coding region whereas the promoter region remains mostly unmethylated. A different pattern is observed in neoplasia: the genome-wide hypomethylation is accompanied by localized hypermethylation. Evidence suggests that methylation is an important factor in carcinogenesis since genome-wide hypomethylation can trigger the chromosome instability and increase the mutation rates, playing a key role in different cancer types and probably at different stages of oncogenesis.<sup>12, 13</sup> Generally, abnormal patterns of methylation signify elevated cancer risk due to heightened susceptibility to cancer cell proliferation. According to Vendramini-Costa and Carvalho,<sup>14</sup> tumor initiation involves irreversible changes in DNA through activation of oncogenes or inactivation of tumor suppressor genes. Further development leads mutated cells to expansion through increased proliferation and suppression of cell death. In the process of invasion of adjacent tissues cancer cells may accumulate other mutations, thus exacerbating their phenotype. Again, the process is quite similar to the forest fire propagation, which accumulates additional strength while invading new territories. Last, the disruption of cell-to-cell communication is an important aspect characterizing precancerous tissue, and it is a central component of a bigger process of tissue disorganization.<sup>15</sup> The viewpoint is that a community of cells is not simply a collection of units dwelling within certain architectural structures. With the destruction of signaling pathways, not only the normal regulation of individual cellular processes is damaged, but also a blow is dealt, so to speak, to the mental capabilities of the community as a whole. Its collective memory is wiped out or distorted, customary division of labor between subpopulations is shifted towards aberrant modalities, and community-wide self-defense mechanisms are weakened or broken. These processes in turn cause a shift in expression profiles

and metabolic dynamics, eventually penetrating to the level of DNA and causing multiple mutations. The mechanisms of tumor initiation play a prominent role in carcinogenesis, and a single catastrophic event indeed can make a fundamental impact on all subsequent events. However, not every event that may be seen as catastrophic on the level of individual cell would necessarily lead to carcinogenesis. Vast majority of those events would fade and disappear without traces. This is because the immune system remains on guard of tissue homeostasis. When tissue homeostasis is perturbed, sentinel macrophages and mast cells release cytokines, chemokines, reactive oxygen species (ROS), and other bioactive mediators that induce mobilization of additional leukocytes.<sup>16</sup> This means that the mutant cell capable of starting the domino-effect of subsequent failures should be able to overcome the tissue's natural defenses; this may happen only if the tissue is already preconditioned for failure and resides on the verge of systemic collapse. All these findings provide just a glimpse of extremely complex and tangled transition of healthy tissue towards precancerous state. Obviously, even a complete knowledge of each and every process contributing to this transition does not automatically lead to understanding the process as a whole. Resorting to the sandpile analogy, it would be as difficult as understanding the phenomenon of avalanche from observations of each sand grain trajectory. This is why systemic approaches are not simply helpful, they are absolutely necessary and unavoidable for synthesizing existing biomolecular knowledge into a coherent picture of carcinogenesis. Thus, recognition of the widespread applicability of concepts, outlined here, will increasingly affect the development of new strategies to treat human cancer.

## ***1.2 Cell cycle regulation***

With advancements on the basic mechanisms of oncogenesis, we have gained a better understanding of the role that the cell cycle regulation plays in malignant transformation and in the development of resistance to chemotherapy, laying the bases for development of a new class of anticancer therapeutics in clinical development.<sup>17</sup>

The fundamental task of the cell cycle is to ensure that DNA is faithfully replicated once during S phase and that identical chromosomal copies are distributed equally to two daughter cells during M phase.<sup>18</sup> The machinery for DNA replication and chromosome segregation is insulated from interruption by extracellular signals, and its essential and autonomous nature implies that damage to the pivotal components would be highly debilitating, if not fatal, to cells. Therefore, genes commanding these processes should not be frequent targets of mutation, deletion, or amplification in cancer. Oncogenic processes exert their greatest effect by targeting particular regulators of G1 phase progression.<sup>19</sup> During the G<sub>1</sub> phase, cells respond to extracellular signals by either advancing toward another division or withdrawing from the cycle into a resting state (G<sub>0</sub>).<sup>20</sup> Unlike transit through the S, G<sub>2</sub>, and M phases, G<sub>1</sub> progression normally relies on stimulation by mitogens and can be blocked by antiproliferative cytokines. Cancer cells abandon these controls and tend to remain in cycle, and because cell cycle exit can facilitate maturation and terminal differentiation, these processes are subverted as well.<sup>21</sup> The decision to divide occurs as cells pass a restriction point late in G<sub>1</sub>, after which they become refractory to extracellular growth regulatory signals and instead commit to the autonomous program that carries them through to division. An appreciation of restriction point control is central to our understanding of how and why cancer cells continuously cycle. The cell cycle is a critical regulator of the processes of cell proliferation and growth as well as of cell division after DNA damage. It governs the transition from quiescence (G<sub>0</sub>) to cell proliferation, and through

its checkpoints, ensures the fidelity of the genetic transcript. It is the mechanism by which cells reproduce, and is typically divided into four phases. The periods associated with DNA synthesis (S phase) and mitosis (M phase) are separated by gaps of varying length called G1 and G2 (Figure 4). Progression of a cell through the cell cycle is promoted by a number of CDKs which, when complexed with specific regulatory proteins called cyclins, drive the cell forward through the cell cycle. There exist corresponding cell cycle inhibitory proteins (CDK inhibitors [CKIs]) that serve as negative regulators of the cell cycle and stop the cell from proceeding to the next phase of the cell cycle (Figure 3). The INK4 (for inhibitor of cdk4) class of CKIs, notably p16lnk4a, p15lnk4b, p18lnk4c, and p19lnk4 days, bind and inhibit cyclin D-associated kinases (CDK2, -4, and -6). The kinase inhibitor protein (KIP) group of CKI inhibitors, p21waf1, p27kip1, and p57kip2, negatively regulate cyclin E/CDK2 and cyclin A/CDK2 complexes.<sup>22</sup>

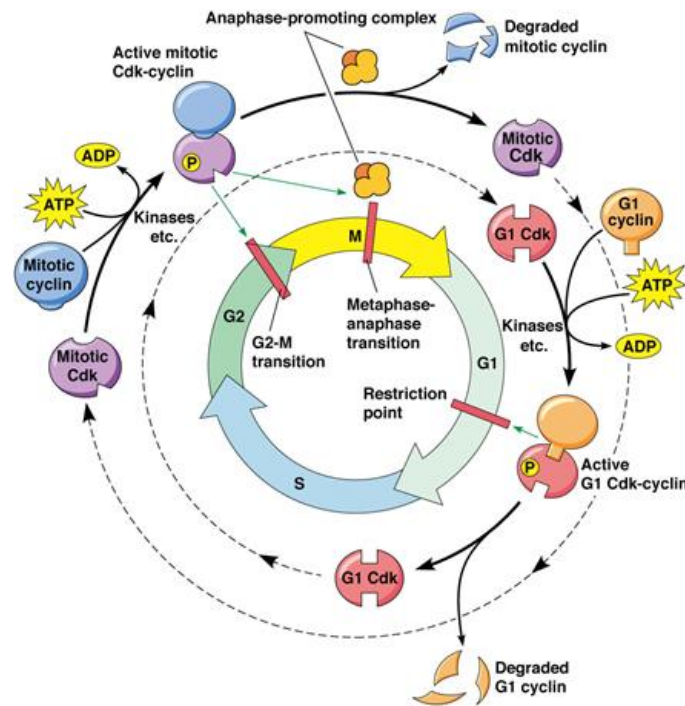


**Figure 4.** *The cell cycle*

The pattern of cyclin expression varies with a cell’s progression through the cell cycle, and this specific cyclin expression pattern defines the relative position of the cell within the cell cycle.<sup>23</sup> At least nine structurally related CDKs (CDK1-CDK9) have been identified, though not all have clearly defined cell cycle regulatory roles. A considerable number of cyclins have been identified to date (cyclin A–cyclin T). CDK/cyclin complexes themselves become activated by phosphorylation at specific sites on the CDK by cdk7/cyclin H, also referred to as CDK-activating kinase (CAK).<sup>24</sup> Cyclin D isoforms (cyclin D1-D3) interact with CDK2, -4, and -6 and drive a cell’s progression through G1. The association of cyclin E with CDK2 is active at the G1/S transition and directs entry into S phase. S phase progression is directed by the cyclin A/CDK2 complex, and the complex of cyclin A with CDK1 (also known as cdc2) is important in G2. CDK1/cyclin B is necessary for mitosis to occur. The cell

responds to mitogenic stimuli and decides to advance through the various phases of the cell cycle only during a limited phase of its cycle. In fact, the cell needs stimulation only during the first two-thirds of its G1 phase where it may decide to continue its advance and complete its cell cycle. This point is termed ‘restriction point’ (R point); it is a central event in normal cellular proliferation control. It has been demonstrated that pRb is the molecular device that serves as the R point switch. pRb is hypophosphorylated in resting G0 cells, is increasingly phosphorylated during progression through G1 and is maintained in a hyperphosphorylated state until late mitosis. pRb phosphorylation seems to be related to mitogenic signals, which converge on the cell cycle machinery, represented by the cyclin D1/cdk4 (cdk6) complex in the early and mid-G1, and composed of cyclin E/cdk2 in late G1.

### ***1.2.1 The cancer and the cell cycle***

In physiological conditions, activation of CDK/Cyclin kinases is tightly controlled both spatially and temporally. However, CDK/Cyclins are dysregulated in several human cancers, which wreaks havoc in the coordinated cycle of cell growth and proliferation and contributes to the uncontrolled proliferation characteristic of cancer cells.<sup>25</sup> In fact, together with mutations in proto-oncogenes, mutations leading to hyperactivation of CDK activity have been reportedly found in human cancer genomes, and confer selective growth advantage to cells, whilst mutations that inactivate checkpoint regulators, tumour suppressor genes or CKIs result in loss of cell cycle inhibition.<sup>26</sup> CDK/Cyclin hyperactivation may result from one of several causes, including gene amplification and protein overexpression of either the CDK or cyclin subunit, alternative splicing and expression of truncated cyclin variants, untimely expression and mislocalization, or constitutive activation of CDK/Cyclins by preventing their inactivation through binding to INK or KIP/CIP inhibitors.<sup>27</sup> A representative panel of mutations which occur in CDKs

and Cyclins may be found in the catalogue of Cosmic Mutations in Cancer which integrates all mutations identified through sequencing of human cancer tissue samples. (Figure 5)

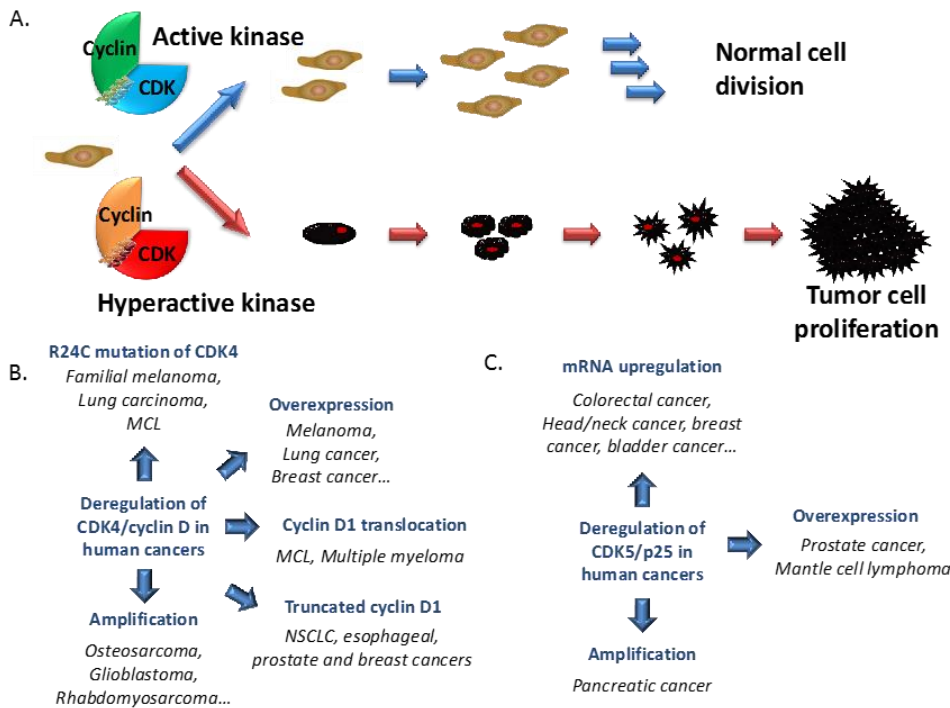


**Figure 5. CDK/Cyclins and Cancer.** (A) Schematic representation of normal cell growth and division regulated by cyclin-dependent kinases. Hyperactivation of these kinases contributes to development of cancer cell proliferation; (B) CDK4/cyclin D in cancers: Among all the CDK/cyclins, the complex CDK4/cyclin D is the one which presents most aberrations in cancers. Hyperactive CDK4/cyclin D is found in several human cancers associated with the R24C mutation of CDK4 which prevents the fixation of the endogenous inhibitor p16INK4A, mutation of p16INK4a itself or CDK4 or cyclin D amplification; (C) CDK5/p25 in cancers.

A second class of growth-deregulating mutations comprises those that target the principal late-G1 cell-cycle checkpoint regulated by pRB. Loss of pocket protein functions may induce cell cycle deregulation and lead to a malignant phenotype. Defects in this pathway, which may be universal in human cancers, include deletion of the *RB* gene itself and deregulation of the CDKs that

phosphorylate and functionally inactivate pRB, either through direct over-activation of CDKs or through genetic loss of their inhibitors.<sup>28</sup> Another frequent proliferative lesion that has the effect of deregulating the cell cycle is uncontrolled expression of Myc.<sup>29</sup> Myc expression is tightly controlled by mitogen availability in normal cells, but it is usually expressed in a deregulated or elevated manner in tumor cells.<sup>30,31</sup> Myc seems to be a strategic controller of cell proliferation that acts pleiotropically to coordinate both cell growth and concomitant progression through the cell cycle.<sup>32</sup> The presence in individual tumors of multiple mutations that affect each of the pathways discussed above suggests that each pathway contributes a discrete type of proliferative function to the neoplastic phenotype. But precisely what such functions are and how and why they interact, remains unknown. In addition to driving aberrant cell division, mutations in the various proliferative control pathways have a profound impact on other cell functions. For example, many of the proliferative lesions in tumor cells also contribute to the inhibition of differentiation, thereby preventing the elimination of progeny cells from the proliferative compartment of many types of tissue. pRB, for example, is essential in differentiation of several tissue types through interactions with factors such as the helix–loop–helix proteins MyoD<sup>26</sup> <sup>33</sup> and Id2. Loss or inhibition of pRB function prevents normal differentiation, a contribution to tumor development distinct from the direct deregulation of cell-cycle progression. Deregulated Myc expression also inhibits differentiation, in part by activation of Id2 expression.<sup>34</sup>

### ***1.3 Apoptosis***

Apoptosis, or programmed cell death (Figure 6), is a normal component of the development and health of multicellular organisms. Apoptosis occurs during the normal development of multicellular organisms and continues throughout adult life. The combination of apoptosis and cell proliferation is responsible for shaping tissues and organs in developing embryos. Cells die in response to a

variety of stimuli and during apoptosis they do so in a controlled, regulated fashion.

There are a number of mechanisms through which apoptosis can be induced in cells. The sensitivity of cells to any of these stimuli can vary depending on a number of factors such as the expression of pro- and anti-apoptotic proteins (eg. the Bcl-2 proteins or the Inhibitor of Apoptosis Proteins), the severity of the stimulus and the stage of the cell cycle. Some of the major stimuli that can induce apoptosis include virus infection, cell stress and DNA damage. In some cases the apoptotic stimuli comprise extrinsic signals such as the binding of death inducing ligands to cell surface receptors called death receptors. These ligands can either be soluble factors or can be expressed on the surface of cells such as cytotoxic T lymphocytes. The latter occurs when T-cells recognize damaged or virus infected cells and initiate apoptosis in order to prevent damaged cells from becoming neoplastic (cancerous) or virus-infected cells from spreading the infection. Apoptosis can also be induced by cytotoxic T-lymphocytes using the enzyme granzyme. In other cases apoptosis can be initiated following intrinsic signals that are produced following cellular stress. Cellular stress may occur from exposure to radiation or chemicals or to viral infection. It might also be a consequence of growth factor deprivation or oxidative stress caused by free radicals. In general intrinsic signals initiate apoptosis via the involvement of the mitochondria. The relative ratios of the various bcl-2 proteins can often determine how much cellular stress is necessary to induce apoptosis.

Upon receiving specific signals instructing the cells to undergo apoptosis a number of distinctive changes occur in the cell. A family of proteins known as caspases is typically activated in the early stages of apoptosis. These proteins breakdown or cleave key cellular components that are required for normal cellular function including structural proteins in the cytoskeleton and nuclear proteins such as DNA repair enzymes. The caspases can also activate other

degradative enzymes such as DNases, which begin to cleave the DNA in the nucleus. This makes apoptosis distinct from another form of cell death called necrosis in which uncontrolled cell death leads to lysis of cells, inflammatory responses and, potentially, to serious health problems. Apoptosis, by contrast, is a process in which cells play an active role in their own death (which is why apoptosis is often referred to as cell suicide).

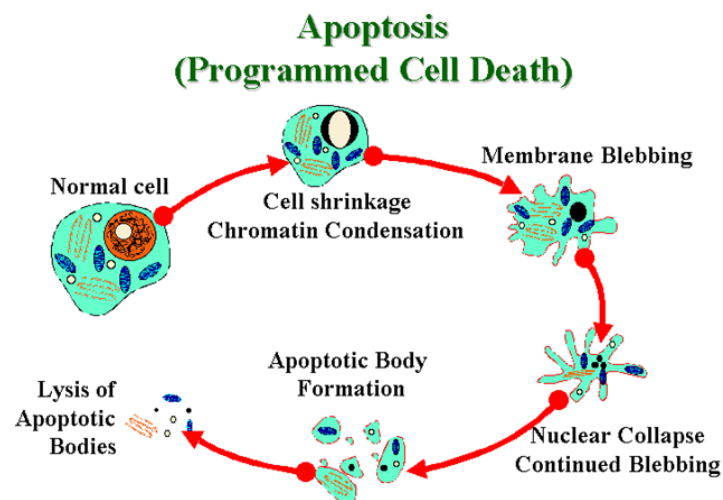
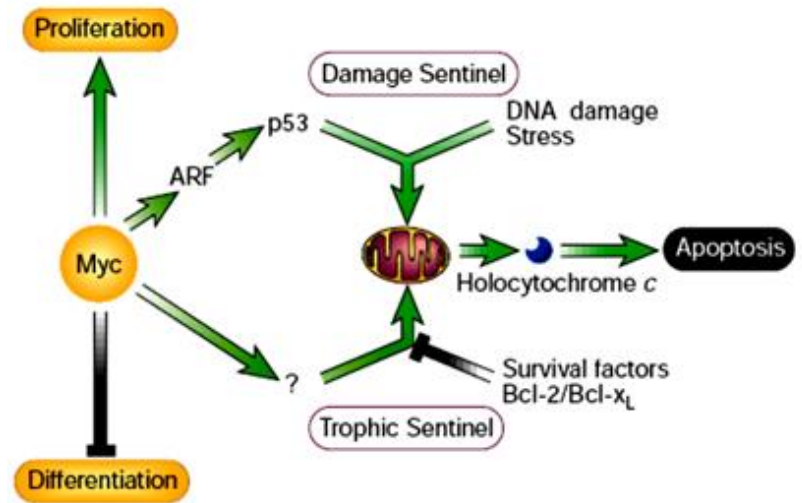


Figure 6. Apoptosis

### 1.3.1 Connecting apoptosis and proliferation in cancer

The central engines of apoptosis are the caspases, cascades of cysteine aspartyl proteases that implement cell death by cleaving a variety of intracellular substrates that trigger cell dissolution. Caspases are synthesized as latent zymogens that are activated by proteolytic cleavage: typically through the action of upstream apical caspases. An activation pathway (extrinsic pathway) is mediated by transmembrane death receptors of the CD95 (Apo-1 or Fas)/TRAIL/tumor-necrosis factor (TNF) receptor 1 family, whose ligation triggers recruitment and assembly of multiprotein complexes that activate apical caspase 8.<sup>35</sup> The other principal apoptotic death-signaling pathway

involves the mitochondrion (intrinsic pathway), which acts as an integrating sensor of multiple death insults by releasing cytochrome *c* into the cytosol where it triggers caspase activation. The mitochondrial pathway is thought to be the principal target of survival signaling pathways, which act by stabilizing mitochondrial function and integrity and suppressing release of cytochrome *c*.<sup>36</sup> Once cytochrome *c* has been released from the mitochondrion, it orchestrates assembly of an intracellular apoptosome complex that recruits apical caspase 9 via the adaptor protein Apaf-1.<sup>37</sup> The anti-apoptotic oncoproteins Bcl-2 and Bcl-xL, which exert their principal effects through stabilization of the mitochondrion, are overexpressed in several tumor types and recent analyses have indicated that loss of Apaf-1 is a relatively frequent event in malignant melanoma that presumably confers resistance to apoptosis.<sup>38</sup> A particularly potent driving force for the suppression of apoptosis in tumor cells is the coupled relationship between cell proliferation and cell death, a phenomenon exemplified by the Myc protein. In addition to its well documented growth-promoting property, Myc was found to be a powerful inducer of apoptosis, especially under conditions of stress, genotoxic damage or depleted survival factors.<sup>39</sup> Consideration of such observations led to the proposal that the innate apoptotic potential of Myc serves as an inbuilt foil to its oncogenic capacity (Figure 7).



**Figure 7.** Activation of growth-deregulating lesions triggers ‘sentinel’

In this example, the oncoprotein Myc is shown activating a p53 damage sentinel through the ARF/MDM-2 pathway, thereby sensitizing the cell to any DNA damage. Myc also promotes release of holocytochrome c from the mitochondrion into the cytosol where it triggers apoptosis. Release of holocytochrome c is inhibited by paracrine ‘survival’ signals that are typically restricted both in supply and location. Clonal outgrowth driven by relentless Myc expression outstrips survival factor availability, triggering the ‘trophic sentinel’ to kill the cell. Another common pathway through which a wide variety of proliferative signals influence the apoptotic program is through induction of ARF, an alternate product of the *INK4a* locus, one of whose functions is to trigger upregulation of p53 through its inhibitory action on MDM-2.<sup>40</sup> Another potent selective pressure in cancers to suppress apoptosis arises from the fact that programmed cell death is the typical response of somatic cells to many forms of stress and damage; in particular damage to cell DNA (a fact exploited by most classical cancer therapeutics). Stress-associated signals that activate apoptosis include many of those encountered by the incipient tumor cell,

including hypoxia and nutrient deprivation, as well as DNA damage arising from telomere erosion, defective repair, oncogene deregulation and therapy. The p53 protein is important in transducing such diverse signals into tumor-suppressive apoptotic or growth-arresting responses, which implies that there is strong selection for tumor cells to lose p53 function.<sup>41</sup> Importantly, differing p53-activating stresses tend to arise at different stages of carcinogenic progression. For example, oncogene deregulation occurs early, as it is a prerequisite for clonal expansion, whereas hypoxia is significant only after the tumor reaches macroscopic size. Consequently, p53 exerts a tumor-suppressive role at multiple stages of carcinogenic progression, (Figure 8) offering an explanation for why loss of p53 has such a profound effect on tumor development.

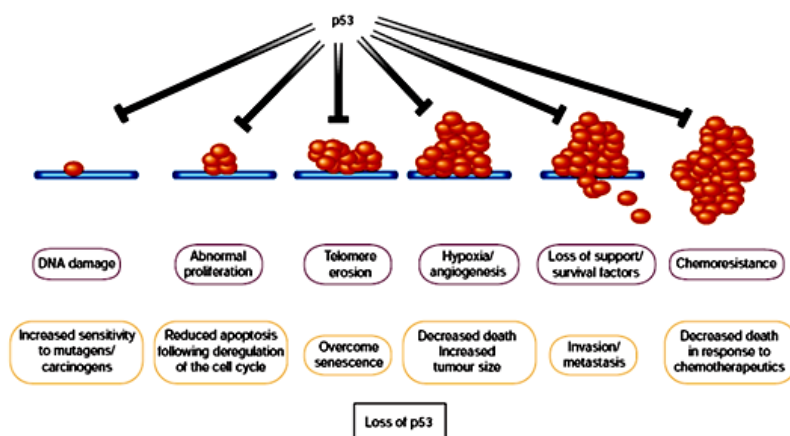


**Figure 8.** Many stress signals encountered during tumor progression activate p53, resulting in apoptosis or growth arrest

Loss either of the ability to activate p53 or of p53 function itself has considerable impact on the ‘success’ of the carcinogenic process, as it increases the chances of a tumor cell surviving progressively adverse conditions. Inability to activate p53 in response to stress signals encountered early during tumor development, such as deregulated proliferation, may be sufficient to allow

the formation of preneoplastic lesions. However, lesions that suppress activation of p53 in response to such oncogene-associated stress signals do not necessarily block activation of p53 by subsequent events encountered during malignant progression, such as DNA damage. Consequently, additional alterations in pathways that activate or respond to p53, or loss of p53 by direct mutation of the gene itself, may be selected during progression to more malignant cancers.

#### ***1.4 Molecular targeting of cell proliferation and apoptosis***

Because deregulated proliferation and inhibition of apoptosis lie at the heart of all tumor development, they present two obvious targets for therapeutic intervention in all cancers. Clearly there are numerous mechanisms through which these two defects can occur, and the success of targeted therapy will depend to a large part on the molecular fingerprinting of individual tumours.<sup>42</sup> Although most existing cancer drugs are anti-mitotic, they act not by targeting the specific lesions responsible for deregulated tumor growth, but by crudely interfering with the basic machinery of DNA synthesis and cell division. Moreover, we now know that the surprising selectivity of such crude agents results largely from the increased sensitivity to apoptosis afforded to tumor cells by their oncogenic lesions. Drugs designed to specifically inhibit growth-deregulating lesions are currently being tested in clinical trials, and include inhibitors of RTKs, Ras, downstream signaling kinases such as the mitogen-activate protein kinase and Akt pathway, and CDKs. At first glance, targeted inhibition of growth-deregulating lesions in cancer would be seem to have limited therapeutic efficacy, as they would at best be cytostatic. However, unexpected therapeutic bonuses may emerge from such an approach because growth deregulation induces a plethora of downstream activities in affected cells and their adjacent tissues. Therapeutic inhibition of the offending oncoprotein in tumors arising from cell lineages where terminal differentiation has been blocked could be sufficient to trigger a resumption of that differentiation

program, permanently expelling the tumor cell from the proliferating compartment.<sup>43</sup>

The second obvious strategy for cancer therapy is to target the lesions that suppress apoptosis in tumor cells. The potent proapoptotic effects of growth-deregulating mutations mean that tumors are peculiarly dependent upon their particular suite of antiapoptotic mutations for continued survival. Thus, although apoptosis in tumor cells is sufficiently suppressed to below a critical threshold to enable them to survive, they remain acutely sensitized to apoptosis. In most, if not all, cancer, this ability to survive results in part from inhibition of the p53 pathway, either by inactivating mutations in p53 itself, perturbation of the signaling pathways that allow activation of p53 in response to stress, or defects in the downstream mediators of p53-induced apoptosis. Reintroduction of p53 function is sufficient to induce apoptosis in many tumor cells, and several mechanisms to reactivate p53 are being considered as therapeutic strategies. These include introduction of wild-type p53 into tumors expressing a mutant protein, or inhibition of negative regulators of p53, such as MDM-2, in those tumors that retain wild-type p53.<sup>41</sup> Regardless of efficiency in cell killing, the success of repairing the apoptotic response in tumor cells depends on the extent to which such therapies confine death to the cancer cells, and allow survival of normal tissue. Many conventional chemotherapies induce significant toxicity, particularly in tissues that normally maintain a proliferative compartment, such as gut epithelium and the hematopoietic system. This DNA damage-induced toxicity is mediated in part through p53, leading to the suggestion that inhibition of p53 in these normal tissues may protect against drug-induced toxicity, thereby improving the tolerance of conventional cancer therapies. However, implicit in the development of drugs that target specific lesions responsible for tumor cell growth is the prediction that these approaches will show significantly more specificity for tumor cell killing than conventional therapies. Although activation of apoptotic pathways can lead to the death of untransformed cells, a

process that is essential in normal development, a fundamental difference exists between tumor cells and their normal counterparts, as normal cells neither have to sustain the pro-apoptotic onslaught that is inherent in deregulated proliferation, nor survive away from their usual environment in the absence of requisite survival signals. Repair or replacement of a single apoptotic signal, be it reactivation of p53 or removal of a survival signal, could well prove too much for a tumor cell already burdened with a heavy apoptotic load. By contrast, the same perturbation may scarcely ruffle the equilibrium of a normal cell, safely buffered in its appropriate soma and enjoying the full gamut of trophic support that ensures normal cell survival.

### ***1.5 p53: molecular target***

p53, (53KD) also known as tumor protein 53 (TP53), is a transcription factor that regulates the cell cycle and apoptosis, in case of cellular insults, and hence functions as a tumor suppressor. p53 contains a natively unfolded amino-terminal transactivation domain (TAD), which can be further subdivided into the subdomains TAD1 and TAD2, followed by a proline-rich region (PRR). The structured DNA-binding and tetramerization domains (OD) are connected through a flexible linker region. (Figure 9) Similarly to the TAD region, the regulatory domain at the extreme carboxyl terminus (CTD) is also intrinsically disordered.<sup>44</sup> The vertical bars, shown in Figure 9, indicate the relative missense-mutation frequency in human cancer for each residue based on the TP53 Mutation Database of the International Agency for Research on Cancer<sup>45</sup>, showing that most cancer mutations are located in the DNA-binding domain. The structure of the DNA-binding domain (PDB code 1TSR) is shown (Figure 9) as a ribbon representation and colored with a rainbow gradient from the amino terminus (blue) to the carboxyl terminus (red).

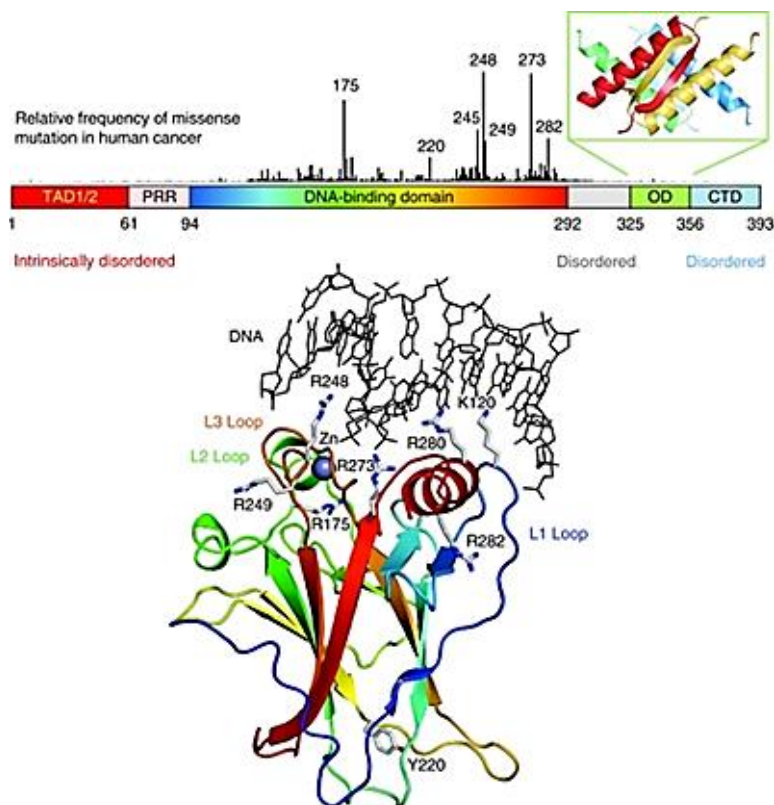


**Figure 9.** Domain structure of p53

p53 has been described as "*the guardian of the genome*", "the guardian angel gene", or the "master watchman", referring to its role in conserving stability by preventing genome mutation. The transcription factor p53 responds to diverse cellular stresses to regulate target genes that induce cell cycle arrest, apoptosis, senescence, DNA repair, or changes in metabolism.<sup>46</sup> In addition, p53 appears to induce apoptosis through nontranscriptional cytoplasmic processes.<sup>47</sup> In unstressed cells, p53 is kept inactive essentially through the actions of the ubiquitin ligase MDM2, which inhibits p53 transcriptional activity and ubiquitinates p53 to promote its degradation.<sup>47</sup> Numerous posttranslational modifications modulate p53 activity, most notably phosphorylation and acetylation. Several less abundant p53 isoforms also modulate p53 activity.

Activity of p53 is ubiquitously lost in human cancer either by mutation of the p53 gene itself or by loss of cell signaling upstream or downstream of p53.

### ***1.5.1 The role of p53 in normal cells***

Activation of p53 can result in a number of cellular responses, and it is possible that different responses are induced by different stress signals. There is evidence that p53 can play a part in determining which response is induced through differential activation of target-gene expression. Although the importance of these responses to tumor suppression is clear, previously unanticipated contributions of these responses to other aspects of human health and disease are being uncovered. The role of p53 in tumor suppression, development and ageing is likely to depend on which cellular response is activated and on the context in which the activation occurs. p53 is an intensively studied protein, its fame stemming mainly from its clear role as a tumor suppressor in humans and other mammals.<sup>48</sup> Loss or mutation of p53 is strongly associated with an increased susceptibility to cancer, and most functions of p53 have been considered in the light of how p53 might protect from malignant progression.<sup>49</sup> Some *p53*-null mice can develop normally<sup>50</sup> an observation that has been taken to rule out major functions for p53 in normal physiology. But recent studies are questioning whether p53 is truly such a single-minded protein, and other functions of p53 that might be profoundly important during normal life are being uncovered. These include roles for p53 in regulating longevity and ageing, glycolytic pathways that might determine endurance and overall fitness, and apoptotic responses during ischemic and other types of stress. Evidence for genetic variations in the activity of the p53 pathway in humans gives these ideas extra relevance.<sup>51</sup> One of the major mechanisms by which p53 functions is as a transcription factor that both positively and negatively regulates the expression of a large and disparate group of responsive genes (Figure 7).<sup>52</sup> Although some of these p53- responsive genes have an important role in mediating cell-cycle

arrest, senescence and apoptosis (the best understood activities of p53), it is now evident that the ability of p53 to influence gene expression has wider reaching effects. Numerous studies have identified p53-regulated genes that could have a role in a number of different and sometimes unexpected responses.<sup>53</sup> Although some of these still need to be fully validated, there is now clear evidence for a role of p53 in the regulation of glycolysis,<sup>54</sup> and autophagy,<sup>55</sup> the repair of genotoxic damage,<sup>56</sup> cell survival and regulation of oxidative stress,<sup>57</sup> invasion and motility,<sup>58</sup> cellular senescence,<sup>59</sup> angiogenesis,<sup>60</sup> differentiation,<sup>61</sup> and bone remodeling.<sup>62</sup> The cellular pathways in which p53 is involved, are schematically represented in Figure 10. In these aspects, its worthy to analyze there is any cancer cells are expressing wild type p53, and if they are expressing, its role in cancer cells has to be studied before clinical use of p53 mediated gene therapy as an anticancer therapy.

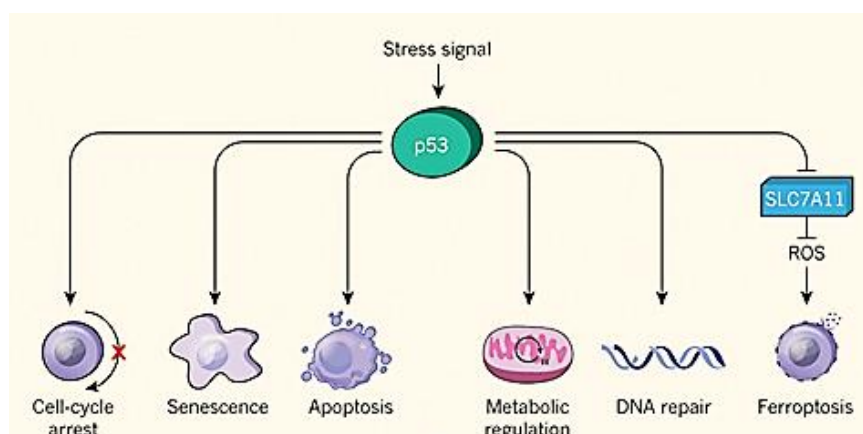


**Figure 10.** Activation and functions of p53

### **1.5.2 The role of p53 in cancers cells**

In the two decades since its original discovery, p53 has found a singularly prominent place in our understanding of human cancer. Although the biochemistry of p53 has been worked out in some detail, our knowledge of the biologic consequences of p53 dysfunction is still quite rudimentary.

p53 dysfunction in cancer cells are mainly due to its mutation (50%), epigenetic modulation at expressional level and low persistence of p53 protein level due to its enhanced turnover. Most p53 mutations found in human cancers are not null mutations but rather encode mutant version of the p53 protein that may have unwanted activities such as a gain-of-function or be dominant negative inhibitors of wt p53 activity. In this regard, it will be important to determine how best to harness the complex properties of p53's ability to induce cellular growth arrest and cell death to generate novel, effective approaches to cancer therapy. Furthermore, a clearer appreciation of the direct interaction epigenetic factors with p53 will lead to development of strategies to inhibit tumor initiation and progression. DNA damage was the first type of stress found to activate p53 and, based on this, p53 has been widely regarded as “the guardian of the genome”.<sup>63</sup> Extensive characterization of the signaling routes that connect DNA damage with p53 have identified a cascade of Ser/Thr kinases that includes ATM, ATR, Chk1 and Chk2, which phosphorylate p53.<sup>64</sup> This signaling cascade is permanently activated in human cancer, suggesting that the cancerous state is intrinsically associated to the generation of DNA damage.<sup>65,66</sup> The constitutive DNA damage present in cancer cells is thought to emanate primarily from the strong generation of reactive oxygen species,<sup>67</sup> as well as, from the aberrant firing of DNA replication origins.<sup>68</sup> Recent characterization of mice genetically manipulated with a knocked-in p53 that cannot be phosphorylated at two of the main residues targeted by ATM/ATR/Chk1/Chk2, namely, Ser18 and Ser23 (Ser15 and Ser20 in human p53), indicates an important role of these phosphorylation sites in some, but not all, the DNA damage induced and p53-dependent responses.<sup>69</sup> In agreement with this, mice carrying p53 S18A/S23A alleles are tumor prone,<sup>70</sup> although this phenotype is considerably milder than in the case of p53-null mice.<sup>71</sup> These data suggest that the activation of p53 in response to DNA damage occurs through multiple pathways, which in addition to the well-established kinase cascade of

ATM/ATR/Chk1/Chk2, probably include other kinases such as p38, JNK/SAPK and c-Abl (Figure 11).<sup>72</sup> Regarding human cancer, the available information gathered from the analysis of epigenetic aberrations indicates that the aforementioned DNA damage signaling kinases are not, in general, significant targets of genetic and epi-genetic inactivation.<sup>73</sup> The only exception to this is found in hematological malignancies, which present a high incidence of mutations in ATM (13–40% depending on the particular type of malignancy).<sup>74</sup> In line with this, a recent large-scale sequencing effort of 210 diverse human cancers has identified ATM among the three most frequently mutated kinases (5% incidence).<sup>75</sup> Based on the above genetic evidence, it can be concluded that DNA damage is conveyed to p53 through multiple redundant pathways in which many transducers participate, but none of them plays a critical role and, therefore, alteration of a single component does not have a significant impact on p53 function.

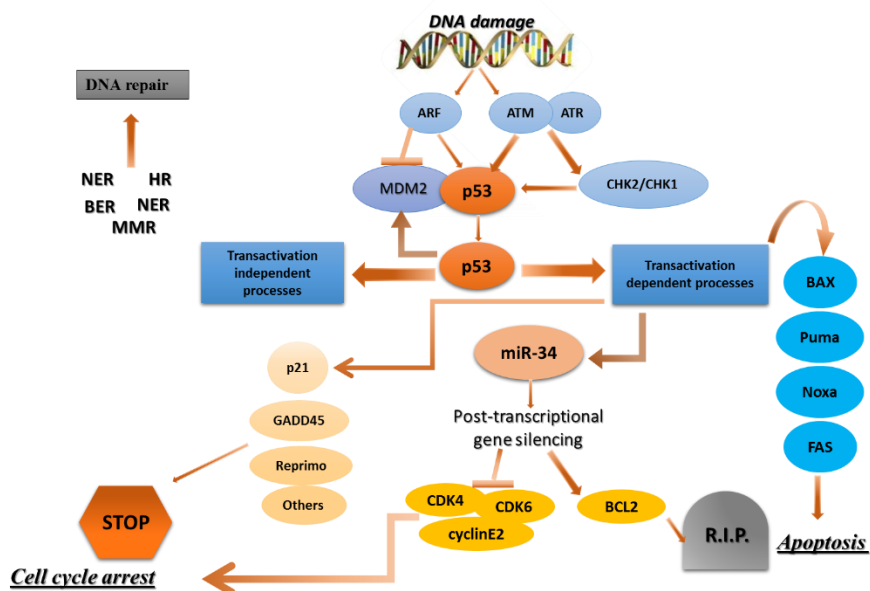


**Figure 11.** p53 is at the center of a complex network of biological interactions that translates stress signals into cell cycle arrest or apoptosis

According, upstream signaling to p53 increases its level and activates its function as a transcription factor in response to a wide variety of stresses, whereas downstream components execute the appropriate cellular response (see below). The principal sensors seem to be MDM2 and MDM4 and their interaction with p53.<sup>76</sup> In non-stressed conditions these proteins bind p53, ubiquitylate it and target it for degradation by the proteasome. In stressed conditions the function of the MDM2–MDM4 complex is blocked by phosphorylation, protein-binding events and/or enhanced degradation. Hence, phosphorylation of MDM4 is essential for the p53 response to ionizing radiation, and the response to oncogene activation depends on the binding of ARF to MDM2. Many p53-activating small molecules function by causing the release of ribosomal proteins from the nucleolus to the nucleoplasm, where they bind to MDM2 and MDM4 and inhibit their function. Molecules that activate wild-type p53 in tumors by disrupting MDM2 activity can compensate for any missing upstream components of the p53 pathway. However, defective downstream p53 signaling might substantially decrease their effectiveness. Therefore, the ability to identify tumors in which downstream p53 signaling is unaffected is important. The development of strategies to ensure that the desired p53 response is initiated when it is reactivated might be necessary and could require the judicious use of drug combinations.

### ***1.6 p53 network: co-activators and associated proteins***

The interaction between p53 and transcriptional co-activators also influences its affinity for promoters. It is therefore plausible that the specific co-factors expressed in a particular cellular context determine the repertoire of p53-target genes induced, and consequently whether the cell undergoes growth arrest or apoptosis, or even a particular apoptotic pathway, may be subject to the availability of co-activators.<sup>76</sup> Once the p53 protein is activated, it initiates a transcriptional program that reflects the nature of the stress signal, the protein

modifications and proteins associated with the p53 protein. The p53 protein binds to a specific DNA sequence, termed the p53- responsive element (RE),<sup>77</sup> and induces the expression of downstream genes. An algorithm that identifies p53-responsive genes in the human and mouse genome has been utilized to detect a number of new genes regulated by the p53 protein.<sup>78</sup> The genes in this p53 network mainly initiate one of three programs that result in cell cycle arrest, DNA repair or apoptosis. The exact criteria that influence p53 to stimulate cell cycle arrest or apoptosis are only partially understood and are the subject of intense study. Several general factors that influence this decision include p53 expression levels, the type of stress signal, the cell type and the cellular context at the time of exposure to stress. Several intriguing observations have recently provided insight into the apparent intricacies of such cell fate determination. The examples described below involve the binding of p53 to its canonical binding sequence in target genes. Note, however, that p53 can also activate target genes through a non-canonical sequence. The first such example is in the p53-induced gene 3 (*PIG3*), which has been implicated in the accumulation of reactive oxygen species and apoptosis induction. *PIG3* can be induced by p53 through a microsatellite sequence within its untranslated region. Another recently described example is the gene encoding the pro-apoptotic phosphatase PAC1, which is induced through binding of p53 to a novel palindromic binding site. This might represent a new mechanism for transcriptional regulation of apoptotic genes by p53, which differs from that already described (see below). Exact discrimination between p53 arrest and apoptotic functions has been critical to the identification of the importance of the latter in tumor suppression.

### ***1.6.1 p53 and the DNA repair***

Soon after having established TP53 as the most frequently altered gene in human tumors in the 1990s,<sup>79</sup> p53 was understood as a major component of the DNA damage response pathway. After the introduction of DNA injuries the

level of p53 protein rises, which in turn induces a transient cell cycle arrest or apoptotic cell death. DNA damage activates p53 through post-translational modifications by specific kinases, such as the strand break sensor ataxia telangiectasia mutated protein (Atm), by acetyltransferases like CREB-binding protein (Cbp)/p300, and by the poly (ADPribose) polymerase 1 (Parp-1), which prevent proteolysis via the Arf-mouse double minute 2 (MDM2) pathway and/or enhance binding of p53 to consensus sequences within the genome.<sup>80</sup> Initially, investigations on a direct participation of p53 in DNA repair were spurred by a number of biochemical observations. Thus, the C-terminal 30 amino acids of p53 were shown to recognize several DNA damage-related structures, such as DNA ends, gaps, and insertion/deletion mismatches. p53 was also demonstrated to catalyze reannealing of short stretches of single- and double-stranded DNA and to promote strand exchange between them. Further, p53 binds to three-stranded heteroduplex joints and four-stranded Holliday junction DNA structures with localization specifically at the junction, suggesting that p53 directly participates in recombinational repair.<sup>81</sup> Moreover, several groups demonstrated a Mg-dependent 3'–5' exonuclease activity intrinsic to p53. Noticeably, the same central region within p53, where tumorigenic mutations are clustered, recognizes DNA sequence specifically, is required for junction specific binding of heteroduplex joints and is necessary and sufficient for the 3'–5' exonuclease activity on DNA.<sup>82</sup> In addition to p53's biochemical activities, numerous reports on physical and functional protein interactions further strengthened the proposal of a direct role of p53 in nucleotide excision repair (NER), base excision repair (BER), and double-strand break (DSB) repair.<sup>83</sup>

### ***1.6.2 p53 and the growth arrest***

p21*WAF1/CIP1* is known to be a p53-downstream gene, and has been suggested to mediate p53-induced growth arrest triggered by DNA damage. The p21

protein is a cyclin-dependent kinase inhibitor that associates with a class of CDKs and inhibits their kinase activities. This will facilitate the accumulation of hypophosphorylated form of pRB that in turn associates with E2F inhibiting its transcriptional activity, leading to cell cycle arrest. As long as pRb is bound to E2F, the cell is prevented from entering into S phase. This G1 arrest affords the cell time to repair the DNA damage. Should repair be unsuccessful, P53 levels drop and CDK-cyclin protein kinase activity resumes, leading to entry into S phase. In the event that the DNA is not repair, p53 triggers apoptosis.<sup>84</sup>

### ***1.6.3 p53 and the apoptosis***

Pivotal to the tumor-suppressor activity of p53 is its ability to activate apoptosis via multiple different pathways. Since the most-studied function of p53 is its role as a transcription factor that can activate transcription of an ever-increasing number of target genes, its transcriptional activation of pro-apoptotic genes, as well as its transcriptional repression of anti-apoptotic genes, has been widely analyzed.<sup>85</sup> However, although a large number of genes regulated by p53 during induction of apoptosis are known no single target gene has been identified whose altered expression alone can sufficiently explain p53 mediated transcription dependent apoptosis, and whose genetic deficiency phenocopies p53 deficiency in vivo. As an additional mode of p53’s pro-apoptotic activity, recent studies have placed non transcriptional pro- apoptotic activities of p53 at the center of an active debate that aims to establish a comprehensive understanding of p53- mediated apoptosis.<sup>86</sup>

#### ***1.6.3.1 p53 role in transcription dependent apoptosis***

The past twenty-five years have seen intensive and varied investigations to better understand the functions that p53 uses to mediate apoptosis. The first indication of the role of p53 in apoptosis was obtained using the M1 mouse myeloid leukemia cell line lacking endogenous p53. Using M1 cells stably

transfected with a temperature-sensitive mutant that acquires the conformation of wild-type p53 at permissive temperature (32°C), it was observed that upon downshift to the permissive temperature, the transfectants underwent rapid loss of viability with the characteristics of apoptosis.<sup>87</sup> Several mechanisms have been implicated in p53-mediated apoptosis. One is p53 activation to up-regulation of pro-apoptotic Bax and down-regulation of pro-survival Bcl-2.<sup>88</sup> More recently it's determined that p53-mediated apoptosis of M1 cells involves rapid activation of the pro-apoptotic Fas/CD95 death pathway-via up-regulation of membrane bound Fas and the intrinsic mitochondrial pathway, which results in activation of caspases 8, 9 and 10. (Figure 12) Either Fas blocking antibody or inhibition of the apical caspases 8 and 10, were each almost as effective as IL-6 in abrogating p53 mediated apoptosis. These observations argue that p53 regulation of the bcl-2 members Bax and Bcl-2, associated with the intrinsic mitochondrial apoptotic pathway, is ancillary to the extrinsic Fas/CD95 apoptotic pathway in mediating p53 induced apoptosis of M1 myeloid leukemia cells.<sup>89</sup>

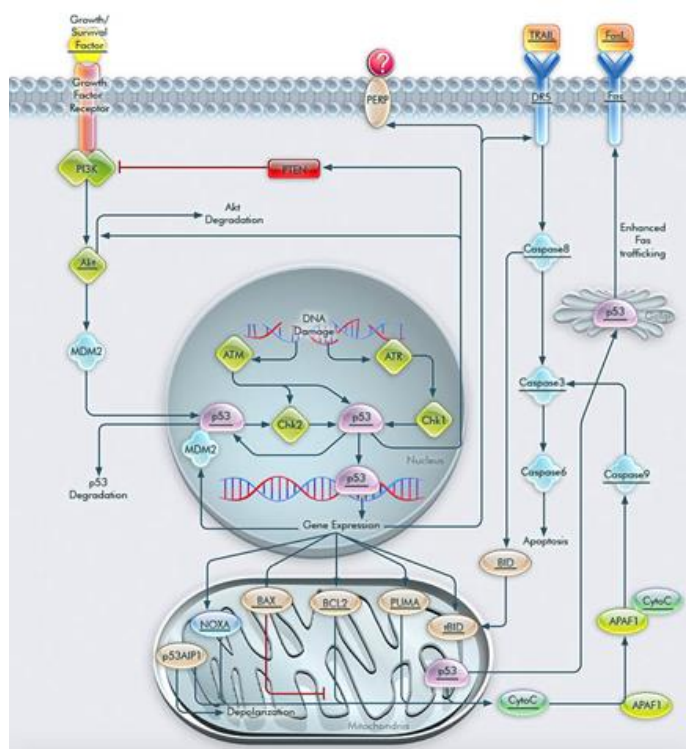


**Figure 12.** p53 mediated apoptosis

In other cell types up-regulation IGF-BP3<sup>90</sup> which sequesters the cell survival factor insulin-like growth factor-1 has been associated with p53 mediated apoptosis. The gene encoding for the cathepsin-D protease, PAG-608 which encodes a nuclear zinc finger protein and the human homolog of the *Drosophila* *lasina* gene have also been implicated as mediators of p53 induced apoptosis in various cell types. Furthermore, a series of p53-induced genes (PIG genes) were documented to encode proteins that respond to oxidative stress, suggesting that p53-mediated apoptosis involves activation of redox-controlling targets followed by increase in ROS, oxidative damage to mitochondria and caspase activation. Along this research line it was recently observed that p53 suppresses Nrf2-dependent transcription of antioxidant response genes, presumably to prevent the generation of antioxidants that could hinder induction of apoptosis.<sup>91</sup> Clearly established is p53’s role as a nuclear

transcription factor with the ability to activate, or repress, the expression of many genes. A number of p53 transcriptional targets, such as the p53-induced genes BAX, PUMA, NOXA, and the p53-repressed genes BCL2 and SURVIVIN, represent genes with the potential to promote or inhibit apoptosis, respectively, in stressed cells. Puma and Noxa are thought to indirectly induce mitochondrial outer membrane permeabilization (MOMP), known to be induced by the activation of Bax and Bak, via interfering with Bax and Bak interaction with prosurvival Bcl-2 family members. Interestingly, it was observed that Puma and Noxa differentially contribute to the regulation of p53-mediated apoptotic pathways. In normal cells, Puma was found to induce mitochondrial outer membrane permeabilization via an ER-dependent pathway; however, upon E1A oncoprotein expression, cells also became susceptible to mitochondrial outer membrane permeabilization induction by Noxa via an ER-independent pathway. In several instances, transcriptional activation by p53 was observed to be dispensable for p53-dependent apoptosis, since mutants p53 which fail to activate transcription could still induce apoptosis.<sup>92</sup> In addition, p53-dependent apoptosis could occur in the presence of inhibitors of transcription and translation.<sup>93</sup> In recent years it has become clear that p53 also harbors a direct proapoptotic function at the mitochondria via engaging in protein-protein interactions with anti- and pro-apoptotic Bcl2 family members, including BclXL and Bak.<sup>94</sup> It has been reported, certain transcriptionally inactive mutants of p53 can still induce apoptosis when over expressed in tumor cells. Also, in response to some stresses, such as hypoxia, p53 induces apoptosis but does not function as a transactivator. Intriguingly has been demonstrated that during p53-dependent apoptosis a fraction cellular p53 protein localizes to mitochondria and induces cytochrome c release; however, this is not observed during p53-mediated cell cycle arrest.<sup>95</sup> Additional support for the concept that p53 has a cytoplasmic role in apoptosis induction resulted from functional analysis of polymorphic variants of p53 (within exon 4 of the p53 gene, a

common single-nucleotide polymorphism (SNP) at codon 72 leads to the incorporation of either an arginine (R72) or a proline (P72) at this position of the protein. When explored the potential mechanisms underlying the observed functional difference between the two p53 variants, made the initially surprising discovery that the greater apoptotic potential of the R72 form correlated with its much better ability to traffic to mitochondria. Based on these data, therefore concluded that the enhanced apoptosis-inducing activity of the R72 protein related, at least in part, to its greater mitochondrial localization. An analysis of whole cell or mitochondrial extracts by immune precipitation-western blot analysis, demonstrated the R72 form of p53 binds better to the mitochondrial death-effectors protein BAK than does the P72 variant, correlating with the difference in apoptotic potential of the two p53 variants. In healthy cells, Bak resides at mitochondria as an inactive monomer. In response to various death stimuli, it undergoes an activating allosteric conformational change that promotes homo-oligomerization. This leads to formation of a pore in the outer mitochondrial membrane, and allows the release of cytochrome c and other caspase cascade (Figure 4). Recently, like BAK, the BCL2 family members BAX and BCL-XL have also been implicated in mitochondrial apoptosis induction by p53 (Figure 12).<sup>96</sup>

**CHAPTER II**  
**SEARCH SETTING**

### **2.1 Aim of the study**

The ability of p53 to respond to stress signals by triggering cell-cycle arrest and cell death by apoptosis is crucial to inhibit tumor development and for the response to anticancer therapy.<sup>49,97,98</sup> Inactivation of p53 by mutation occurs in about half of all human tumors. Tumors that retain wild-type p53 often acquire an alternative mechanism for its inactivation, largely through deregulation of MDM2 (murin double minute-2) protein. Negative regulation of p53 activity and stability is enhanced in many human tumors and effectively impairs the activities of the p53 pathway. Therefore, recovery of p53 activity in cancer cells by antagonizing MDM2 has been proposed as a novel approach for treating cancer and validated *in vitro* by macromolecular studies. MDM2 and p53 are part of an auto-regulatory feedback loop (Figure 13).<sup>99,100</sup> MDM2 is transcriptionally activated by p53 and MDM2, in turn, inhibits p53 activity in several ways. MDM2 binds to the p53 transactivation domain and thereby inhibits p53-mediated transactivation. MDM2 also contains a signal sequence that is similar to the and, after binding to p53, it induces its nuclear export. Nuclear export signal of various viral proteins. As p53 is a transcription factor, it needs to be in the nucleus to be able to access the DNA; its transport to the cytoplasm by MDM2 prevents this. Finally, MDM2 is an ubiquitin ligase, so is able to target p53 for degradation by the proteasome. In normal cellular conditions, p53 is constantly degraded by MDM2, and is therefore present at low levels.<sup>101</sup>



observed in soft-tissue tumours, osteosarcomas and oesophageal carcinomas. Furthermore, many reports describe the overexpression of MDM2 in different types of tumour.<sup>103</sup> The presence of high levels of MDM2 in these tumours might be an important element for their survival, because it decreases their ability to activate p53.<sup>104,105</sup> The design of compounds that prevent the interaction between p53 and MDM2 is therefore an attractive strategy for activating p53 tumour-suppressor activity in tumours. The structures of p53 and MDM2 have been determined by X-RAY CRYSTALLOGRAPHY,<sup>106</sup> p53<sub>15-29</sub> binds into a large cleft that is present at the surface of MDM2 (Figure 14A). The residues 19–25 form an  $\alpha$ -helix and residues 17, 18 and 26–29 take a more extended conformation. Thr18 is particularly important for the stability of the helix and the regulation of the p53–MDM2 interaction by phosphorylation.<sup>107</sup> A detailed structural analysis of the interface between p53 and MDM2 reveals many factors that must be considered when aiming to inhibit this interaction. Only one of the two partners (MDM2) has a structurally well-defined binding site. The inhibitors should therefore aim to mimic the other partner (p53). One of the two interfaces (p53) is formed by only one segment of contiguous aminoacids, allowing the design of peptidic inhibitors (p53 mimics). Three residues — Phe19, Trp23 and Leu26 (Figure 14B) — contribute to a large extent to the interaction and consequently to the binding energy of the p53 peptides. The inhibitors of the p53–MDM2 interaction will have to contain mimics of these amino acids. There are only three hydrogen bonds connecting p53 to MDM2, and at least the most buried one will have to be preserved to ensure sufficient affinity of the inhibitors.<sup>108</sup>

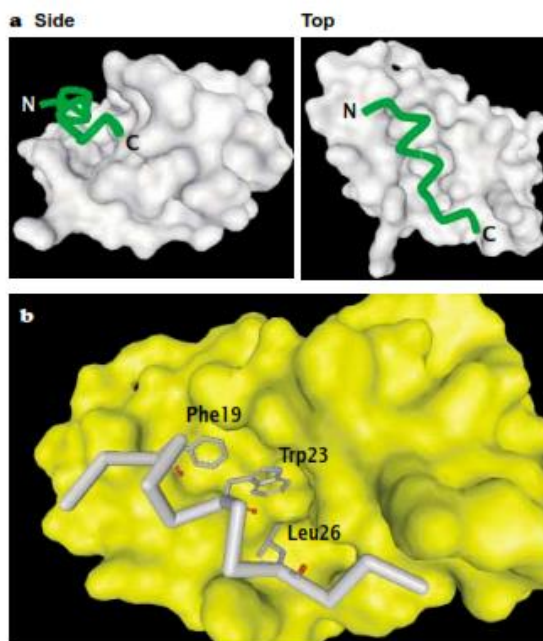


**Figure 14.** Structure of the p53–MDM2 complex. (A): the surface of MDM2<sub>25–109</sub> is in white and the backbone of p53 is in green. Two different views of the complex are presented, and the amino (N) and carboxyl (C) termini of the p53 peptide are indicated. (B): The p53<sub>17–29</sub> backbone is in grey and the side chains of Phe19, Trp23 and Leu26 are represented. The surface of MDM2<sub>25–109</sub> is in yellow

According to these findings, and as part of my PhD program aimed to identify *small-molecules* endowed with antitumor activity, different series of compounds were designed as potential p53 modulators.

Specifically, my research work has been focused on two different projects:

- 1) the synthesis of *small molecules* designed as modulators of apoptosis, mediated by p53;
- 2) the design and synthesis of DTNQ derivatives as antitumour agents potentially involved in the p53-MDM2 interaction.

Finally, the aim of this study was to identify of suitable *leads* allowing further understanding about the molecular complexity of p53 network, thus improving the antitumor therapeutic arsenal

---

**CHAPTER III**  
**DESIGN, SYNTHESIS, RESULTS AND**  
**DISCUSSION OF POTENTIAL p53 MODULATORS**  
**(SERIES 1 AND SERIES 2)**

### 3.1 Background and design

Several low molecular weight inhibitors, have been identified and reported, so, Vassilev et al.<sup>109</sup> identified the first group of molecules that target the MDM2-p53 interaction (Figure 15). These imidazoline derivatives, defined as Nutlins, specifically bind and dissociate MDM2 from p53, leading to extensive p53 activation and induction of a full-blown p53 response, which can trigger tumor shrinkage. The derivative Nutlin-3 is currently undergoing phase I clinical evaluation against advanced solid tumors and hematological malignancies.

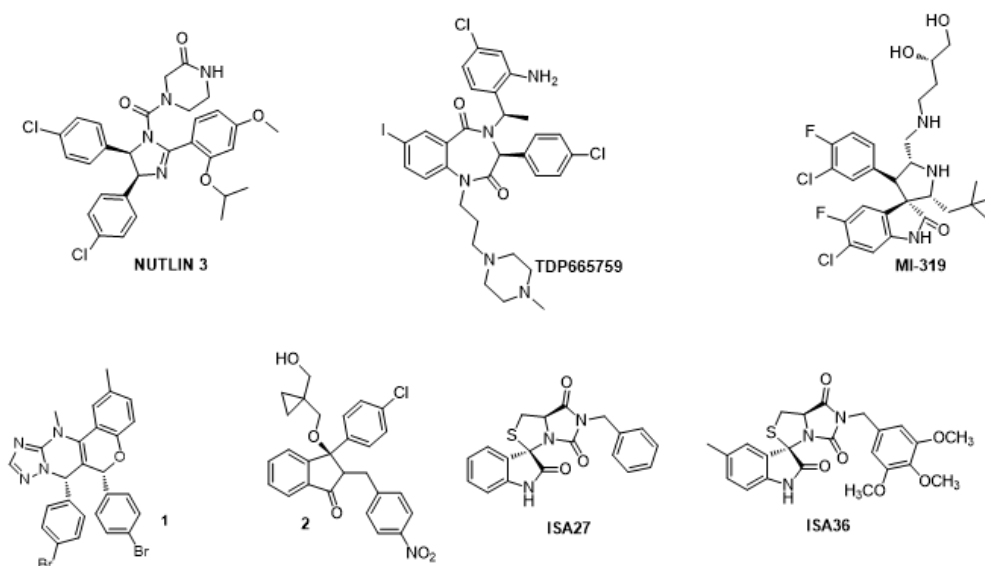
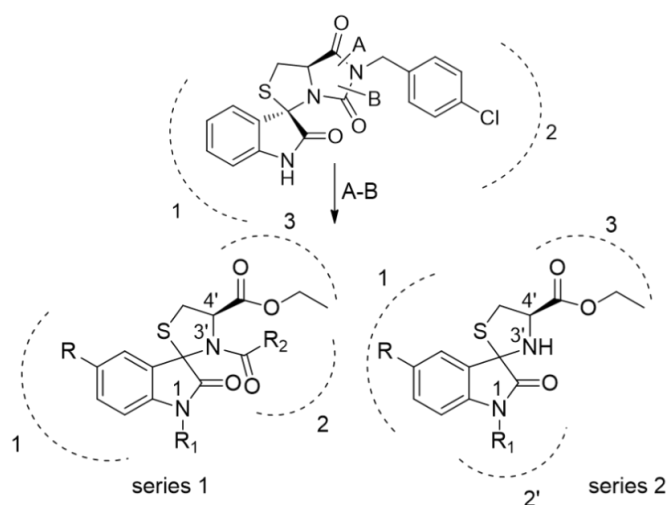


Figure 15. Structures of different inhibitors of p53-MDM2 interaction

The benzodiazepines<sup>110</sup> and the spirooxindole-based compounds<sup>111</sup> are other classes of *small molecules* that have been found to target the p53-MDM2 interaction. These results led to the preclinical development of **TDP665759** and **MI-319**, which disrupt the binding of MDM2 to p53 in vitro and suppress the growth of tumor cells both in vitro and in vivo. Both compounds limit tumor growth without causing major toxicity in the surrounding tissue. Although these

products induce high levels of p53, they are unable to activate the apoptotic cascade; other *small-molecules* inhibitors include chromenotriazolopyrimidines (**1**)<sup>112</sup> and oxindoles (**2**).<sup>113</sup> Most of the inhibitors we have described above share a common structural motifs, such as a rigid heterocyclic scaffold highly functionalized with appropriate aryl/alkyl groups, which are supposed to mimic the critical p53 residues binding MDM2 [Paragraph 2.1]. My research group has previously reported a series of spiro(oxindole-3,3'-thiazolidine)-based derivatives potentially able to mimic at least two critical p53 residues that bind MDM2.<sup>114</sup> Compounds (3*R*,7*aR*)-6-(4-Chlorobenzyl)-1*H*-spiro[imidazo[1,5-*c*]thiazole-3,3-indoline]-2',5,7(6*H*,7*aH*)-trione (**ISA27**) and (3*R*,7*aR*)-5'-methyl-6-(3,4,5-trimethoxybenzyl) -1*H*-spiro[imidazo[1,5-*c*]thiazole-3,3 indoline] 2',5,7 (6*H*,7*aH*) -trione (**ISA36**) inhibited cell growth of different human tumor cells at micromolar concentrations. In particular **ISA27** induced apoptotic cell death after 24h of treatment at cytotoxic concentrations but did not alter the normal course of cell cycle. **ISA27** also induced a time-dependent increment of p53 expression, indicating that the activity profiles of the compound might be regulated by this protein. More concretely, NMR studies (<sup>1</sup>H proton) performed on compounds **ISA27** and **ISA36** demonstrated the ability of these compounds to block p53-MDM2 interaction.<sup>114</sup> Encouraged by the results obtained and aiming to improve the pharmacological profile of these compounds, new inhibitors of p53-MDM2 interaction were designed by structural modifications of **ISA27**. We considered of interest to manipulate the spiro (oxindole-3,3'-thiazolidine) nucleus of **ISA27**, by opening of imidazole ring, with the aim of altering its conformational properties. The opening of this ring would allow us to obtain more flexible structures (Figure 16, series 1 and 2) with a potential third point of diversification through the 4'-carboxyl group of the thiazolidine moiety. This ring could allow the aromatic and/or alkyl side chains to assume more appropriate orientations to interact with the binding site.



**Figure 16.** Design of new series 1 and 2. Dashed lines define hypothetical interaction subsites

Therefore, during the first year of my PhD programme I have been involved in the synthesis of two small libraries of compounds, both series retain the ester group at position C-4', while the oxindole moiety carries either a weak releasing (CH<sub>3</sub>) or a withdrawing (Br) electron groups (R). Series 1 contains a substituted phenyl, benzyl, or a cyclohexyl side chains on the N-3' (R<sub>2</sub>), while these groups were positioned on N-1 in the series 2 (R<sub>1</sub>).

### 3.2 Chemistry

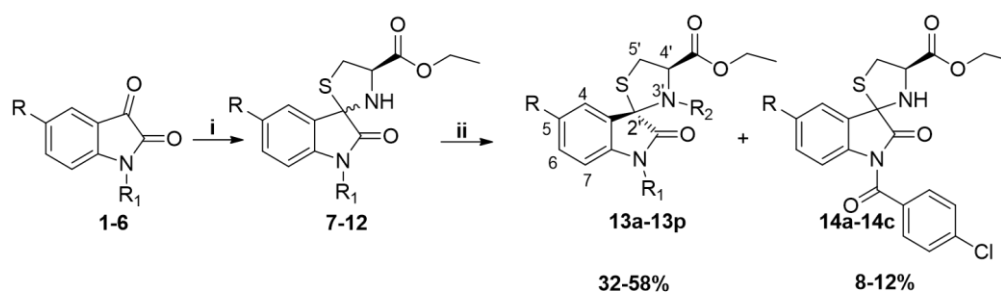
#### 3.2.1 Chemistry 1<sup>st</sup> series

The new (2'*S*,4'*R*) -ethyl 3'-substituted-2-oxospiro [indoline-3,2' thiazolidine]-4'-carboxylate derivatives (**13a-f**, **13l-n**) were prepared applying the synthetic route shown in Scheme 1.<sup>115</sup> Starting spirooxindolethiazolidine skeletons (**7-12**) were constructed by condensation between the isatin derivatives (**1-6**) and *L*-cysteine ethyl ester in EtOH. These derivatives were obtained with 80-90%

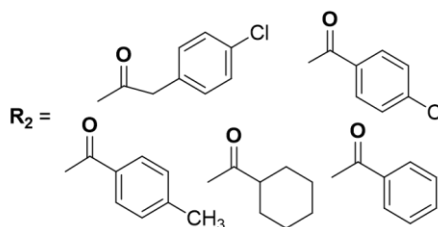
yields, as (2'R)/(2'S) epimeric mixtures ranging from 60/40 to 40/60 ratios as my research group previously described.<sup>114,116</sup>

The 3'-acyl derivatives were obtained by reaction of compounds **7-12** with the corresponding 2-(4-chlorophenyl) acetyl, 4-chlorobenzoyl, 4-methylbenzoyl, benzoyl, or cyclohexanecarbonyl chlorides in THF using TEA as base.

**Scheme 1.** Synthesis of 2-Oxospiro[indoline-3,2'-thiazolidine]-4'-carboxylate derivatives (Series 1 and 2)



- |        |                     |                                  |
|--------|---------------------|----------------------------------|
| 1, 7,  | R = H               | R <sub>1</sub> = H               |
| 2, 8,  | R = CH <sub>3</sub> | R <sub>1</sub> = H               |
| 3, 9,  | R = Br              | R <sub>1</sub> = H               |
| 4, 10, | R = H               | R <sub>1</sub> = CH <sub>3</sub> |
| 5, 11, | R = CH <sub>3</sub> | R <sub>1</sub> = CH <sub>3</sub> |
| 6, 12, | R = Br              | R <sub>1</sub> = CH <sub>3</sub> |



Reagents and conditions: (i): *L*-CysOEt, NaHCO<sub>3</sub> in ETOH; (ii): R<sub>2</sub>- TEA, in THF, 2 h, room temp.  
(See Table 1 for the correspondence between number of final products and substituent R, R<sub>1</sub>, and R<sub>2</sub>)

In these conditions, all final products (**13a-f** and **13h-q**) were obtained as single diastereomers in 32-58% overall yields. These stereoselectivities in the acylation reactions of thiazolidine derivatives have been previously observed by my research group<sup>116</sup> and other authors<sup>117</sup> and can be explained by the fact that

thiazolidines undergo rapid ring opening and closure reactions. This favors the formation of thermodynamically more stable diastereoisomers. Moreover, the reaction of intermediates **7-9** ( $R_1=H$ ) with 4-Cl-benzoyl chloride also gave the 1-substituted derivatives **14a-c** with 8-12% yields.

In the synthesis of the 3-cyclohexylcarboxy derivatives **13n-q**, two isomers were obtained in a 11/1 to 6/1 ratio (estimated by H-NMR), which differs for the cis/trans configuration at the N3'-COC<sub>6</sub>H<sub>11</sub> amide bond.<sup>118</sup> (Figure 17)

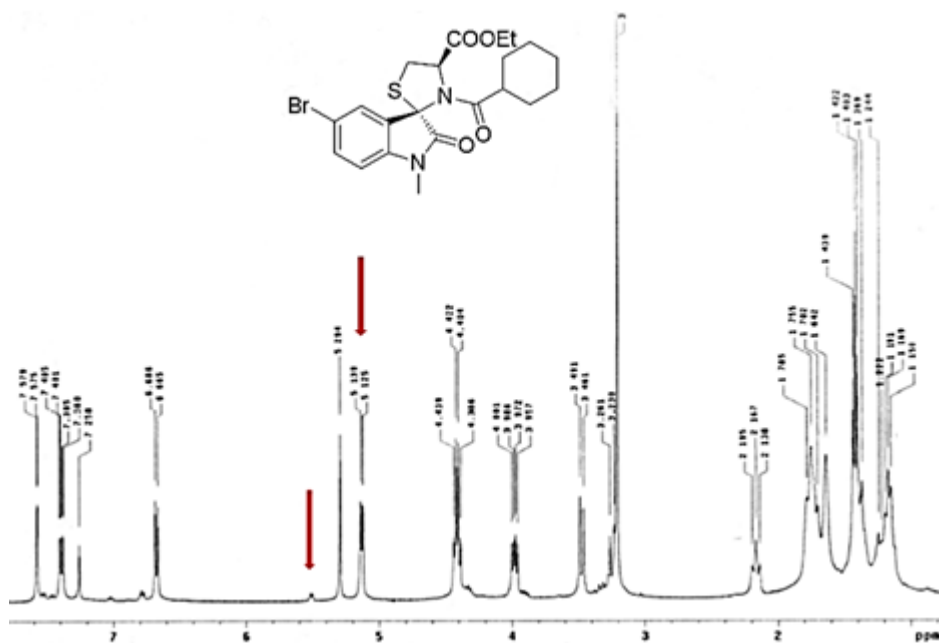
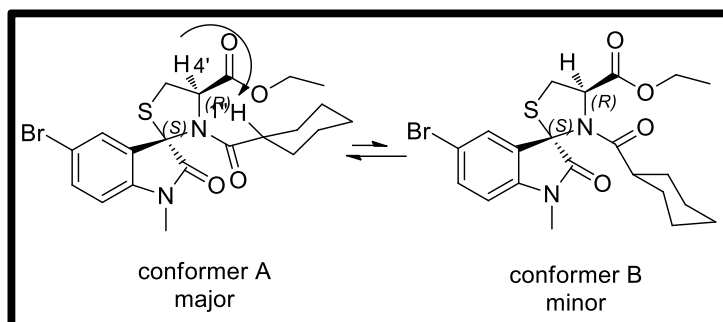


Figure 17. <sup>1</sup>H NMR spectrum of compound 13n (SM13)

The major isomer (cis) in these mixtures was identified on the basis of the ROE observed in the ROESY spectrum of **13n** between the H-1'' of the cyclohexanecarbonyl group and the H-4' of the thiazolidine (Figure18), Cis/trans isomerization about amide bond was evidenced by 2D NMR.



**Figure 18.** ROE interaction observed between H-4' and H-1'' in the ROESY spectrum of compound 13n (SM13)

In fact, interconversion was demonstrated by an exchange cross-peak between the H-4' hydrogen signals of the two isomers.<sup>100</sup> (Figure 19).

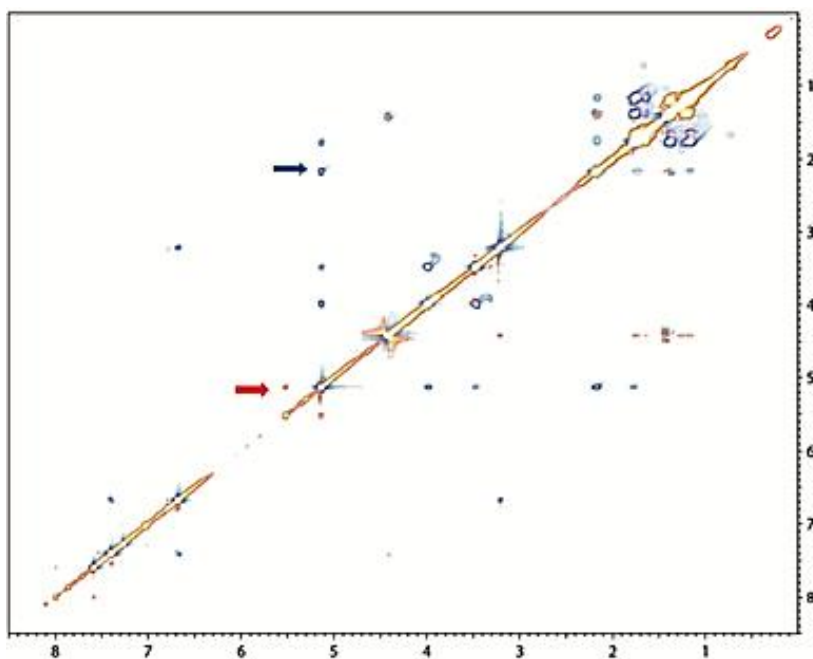
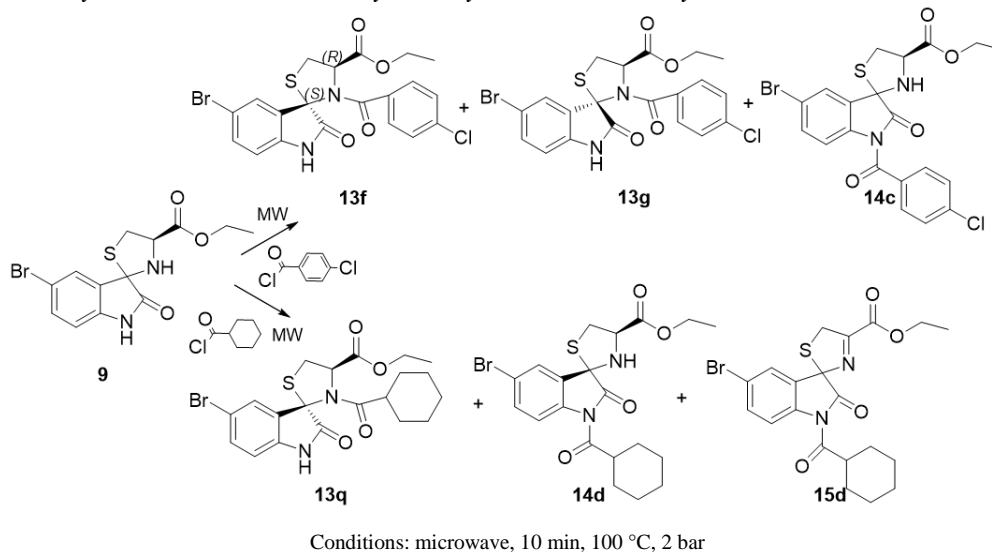


**Figure 19.** Roesy spectrum of compound 13n. Red arrow indicates the chemical exchange peak between H-4' signals of the two isomers of 13n (same sign as the diagonal peaks). Blue arrow indicates the ROE interaction between H-4' and H-1'' of the major isomer (opposite sign as the diagonal peaks)

Changes in the condition of reactions that involve an increase of the reaction time (from 2 h to 12 or 24 h) do not significantly modify the above-described results, while increase of temperature resulted in a general decrease of reaction yields. However, with the use of microwave (Scheme 2),<sup>100</sup> the reaction of intermediate **9** with 4-chlorobenzoyl chloride led to a mixture of two diastereoisomers (2'*S*,4'*R*)-**13f** and (2'*R*,4'*R*)-**13g** and the 1-substituted derivative **14c** in 33%, 15%, and 9% yields, respectively. In the same conditions and using cyclohexanecarbonyl chloride as acylation agent, we observed the formation of only a diastereoisomer (2'*S*,4'*R*)-**13q** (42%), the 1-cyclohexanecarbonyl derivative **14d** (25%), and a minor product with structure of 2-oxo-5'H-spiro[indoline-3,2'-thiazole]-4'-ethylloxycarbonyl **15d** with a 15% yield.

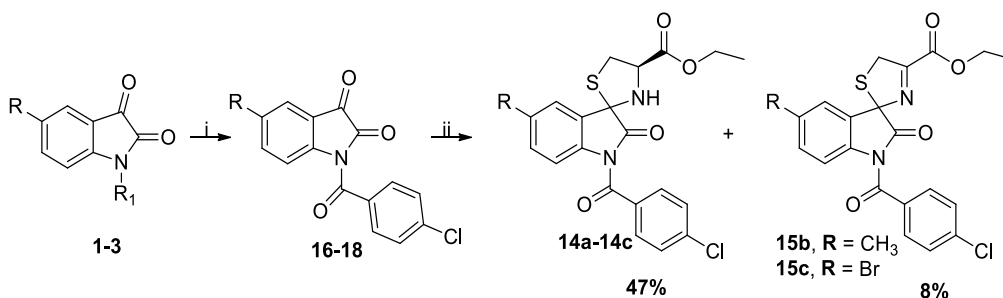
**Scheme 2.** Reaction of ethyl 5-bromo-2-oxospiro [indoline-3,2' thiazolidine]-4'-carboxylate with 4-chlorobenzoyl and cyclohexanecarbonyl chlorides



### 3.2.2 Chemistry 2<sup>nd</sup> series

The 1-(4-chlorobenzoyl)-2-oxospiro[indoline-3,2'-thiazolidine] derivatives (**14a-c**) were prepared using an alternative synthetic route as shown in Scheme 3.<sup>100</sup> Treatment of isatins **1-3** with 4-chlorobenzoyl chloride in DCM and TEA gave the corresponding intermediates **16-18** which were condensed with cysteine ethyl ester in EtOH. In this condition, compounds **14a-c** were obtained as single (2'*S*,4'*R*) diastereoisomer in 47% yields according to their 1D and 2D NMR spectra. In addition, working with the 5-substituted intermediates **17** and **18**, we also observed the formation of thiazoline derivatives **15b** and **15c** with 8% yields.

**Scheme 3.** Synthesis of (2'*S*,4'*R*) -ethyl 2-oxospiro[indoline-3,2'-thiazolidine]-4'-carboxylate derivatives (**14**) and ethyl 2-oxo 5'*H*-spiro[indoline-3,2'-thiazole]-4'-carboxylate derivatives (**15**)



**1, 16, 14a** R = H  
**2, 17, 14b** R = CH<sub>3</sub>  
**3, 18, 14c** R = Br

Reagents and conditions: (i): 4-Cl-C<sub>6</sub>H<sub>4</sub>COCl, TEA in THF, 2h, room temp.; (ii): L-Cys-OEt, NaHCO<sub>3</sub> in EtOH

Moreover, the reaction of **1-3** with cyclohexanecarbonyl chloride did not lead to the desired 1-(cyclohexylcarbonyl) derivative, recovering the starting materials. Poor reactivity of cyclohexane carbonyl chloride could be explained,

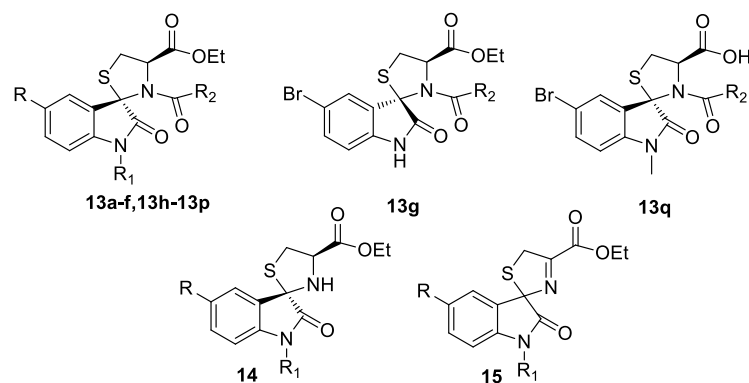
if compared to 4-chlorobenzoyl chloride, by considering a higher steric hindrance of the first. Modifications of reaction conditions including changes of solvent, increase of temperature, or use of microwaves led to the same negative results.<sup>100</sup>

### ***3.3 Biological effects of the spiro-oxo-indole-thiazolidine synthesized***

#### ***3.3.1 Antiproliferative activity***

The synthesized compounds were examined, in the Department of Molecular and Cell Biology of the University of Naples “Federico II”, for their antiproliferative activity against two tumor cell lines: the human breast adenocarcinoma MCF-7 and human colon carcinoma HT-29 at 24 h. The obtained IC<sub>50</sub> values are summarized in Table 1.<sup>100</sup> **ISA27**, considered our hit compound, showed a similar micromolar antiproliferative activity against the two tumoral cell lines used in the assay. The opening derivatives **13a**, **13b**, and **13c** showed an elevated activity with IC<sub>50</sub> values in the micromolar range against MCF-7 and submicromolar against HT29 cell lines. Exchange of the 4-chlorobenzyl group for 4-chlorophenyl gave compounds **13d-f**, more active against MCF-7 cells, while **13f** was 6-fold more active against the HT29 cell line. The activity data for compounds **13a-f** and **13h-j** (IC<sub>50</sub> from 0.08 to >4.0 μM) indicated that the nature of the substituents on the oxoindole moiety markedly affects the antiproliferative activity profile of these compounds. Contrary to what was observed in the precedent series (**ISA27**)<sup>99</sup> presence of an electron-withdrawing group, such as the bromide group, at position C-5 of the indole system caused an increase of the activity of the corresponding analogues **13c**, **13f**, and **13j** in both cell lines but particularly on HT29 cell.

**Table 1.** Antiproliferative activity of spiro[indoline-3,2'-thiazolidine] (**13** and **14**) and spiro[indoline-3,2'-thiazole] (**15**) derivatives



Compd	R	R <sub>1</sub>	R <sub>2</sub>	IC <sub>50</sub> (μM ± SD) <sup>a</sup>	
				MCF-7 <sup>b</sup>	HT29 <sup>c</sup>
ISA27	H	H		1.21±0.6	1.60±0.4
13a	H	H	CH <sub>2</sub> C <sub>6</sub> H <sub>4</sub> (4-Cl)	> 5	1.00±0.20
13b	CH <sub>3</sub>	H	CH <sub>2</sub> C <sub>6</sub> H <sub>4</sub> (4-Cl)	4.81±1.0	0.78±0.20
13c	Br	H	CH <sub>2</sub> C <sub>6</sub> H <sub>4</sub> (4-Cl)	2.90±0.8	0.66±0.10
13d	H	H	C <sub>6</sub> H <sub>4</sub> (4-Cl)	2.15 ±0.7	3.69±0.90
13e	CH <sub>3</sub>	H	C <sub>6</sub> H <sub>4</sub> (4-Cl)	2.12±0.7	1.09±0.60
13f	Br	H	C <sub>6</sub> H <sub>4</sub> (4-Cl)	0.90±0.2	0.11±0.09
13g	Br	H	C <sub>6</sub> H <sub>4</sub> (4-Cl)	3.0 ±0.20	2.00±0.80
13h	H	CH <sub>3</sub>	C <sub>6</sub> H <sub>4</sub> (4-Cl)	4.52±1.1	0.18±0.09
13i	CH <sub>3</sub>	CH <sub>3</sub>	C <sub>6</sub> H <sub>4</sub> (4-Cl)	1.23±0.4	0.12±0.07
13j	Br	CH <sub>3</sub>	C <sub>6</sub> H <sub>4</sub> (4-Cl)	0.52±0.3	0.08±0.01
13k	Br	CH <sub>3</sub>	CH <sub>2</sub> C <sub>6</sub> H <sub>4</sub> (4-Cl)	0.27±0.1	0.36±0.09
13l	Br	CH <sub>3</sub>	C <sub>6</sub> H <sub>5</sub>	0.31±0.1	0.21±0.2
13m	Br	CH <sub>3</sub>	C <sub>6</sub> H <sub>4</sub> (4-CH <sub>3</sub> )	0.06±0.05	0.09±0.05
13n	Br	CH <sub>3</sub>	Cyclohexyl	0.04±0.01	0.07±0.01
13o	CH <sub>3</sub>	CH <sub>3</sub>	Cyclohexyl	1.20±0.6	1.10±0.6
13p	H	CH <sub>3</sub>	Cyclohexyl	2.30±0.8	1.90±0.8
13q	Br	H	Cyclohexyl	0.22±0.1	0.56±0.1
13r	Br	CH <sub>3</sub>	Cyclohexyl	2.01±0.9	1.90±0.7
14a	H	COC <sub>6</sub> H <sub>4</sub> (4-Cl)	H	1.01±0.6	1.03±0.8
14b	CH <sub>3</sub>	COC <sub>6</sub> H <sub>4</sub> (4-Cl)	H	3.46±0.9	0.23±0.1
14c	Br	COC <sub>6</sub> H <sub>4</sub> (4-Cl)	H	0.15±0.1	0.02±0.01
14d	Br	Cyclohexyl	H	2.08±0.8	1.40±0.8
15b	CH <sub>3</sub>	COC <sub>6</sub> H <sub>4</sub> (4-Cl)		2.78±0.9	0.21±0.1
15c	Br	COC <sub>6</sub> H <sub>4</sub> (4-Cl)		0.86±0.4	0.20±0.1
15d	Br	Cyclohexyl		1.63±0.6	0.85±0.4

<sup>a</sup>Data represent mean values (±SD) of three independent determinations. <sup>b</sup>Human breast adenocarcinoma cell line. <sup>c</sup>Human colon carcinoma cell line

We observed that the configuration at the 2' carbon has a notable influence on the cytotoxic activity on this cell line. In fact, (2'*R*,4'*R*) **13g** was 18-fold less potent than its diastereoisomer (2'*S*,4'*R*)-**13f** on HT29 cells and 3-fold less potent on the MCF7 cell line. The introduction of a methyl group at N-1 improved the activity of compounds **13h-j** compared to the non methylated analogues (**13d-f**), especially on the colon cell line. The most potent compound of this subseries, **13j**, gave IC<sub>50</sub> values of 520 and 80 nM in MCF-7 and HT29 cell lines, respectively. Modifications of **13j** at the N-3' position produced different effects: the introduction of 4-Cl-benzoyl group increased (2-fold) the antiproliferative activity of analogue **13k** on MCF-7 cells and reduced (4-fold) its activity on HT29 cells. A similar behavior was observed with compound **13l**, which contains a phenyl group at the N-3' position. The introduction of a 4-CH<sub>3</sub>-phenyl or a cyclohexyl group led to compounds **13m** and **13n**, which showed an antiproliferative activity in the nanomolar range (IC<sub>50</sub> < 100 nM, for both cell lines). In particular, **13n** was 14-fold more potent than its analogue **13j** on MCF-7 cells. Further modifications of this compound involving substitution or loss of the bromine atom at the C5 (compounds **13o** and **13p**), lack of the CH<sub>3</sub> group at N1 (compound **13q**), and ethyl ester hydrolysis to carboxylic acid (**13r**) all resulted in a loss of activity in the resulting compounds. These derivatives were less potent than **13n** against MCF-7 (from 5- to 60-fold) and HT29 (from 8- to 28-fold) cell lines. Furthermore, switching the 4-Cl-benzoyl or cyclohexylcarbonyl groups from position N3' to position N1 led to contrasting results. 4-chlorobenzoyl derivative **14c** showed cytotoxic activity in the nanomolar range on both cell lines (IC<sub>50</sub> of 150 and 20 nM) and was ~6-fold more potent than its regioisomer **13f**. Derivative **14a** was also 2- to 3-fold more potent than its regioisomer **13d**, while compound **14b** containing a CH<sub>3</sub> group at C-5 position showed a slight decrease of activity on MCF-7 cells compared to its analogue **13e**. In contrast compound **14b** was 4-fold more potent than **13e**

against HT29 cells. Surprisingly, the same change of the position for cyclohexyl carbonyl group (**13q** versus **14d**) led to a considerable decrease in activity. In fact, **14d** was 10-fold less potent than its regioisomer **13q** on MCF-7 cells. Finally, the presence of a more planar thiazoline ring in the structure produced different effects: derivative **15b** retained the cytotoxic activity of its thiazolidine analogue **14b**, while compound **15c** was 6- and 10-fold less active than **14c** on both cell lines. In contrast, compound **15d** showed a slight increase of activity (~1.5-fold) on both cell lines compared to **14d**. Considering the interesting data of cytotoxicity for the most active compound, **13n** or **SM13**, was also analyzed against a panel of human tumor cell lines, including PC3 (prostate), U937 (leukemia), Calu (lung), HEPG2 (liver), and C643 (anaplastic thyroid) human cell lines (Table 2). Doxorubicin and nutlin-3 were used as reference cytotoxic agents. Data on the MCF-7 cell line are also reported in Table 2. In all tested cell lines, **SM13** showed marked cytotoxic potency with IC<sub>50</sub> in the range 0.07-0.55 μM, while nutlin-3 was much less effective in our panel, in accordance with some data found in the literature.<sup>119</sup> **SM13** was 18-fold more potent than doxorubicin on the Calu cell line and was equipotent to doxorubicin in PC3 and U937 cell lines. Table 2 also shows that **SM13** inhibited the cellular growth of a human gingival fibroblast (HGF) normal cell line at low micromolar concentration. This cytotoxicity was similar to that shown by nutlin-3 on the same line and was 4 times less than that caused by doxorubicin. These data seem to indicate that **SM13** has a good profile of cell selectivity.<sup>100</sup>

**Table 2.** Antiproliferative activity of 13n (SM13) on multiple human tumor cell lines and one normal cell line

Origin tumor	Cell line	SM13 (13n)	IC <sub>50</sub> (μM±SD) <sup>a</sup>	
			Nutlin-3	Dox
Breast	MCF-7	0.04±0.01	2.9±0.31	0.02±0.01
Prostate	PC3	0.41±0.21	30.3±1.90	0.75±0.10
Leukemia	U937	0.07±0.01	15.6±1.90	0.12±0.03
Lung	Calu	0.10±0.06	27.2±0.30	1.81±0.33
Liver	HEPG2	0.14±0.06	10.2±0.10	0.08±0.01
Anaplastic thyroid	C643	0.55±0.08	23±1.20	0.07±0.01
<b>Origin normal</b>				
Human gingival fibroblast	HGF	1.60±0.15	1.40±0.36	0.50±0.15

<sup>a</sup>Data represent mean values (±SD) of three independent determinations at 24 h

### 3.3.2 Modulation of p53-MDM2 interaction *in vitro*

To test the effective ability of **SM13** to inhibit p53–MDM2 interaction, we performed an *in vitro* binding assay using ImmunoSet p53/MDM2 complex ELISA (Figure 20). Nutlin-3 and compound 3 were also evaluated as references. In this assay and for all compounds, the minimum effective concentration was determined at 5 μM. At this concentration, the percentage inhibition was 19% for nutlin-3 and 25% for 3, while compound **SM13** has proved to be more effective inhibiting 30% of p53MDM2 interaction.<sup>100</sup>

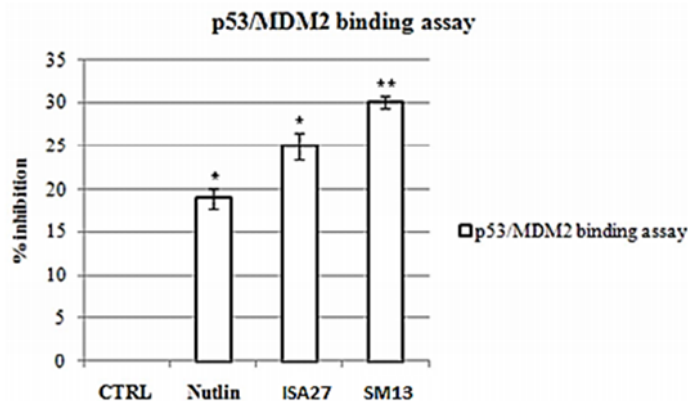


**Figure 20.** Binding assay using ImmunoSet<sup>TM</sup> p53/MDM2 complex ELISA set. Data was presented as % of inhibition referred to control (only standards) using 5  $\mu$ M of Nutlin-3, ISA27 and SM13

### 3.3.3 Modulation of p53-MDM2 interaction in cell

In order to confirm the ability of **SM13** to inhibit the MDM2-p53 interaction in cell, the expression levels of these two proteins were evaluated by western blot after 24, 48, and 72h of **SM13** treatment and after 24h with nutlin-3. Compound concentrations close to their IC<sub>50</sub> on the MCF-7 cell line were used in this assay (i.e. 50 nM for **SM13** and 3  $\mu$ M for nutlin-3). In these conditions, **SM13** induced the accumulation of p53 and MDM2 proteins, (Figure 21A, 21B). To determine whether **SM13** was able to prevent MDM2-p53 interaction, p53 expression levels were measured after MDM2 immunoprecipitation (Figure 21C, 21D). Cells were treated with **SM13** for 24, 48, and 7h or with nutlin-3 for 24 h, MDM2 was immunoprecipitated. The samples underwent western blot to visualize p53 and to evaluate its association with MDM2.

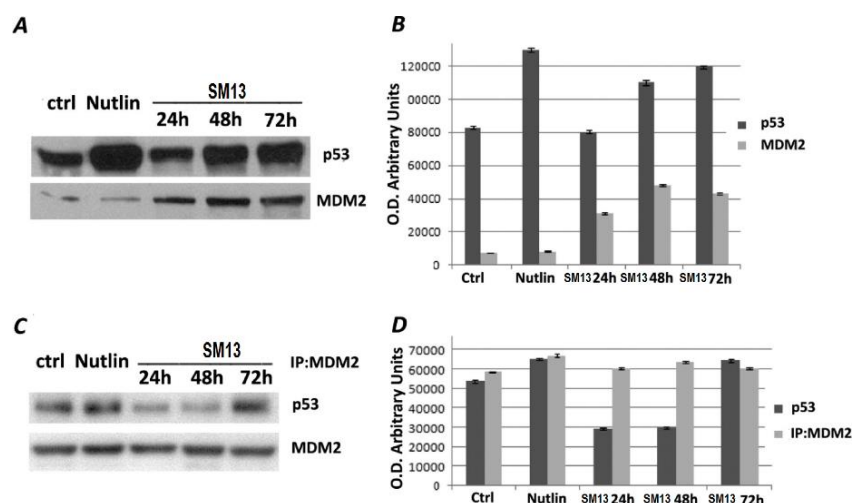


**Figure 21.** (A) MCF-7 cells were treated with 50 nM SM13 for 24, 48, and 72 h or 3  $\mu$ M nutlin-3 for 24 h. Total cell lysates were analyzed by Western blotting for p53 and MDM2 with specific antibodies. (C) A similar experiment was performed for p53 after MDM2 immunoprecipitation. (B, D) Immunoblots were quantified by ImageQuant densitometric analysis. Protein expression levels were measured in arbitrary densitometric units, and data show the mean values  $\pm$  SEM calculated from relative protein expression levels determined in three separate experiments

Treatment with **SM13** reduced the MDM2-p53 interaction as evidenced by a significant decrease in the p53 levels bound to MDM2 at 24 and 48 h. Nutlin-3 seems to be inactive in this immunoprecipitation assay. We can hypothesize that nutlin acts more quickly than **SM13**; its unresponsiveness to the test may be due to a recombination of p53 and MDM2 within 24 h. Interestingly, this recombination is also observed for **SM13** after 72 h.<sup>100</sup>

### 3.3.4 Cell-cycle progression

To investigate the effect in the reduction of tumor cell survival mediated by **SM13**, MCF-7 cell cycle was analyzed after 24, 48, and 72 h of treatment; again, nutlin-3 was used for comparison. Nutlin-3 (3  $\mu$ M) induced cell cycle arrest, as shown by G0/G1 phase block and in accordance with literature data.<sup>94</sup> **SM13**

(50 nM) did not significantly affect cell cycle. Indeed, **SM13** treated cells showed the same distribution in G1, S, and G2/M phases of untreated cell at 24, 48, and 72 h (Figure 22A, 22B, and 22C). When the same experiment was performed with increasing concentration of **SM13** (500 nM, 1  $\mu$ M, 5  $\mu$ M), no difference in cell cycle effect was found compared to initial concentration (Figure 22D).<sup>100</sup>

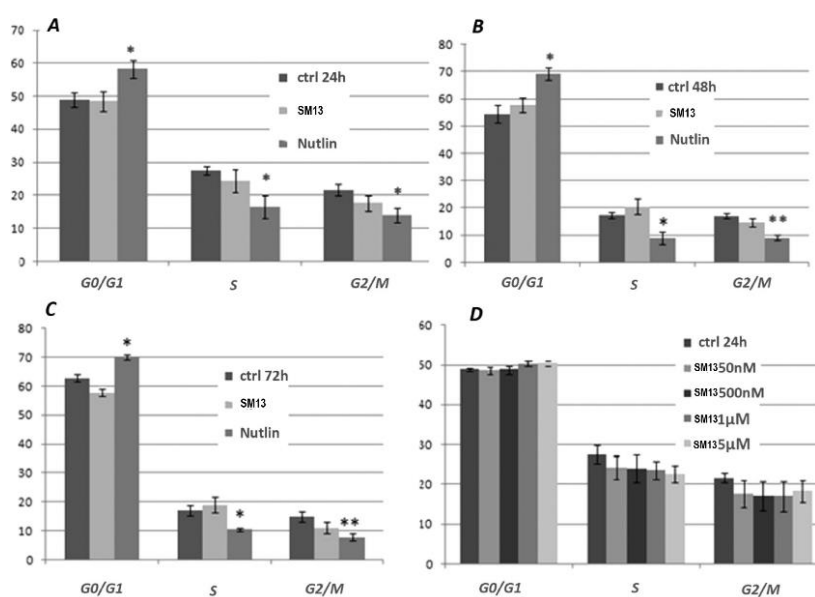


**Figure 22.** Effects of SM13 on cell cycle progression analyzed for DNA content by FACS in breast cancer MCF-7 cells untreated or treated with 50 nM of SM13 or 3  $\mu$ M nutlin-3 at (A) 24, (B) 48, and (C) 72 h and (D) MCF-7 cells untreated or treated with 50, 500, 1000, and 5000 nM 4h at 24 h. The distribution and percentage of cells in G1, S, and G2/M phases of the cell cycle are indicated. Data points are mean values  $\pm$  SEM. Significance is assumed at (\*)  $p < 0.05$ , (\*\*)  $0.01 < p < 0.05$ , (\*\*\*)  $p < 0.01$

### 3.3.5 Apoptotic cell-death

To study if the mechanism of cell death induced by **SM13** influence apoptosis, cell death with preliminary, qualitative assessment of apoptosis by subG1 analysis was evaluated. The treatment with **SM13** (50 nM) showed a strong

increase of the subG1 peak, which rose in a time dependent manner (Figure 23). Nutlin-3 (3  $\mu$ M) also induced a significant increase of cell death.

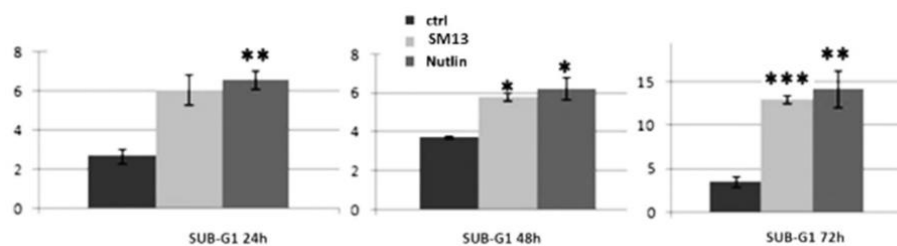


**Figure 23.** Representative subG1 populations calculated from FACS histograms. MCF-7 cells were incubated with 50 nM 4n or with 3  $\mu$ M nutlin3 for 24, 48, and 72 h. Data are expressed as the percentage of subG1 cells

However, the subG1 peak may consist of apoptotic and necrotic cells. To discriminate between the two possibilities, an annexin V binding assay was performed. **SM13** and nutlin-3 induced a significant increase of cell fraction in early apoptosis (Figure 24). In particular, the apoptotic cell percentage increased from 4% of untreated cells to 10% and 12% of cells after 48 and 72 h of **SM13** treatment. Nutlin-3 determined a lower increase of early apoptosis compared to **SM13**.

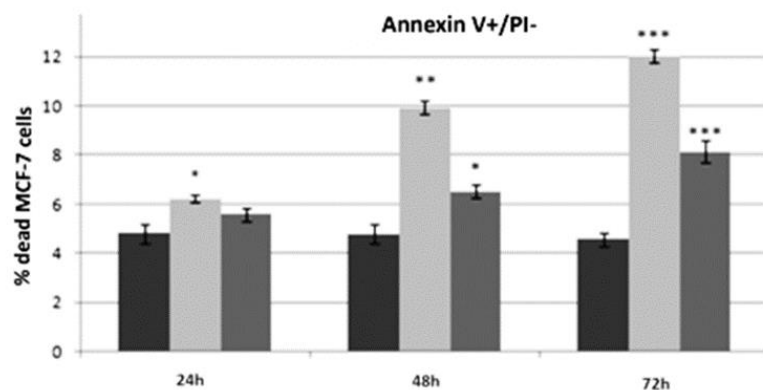


**Figure 24.** The cells were analyzed by FACS for the occurrence of apoptosis (FITC-annexin binding). Values represent the mean  $\pm$  SEM. Significance is assumed at (\*)  $p < 0.05$ , (\*\*)  $0.01 < p < 0.05$ , (\*\*\*)  $p < 0.01$

So it has been evidenced that, although p53 plays a pivotal role in regulating cell cycle and apoptosis, treatment of MCF-7 cells with **SM13** or nutlin-3 has a different impact on both mechanisms. Indeed, whereas nutlin-3 determined a cell cycle arrest, **SM13** induced apoptotic cell death. To investigate the cell death mechanism induced by **SM13**, the p53 dependent apoptotic pathway was analyzed by Western blot. The analysis of the expression levels of p53 and p53 transcriptional targets, such as p21 and p27, showed a progressive increase of these proteins during the treatment with **SM13** in a time dependent manner (Figure 25). However, these increases do not seem to be sufficient to induce cell cycle arrest. On the contrary, nutlin-3 showed a greater accumulation of p21 than 4n at 24, 48, and 72 h, inducing cell cycle arrest (Figure 25A and 25B). The cells committed to die via p53 dependent apoptosis typically follow the mitochondrial pathway, although p53 can also modulate cell death through death receptors. p53 has been reported to trigger apoptosis by modulation of gene transcription of Bcl-2 family members and by physical interaction with these proteins.

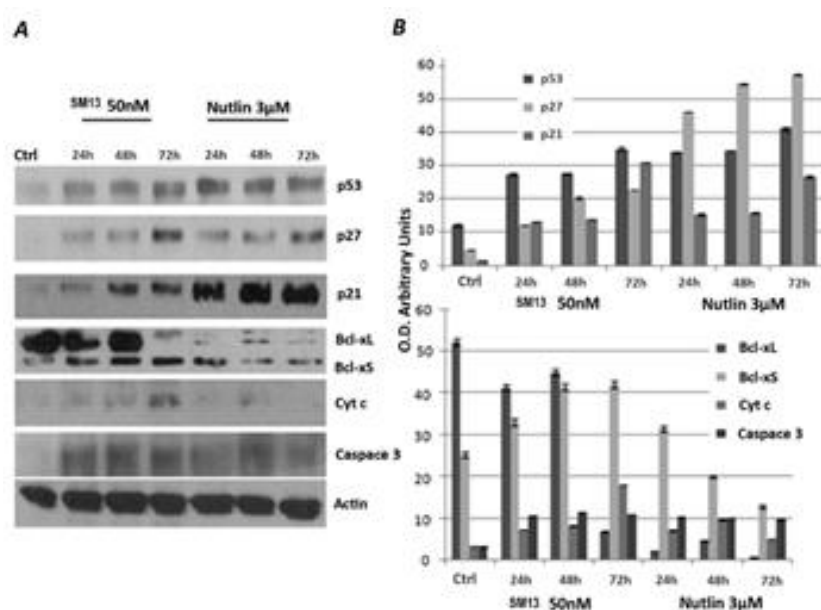


**Figure 25.** (A) MCF-7 cells were treated with 50 nM SM13 or 3 µM nutlin for the indicated time intervals. Total cell lysates were analyzed by Western blotting for phosphotyrosine p53, p21, p27, Bcl-xL/S, cytochrome c, and caspase-3 with specific antibodies. (B) Immunoblots were quantified by ImageQuant densitometric analysis. Protein expression levels were measured in arbitrary densitometric units, and data show the mean values  $\pm$  SEM calculated from relative protein expression levels determined in three separate experiments: (\*)  $p < 0.05$  vs protein expression levels in untreated control cells.

Western blot results indicated that **SM13** and nutlin regulate Bcl-2 members, reducing the antiapoptotic Bcl-xL protein and increasing the pro apoptotic Bcl-xS protein, although the two drugs affect BclxL/S expression at different times. The induction of 4n-mediated apoptosis was confirmed by the release of cytochrome c from mitochondria to the cytosol, which increased at various time intervals and became particularly evident at 72 h of drug treatment. Also nutlin-3 affects cytochrome c release at 48 h even if at lower levels compared to **SM13**. One of the final effectors of the apoptotic process is caspase-3, which is activated by extrinsic and intrinsic or mitochondrial pathways. The cleavage of caspase-3 is a clear indicator of apoptosis; hence, we analyzed the p53 fragment with a specific antibody. Western blot analysis revealed that both **SM13** and

nutlin-3 induced an accumulation of the cleavage product of caspase-3. All these findings suggest that in the MCF-7 breast cancer cell line, cell cycle arrest is the main molecular mechanism mediated by nutlin-3. On the contrary, 50 nM of **SM13** did not block cell cycle progression but rather it induced apoptosis.<sup>100</sup>

### **3.4 Molecular modeling studies**

To study the exact binding mode and to better rationalize the reasons behind the activity of our indoline-3,2'-thiazolidines, in the Department of Pharmacy of the University of Naples "Federico II", molecular docking studies were carried on **SM13** which is the most potent antiproliferative agent in this series (Figure 26). In particular, in the binding pose predicted for **SM13** the ligand is inserted into the MDM2 binding site so that the 3-cyclohexylcarboxylic substituent is buried in the so-called Trp23 pocket, making favorable van der Waals contacts with Ile61, Val75, Phe86, Phe91, and Ile99 side chains. On the other hand, the MDM2 Phe19 subpocket is occupied by the ligand ethyl ester chain that is able to make direct contacts with Ile61 and Met62 side chains. The presence of this interaction could partially explain why hydrolysis of the ethyl ester chain to the corresponding carboxylic acid results in the loss of activity [Table 1; Paragraph 3.3.1].

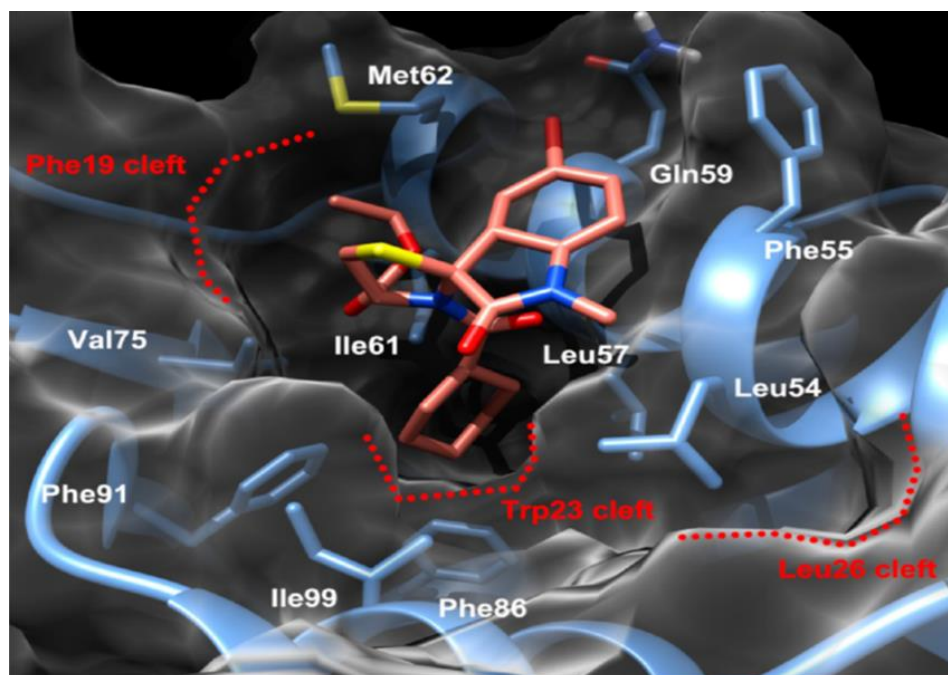


**Figure 26.** Predicted binding mode for SM13 in the MDM2 binding site. The ligand is represented as pink stick, while the protein is represented as blue sticks and ribbons and transparent white surface.

On the other hand, reduction of membrane penetration cannot be ruled out. Interestingly, the Leu26 cleft does not seem to be completely filled by the 5-bromo-2-oxindole nucleus that instead forms additional hydrophobic interactions with Leu54 through its N-1methyl substituent. This latter hydrophobic interaction could explain why **13d–f** are generally less active than their methylated analogues **13h–j**. In this position, *edge–face*  $\pi–\pi$  interaction with the Phe55 residue is also established in a shallow and rather lipophilic portion of the MDM2 protein in which the 5-bromine atom fills the crevice between Phe55, Met62, and Gln59. Indeed, the interaction with the Phe55 residue has already been detected through X-ray studies for other structurally unrelated ligands in a very recent work by Olson’s group.<sup>120</sup> Interestingly, the ligand N3’-COC<sub>6</sub>H<sub>11</sub> amide bond adopts a *cis* configuration as already suggested by ROESY experiments.<sup>100</sup> [Figure 19]

**CHAPTER IV**  
**EXPERIMENTAL SECTION FOR SERIES 1 AND 2**

#### 4.1 Chemistry

Reagents, starting materials, and solvents were purchased from commercial suppliers and used as received. Analytical TLC was performed on plates coated with a 0.25 mm layer of silica gel 60 F254 Merck and preparative TLC on 20 cm × 20 cm glass plates coated with a 0.5 mm layer of silica gel PF254 Merck. Silica gel 60 (300-400 mesh, Merck) was used for flash chromatography. Melting points were determined by a Kofler apparatus and are uncorrected. Optical rotations were measured on an Atago Polax 2-L polarimeter. <sup>1</sup>H NMR and <sup>13</sup>C NMR spectra were recorded with a Varian-400 spectrometer, operating at 400 and 100 MHz, respectively. Chemical shifts are reported in δ values (ppm) relative to internal Me<sub>4</sub>Si, and J values are reported in hertz (Hz). ROESY experiment was recorded at 25°C in the phase-sensitive mode using the method from States. Data block sizes were 2048 addresses in t<sub>2</sub> and 512 equidistant t<sub>1</sub> values. Before Fourier transformation, the time domain data matrices were multiplied by shifted sin 2 functions in both dimensions. A mixing time of 500 ms was used. ESIMS experiments were performed on an AppliedBiosystem API 2000 triple-quadrupole spectrometer. Starting spiro(oxindolethiazolidine) ethyl ester derivatives (7-12) were synthesized as described in refs 100 and 102. As an example, here we described the synthesis of (3*RS*,4'*R*)-ethyl 5-bromo-1-methyl-2-oxospiro[indoline-3,2'-thiazolidine]-4'-carboxylate (12). Combustion microanalyses were performed on a Carlo Erba CNH 1106 analyzer, and all reported values are within 0.4% of calculated values. These elemental analyses confirmed >95% purity.

#### ***Synthesis of (3*RS*,4'*R*) -Ethyl 5-Bromo-1-methyl-2-oxospiro[indoline-3,2'-thiazolidine]-4'-carboxylate. (12)***

NaHCO<sub>3</sub> (1.0 g, 12 mmol) and 5-bromo-1-methyl isatin (6, 2.4 g, 10 mmol) were added to a solution of *L*-Cys-OEt (2.3 g, 12 mmol) in ethanol (100 mL), and the suspension was stirred at room temperature for 12 h. Then the suspension was

filtered, and the filtrate was concentrated. Spiro(oxindolethiazolidine) ethyl ester residue was dissolved in DCM and washed with water (3 × 50 mL). The combined organic layer was dried over anhydrous sodium sulfate, filtered, and concentrated. A 5:1 diastereoisomeric mixture of the title's compound was obtained as an oil with 73% yield.

<sup>1</sup>H NMR (400 MHz, CDCl<sub>3</sub>) δ 1.36 (3H, m, CH<sub>3</sub>), 3.10 and 3.12 (3H, s, CH<sub>3</sub>), 3.31 and 3.43 (1H, m, H-5'a), 3.71 and 3.93 (1H, m, H-5'b), 4.25 (4H, m, CH<sub>2</sub>), 4.46 and 4.66 (2H, m, H-4'), 6.69 and 6.75 (1H, d, J = 8.0 Hz, H-7), 7.48 (1H, d, H-6), 7.60 and 7.71 (1H, s, H-4'). The compound was used in the next reaction without further purification.

***General Procedure for the Synthesis of the (2'R or 2'S,4'R) - Ethyl 3'-Substituted-2-Oxospiro[indoline-3,2'-thiazolidine] 4'-carboxylate Derivatives. (13a-q)***

To a solution of (2'R,4'R)- and (2'S,4'R)-ethyl 2-oxospiro[indoline-3,2'-thiazolidine]-4'-carboxylate derivatives (7-12, 200 mg, 5 mmol) in dry THF (50 mL) was added a solution of corresponding 4-chlorobenzoyl or 4-methylbenzoyl or 4-chlorophenylacetyl or cyclohexanecarbonyl chlorides (5.5 mmol) in THF (10 mL) and TEA (10 mmol). The reaction mixture was stirred at room temperature for 2 h, and water was then added. The organic solution was washed with water (3 × 100 mL), dried over Na<sub>2</sub>SO<sub>4</sub>, and evaporated in vacuo. Flash chromatography on silica gel, using ethyl acetate/n-hexane as eluent, overall yielded the corresponding final derivatives as oil.

***(2'S,4'R)-Ethyl 3'-(2-(4-Chlorophenylacetyl)-2-oxospiro-[indoline-3,2'-thiazolidine]-4'-carboxylate. (13a)***

Overall yield 43%. [ $\alpha$ ]<sub>D</sub><sup>25</sup> -7.1° (c 0.1, MeOH). <sup>1</sup>H NMR (400 MHz, CDCl<sub>3</sub>) δ 1.40 (t, 3H, CH<sub>3</sub>); 3.44 (d, 1H, J = 12.0 Hz, H-5'a); 3.63 (s, 2H, CH<sub>2</sub>); 3.95 (dd, 1H, J = 6.0 and 11.6 Hz, H-5'b); 4.39 (q, 2H, CH 5.08 (d, 1H, J = 6.0, H-4');

6.76 (d, 1H,  $J = 8.4$  Hz, H-7); 7.04 (t, 1H, H-6); 7.15 (d, 2H,  $J = 8.0$  Hz, aryl); 7.24 (t, 1H,  $J = 7.9$  Hz, H-5); 7.28 (d, 2H, aryl); 7.43 (s, 1H, NH); 7.47 (d, 1H, H-4).  $^{13}\text{C}$  NMR (100 MHz,  $\text{CDCl}_3$ )  $\delta$  14.5 ( $\text{CH}_3$ ), 34.6 (C-5'), 41.4 ( $\text{CH}_2$ ), 62.5 (CH), 64.3 (C-4'), 73.9 (C-2'), 109.3, 115.8, 123.5, 128.0, 128.9, 130.2, 134.4, 136.2, and 143.1 (aryl), 170.1, 173.9, and 178.0 (C=O). ESIMS  $m/z$  calcd for  $\text{C}_{21}\text{H}_{19}\text{ClN}_2\text{O}_4\text{S}$ , 430.08; found 430.16.

***(2'S,4'R)-ethyl-5-methyl-3'-(2-(4-chlorophenyl)acetyl)-2-oxospiro[indoline-3,2'-thiazolidine]-4'-carboxylate. (13b)***

Overall yield 39%.  $[\alpha]_{\text{D}}^{25} -13.6^\circ$  ( $c$  0.25, MeOH).  $^1\text{H}$  NMR (400 MHz,  $\text{CDCl}_3$ )  $\delta$  1.42 (t, 3H,  $\text{CH}_3$ ); 2.04 (s, 3H,  $\text{CH}_3$ ); 3.37 (d, 1H,  $J = 12.4$  Hz, H-5'a); 3.61 (s, 2H,  $\text{CH}_2$ ); 3.98 (dd, 1H,  $J = 6.0$  and 11.6 Hz, H-5'b); 4.43 (q, 2H,  $\text{CH}_2$ ); 5.04 (d, 1H,  $J = 6.0$ , H-4'); 6.70 (d, 1H,  $J = 8.0$  Hz, H-7); 7.08 (d, 1H, H-6); 7.19 (d, 2H,  $J = 8.0$  Hz, aryl); 7.31 (d, 2H, aryl); 7.40 (s, 1H, H-4); 7.79 (s, 1H, NH).  $^{13}\text{C}$  NMR (100 MHz,  $\text{CDCl}_3$ )  $\delta$  14.2 ( $\text{CH}_3$ ), 21.7 ( $\text{CH}_3$ ), 34.8 (C-5'), 41.6 ( $\text{CH}_2$ ), 62.3 ( $\text{CH}_2$ ), 64.7 (C-4'), 74.2 (C-2'), 109.8, 123.2, 128.5, 129.6, 130.7, 133.0, 137.4, and 142.8 (aryl), 170.6, 173.4, and 178.3 (C=O). ESIMS  $m/z$  calcd for  $\text{C}_{22}\text{H}_{21}\text{ClN}_2\text{O}_4\text{S}$ , 444.09; found 444.15.

***(2'S,4'R)-ethyl-5-bromo-3'-(2-(4-chlorophenyl)acetyl)-2-oxospiro[indoline-3,2'-thiazolidine]-4'-carboxylate. (13c)***

Overall yield 37%.  $[\alpha]_{\text{D}}^{25} -29.1^\circ$  ( $c$  0.4, MeOH).  $^1\text{H}$  NMR (400 MHz,  $\text{CDCl}_3$ )  $\delta$  1.43 (t, 3H,  $\text{CH}_3$ ); 3.42 (d, 1H,  $J = 12.6$  Hz, H-5'a); 3.65 (s, 2H,  $\text{CH}_2$ ); 4.01 (dd, 1H,  $J = 6.0$  and 12.0 Hz, H-5'b); 4.45 (q, 2H,  $\text{CH}_2$ ); 5.00 (d, 1H,  $J = 6.0$ , H-4'); 6.73 (d, 1H,  $J = 7.6$  Hz, H-7); 7.23 (d, 2H,  $J = 8.0$  Hz, aryl); 7.31 (d, 2H, aryl); 7.48 (d, 1H, H-6); 7.95 (s, 1H, H-4); 8.04 (s, 1H, NH).  $^{13}\text{C}$  NMR (100 MHz,  $\text{CDCl}_3$ )  $\delta$  14.3 ( $\text{CH}_3$ ), 21.9 ( $\text{CH}_3$ ), 34.6 (C-5'), 41.5 ( $\text{CH}_2$ ), 62.4 ( $\text{CH}_2$ ), 64.9 (C-4'), 74.4 (C-2'), 109.5, 116.2, 123.4, 128.2, 129.0, 131.1, 132.5, 133.3, 137.2,

and 143.2 (aryl), 170.2, 173.5, and 178.9 (C=O). ESIMS m/z calcd for C<sub>21</sub>H<sub>18</sub>BrClN<sub>2</sub>O<sub>4</sub>S, 507.99; found 508.04.

**(2'S, 4'R)-ethyl 3'-(4-chlorobenzoyl)-2-oxospiro[indoline-3,2'-thiazolidine]-4'-carboxylate. (13d)**

Overall yield 49%. [ $\alpha$ ]<sub>D</sub><sup>25</sup> -16.3° (c 0.1, MeOH). <sup>1</sup>H NMR (400 MHz, CDCl<sub>3</sub>)  $\delta$  1.36 (t, 3H, CH<sub>3</sub>); 3.40 (d, 1H, J = 11.6 Hz, H-5'a); 3.95 (dd, 1H, J = 6.0 and 11.6 Hz, H-5'b); 4.38 (q, 2H, CH<sub>2</sub>); 4.87 (d, 1H, J = 6.0 Hz, H-4'); 6.77 (d, 1H, J = 8.0 Hz, H-7); 7.05 (t, 1H, J = 7.6 Hz, H-6); 7.20 (t, 1H, H-5); 7.33 (d, 2H, aryl, J = 7.6 Hz); 7.44 (d, 2H, aryl); 7.73 (d, 1H, H-4); 8.54 (s, 1H, NH). <sup>13</sup>C NMR (100 MHz, CDCl<sub>3</sub>)  $\delta$  14.5 (CH<sub>3</sub>), 34.5 (C-5'), 62.8 (CH<sub>2</sub>), 66.8 (C-4'), 72.4 (C-2'), 110.7, 123.2, 125.5, 126.3, 128.4, 129.0, 130.3, 134.3, 137.1, and 141.2 (aryl), 168.4, 170.6, and 177.1 (C=O). ESIMS m/z calcd for C<sub>20</sub>H<sub>17</sub>ClN<sub>2</sub>O<sub>4</sub>S, 416.06; found, 416.14.

**(2'S,4'R)-ethyl 3'-(4-chlorobenzoyl)-5-methyl-2-oxospiro[indoline-3,2'-thiazolidine]-4'-carboxylate. (13e)**

Overall yield 58%. [ $\alpha$ ]<sub>D</sub><sup>25</sup> -5.7° (c 0.1, MeOH). <sup>1</sup>H NMR (400 MHz, CDCl<sub>3</sub>)  $\delta$  1.38 (t, 3H, CH<sub>3</sub>); 2.34 (s, 3H, CH<sub>3</sub>); 3.34 (d, 1H, J = 11.6 Hz, H-5'a); 3.98 (dd, 1H, J = 6.0 and 11.6 Hz, H-5'b); 4.38 (q, 2H, CH<sub>2</sub>); 4.85 (d, 1H, J = 6.0 Hz, H-4'); 6.72 (d, 1H, J = 8.0 Hz, H-7); 7.03 (d, 1H, H-6); 7.33 (d, 2H, J = 8.0 Hz, aryl); 7.44 (d, 2H, aryl); 7.54 (s, 1H, H-4); 8.06 (s, 1H, NH). <sup>13</sup>C NMR (100 MHz, CDCl<sub>3</sub>)  $\delta$ : 14.5 (CH<sub>3</sub>), 21.5 (CH<sub>3</sub>), 34.5 (C-5'), 62.7 (CH<sub>2</sub>), 66.7 (C-4'), 72.5 (C-2'), 110.2, 126.1, 128.4, 129.0, 130.8, 133.6, 136.2, and 138.4 (aryl), 167.6, 170.1, and 176.2 (C=O). ESIMS m/z calcd for. per C<sub>21</sub>H<sub>19</sub>ClN<sub>2</sub>O<sub>4</sub>S, 430.08; found, 430.08.

**(2'S,4'R)-ethyl 5-bromo-3'-(4-chlorobenzoyl)-2-oxospiro[indoline-3,2'-thiazolidine]-4'-carboxylate. (13f)**

Overall yield 46%.  $[\alpha]_{\text{D}}^{25}$  -9.8° (*c* 0.24, MeOH).  $^1\text{H}$  NMR (400 MHz,  $\text{CDCl}_3$ )  $\delta$  1.40 (t, 3H,  $\text{CH}_3$ ); 3.35 (d, 1H,  $J = 12.0$  Hz, H-5'a); 3.89 (dd, 1H,  $J = 6.0$  and 11.8 Hz, H-5'b); 4.42 (q, 2H,  $\text{CH}_2$ ); 4.84 (d, 1H,  $J = 6.0$  Hz, H-4'); 7.36-7.50 (m, 5H, H-7, aryl); 7.78-7.81 (m, 2H, H-6, H-4); 8.04 (s, 1H, NH).  $^{13}\text{C}$  NMR (100 MHz,  $\text{CDCl}_3$ )  $\delta$  14.5 ( $\text{CH}_3$ ), 35.3 (C-5'), 63.1 ( $\text{CH}_2$ ), 66.7 (C-4'), 72.3 (C-2'), 116.8, 118.8, 128.4, 128.6, 128.7, 129.2, 131.2, 139.3, and 140.9 (aryl), 168.7, 170.1, and 173.6 (C=O). ESIMS *m/z* calcd for. per  $\text{C}_{20}\text{H}_{16}\text{BrClN}_2\text{O}_4\text{S}$ , 493.97; found, 494.09.

**(2'R,4'R)-ethyl 5-bromo-3'-(4-chlorobenzoyl)-2-oxospiro[indoline-3,2'-thiazolidine]-4'-carboxylate. (13g)**

Overall yield 15%.  $[\alpha]_{\text{D}}^{25}$  -6.9° (*c* 0.11, MeOH).  $^1\text{H}$  NMR (400 MHz,  $\text{CDCl}_3$ )  $\delta$  1.24 (t, 3H,  $\text{CH}_3$ ); 3.61-3.62 (m, 2H, H-5'a, H-5'b); 4.25 (q, 2H,  $\text{CH}_2$ ); 5.43 (t, 1H,  $J = 9.6$  Hz, H-4'); 7.45 (d, 2H,  $J = 8.4$  Hz, aryl); 7.61 (d, 1H,  $J = 9.2$  Hz, H-7); 7.79 (s, 1H, H-4); 8.05 (d, 2H, aryl); 8.90 (d, 1H, H-6); 9.51 (s, 1H, NH).  $^{13}\text{C}$  NMR (100 MHz,  $\text{CDCl}_3$ )  $\delta$  14.4 ( $\text{CH}_3$ ), 34.0 (C-5'), 62.4 ( $\text{CH}_2$ ), 66.9 (C-2'), 78.8 (C-4'), 115.2, 122.2, 129.1, 129.6, 133.4, 134.7, 135.9, and 138.5 (aryl), 165.4, 170.0, and 172.5 (C=O). ESIMS *m/z* calcd for. per  $\text{C}_{20}\text{H}_{16}\text{BrClN}_2\text{O}_4\text{S}$ , 493.97; found, 494.09.

**(2'S,4'R)-ethyl 3'-(4-chlorobenzoyl)-1-methyl-2-oxospiro[indoline-3,2'-thiazolidine]-4'-carboxylate. (13h)**

Overall yield 56%.  $[\alpha]_{\text{D}}^{25}$  -8.9° (*c* 0.2, MeOH).  $^1\text{H}$  NMR (400 MHz,  $\text{CDCl}_3$ )  $\delta$  1.36 (t, 3H,  $\text{CH}_3$ ); 3.29 (s, 3H,  $\text{CH}_3$ ); 3.38 (d, 1H,  $J = 11.6$  Hz, H-5'a); 3.97 (dd, 1H,  $J = 6.0$  and 11.6 Hz, H-5'b); 4.38 (q, 2H,  $\text{CH}_2$ ); 4.85 (d, 1H,  $J = 5.6$  Hz, H-4'); 6.84 (d, 1H,  $J = 8.0$  Hz, H-7); 7.10 (t, 1H,  $J = 8.0$  Hz, H-6); 7.31-7.38 (m,

3H, H-5, aryl); 7.41 (d, 2H, aryl); 7.76 (d, 1H,  $J = 7.6$  Hz, H-4); 8.51 (s, 1H, NH).  $^{13}\text{C}$  NMR (100 MHz,  $\text{CDCl}_3$ )  $\delta$  14.5 ( $\text{CH}_3$ ), 26.1 ( $\text{CH}_3$ ), 34.5 (C-5'), 62.8 ( $\text{CH}_2$ ), 66.7 (C-4'), 72.5 (C-2'), 108.5, 123.4, 125.2, 128.4, 129.0, 130.4, 134.1, 137.3, and 141.4 (aryl), 168.1, 170.7, and 177.2 (C=O). ESIMS  $m/z$  calcd for  $\text{C}_{21}\text{H}_{19}\text{ClN}_2\text{O}_4\text{S}$ , 430.08; found, 430.08.

***(2'S,4'R)-ethyl 3'-(4-chlorobenzoyl)-1,5-dimethyl-2-oxospiro[indoline-3,2'-thiazolidine]-4'-carboxylate. (13i)***

Overall yield 41%.  $[\alpha]_{\text{D}}^{25} -15.2^\circ$  ( $c$  0.4, MeOH).  $^1\text{H}$  NMR (400 MHz,  $\text{CDCl}_3$ )  $\delta$  1.37 (t, 3H,  $\text{CH}_3$ ); 2.35 (s, 3H,  $\text{CH}_3$ ); 3.33 (d, 1H,  $J = 12.0$  Hz, H-5'a); 3.49 (s, 3H,  $\text{CH}_3$ ); 4.00 (dd, 1H,  $J = 5.8$  and  $12.0$  Hz, H-5'b); 4.38 (q, 2H,  $\text{CH}_2$ ); 4.85 (d, 1H,  $J = 5.8$  Hz, H-4'); 6.76 (d, 1H,  $J = 7.8$  Hz, H-7); 7.12 (d, 1H, H-6); 7.33 (d, 2H,  $J = 7.6$  Hz, aryl); 7.41 (d, 2H, aryl); 7.56 (s, 1H, H-4).  $^{13}\text{C}$  NMR (100 MHz,  $\text{CDCl}_3$ )  $\delta$  14.5 ( $\text{CH}_3$ ), 22.9 ( $\text{CH}_3$ ), 29.8 ( $\text{CH}_3$ ), 34.5 (C-5'), 62.8 ( $\text{CH}_2$ ), 66.7 (C-4'), 72.5 (C-2'), 108.5, 123.4, 125.2, 128.4, 129.0, 130.4, 134.1, 137.3, and 141.4 (aryl), 168.1, 170.7, and 177.2 (C=O). ESIMS  $m/z$  calcd for  $\text{C}_{22}\text{H}_{21}\text{ClN}_2\text{O}_4\text{S}$ , 446.09; found, 446.11.

***(2'S,4'R)-ethyl-5-bromo-3'-(4-chlorobenzoyl)-1-methyl-2-oxospiro[indoline-3,2'-thiazolidine]-4'-carboxylate. (13j)***

Overall yield 54%.  $[\alpha]_{\text{D}}^{25} -21.2^\circ$  ( $c$  0.4, MeOH).  $^1\text{H}$  NMR (400 MHz,  $\text{CDCl}_3$ )  $\delta$  1.48 (t, 3H,  $\text{CH}_3$ ); 3.32 (d, 1H,  $J = 12.4$  Hz, H-5'a); 3.48 (s, 1H,  $\text{CH}_3$ ); 3.94-3.99 (m, 1H, H-5'b); 4.40 (q, 2H,  $\text{CH}_2$ ); 4.87 (d, 1H,  $J = 6.2$  Hz, H-4'); 7.38-7.47 (m, 4H, aryl); 7.52 (d, 1H,  $J = 8.0$  Hz, H-6); 7.79-7.83 (m, 2H, aryl).  $^{13}\text{C}$  NMR (100 MHz,  $\text{CDCl}_3$ )  $\delta$  14.7 ( $\text{CH}_3$ ), 25.1 ( $\text{CH}_3$ ), 35.3 (C-5'), 63.2 ( $\text{CH}_2$ ), 66.7 (C-4'), 72.8 (C-2'), 116.9, 128.7, 128.9, 129.0, 129.1, 131.4, 133.5, 137.9, 139.1 (aryl), 168.5, 169.4, and 175.4 (C=O). ESIMS  $m/z$  calcd for  $\text{C}_{21}\text{H}_{18}\text{BrClN}_2\text{O}_4\text{S}$ , 507.99; found, 508.04.

**(2'S,4'R)-ethyl-5-bromo-3'-(2-(4-chlorophenyl)acetyl)-1-methyl-2 oxospiro [indoline-3,2'-thiazolidine]-4'-carboxylate. (13k)**

Overall yield 38%.  $[\alpha]^{25}_{\text{D}} -26.3^{\circ}$  (*c* 0.4, MeOH).  $^1\text{H}$  NMR (400 MHz,  $\text{CDCl}_3$ )  $\delta$  1.41 (t, 3H,  $\text{CH}_3$ ); 3.20 (s, 3H,  $\text{CH}_3$ ); 3.47 (d, 1H,  $J = 12.0$  Hz, H-5'a); 3.63 (s, 2H,  $\text{CH}_2$ ); 3.94 (dd, 1H,  $J = 6.0$  and 11.6 Hz, H-5'b); 4.38 (q, 2H,  $\text{CH}_2$ ); 5.06 (d, 1H,  $J = 6.0$ , H-4'); 6.66 (d, 1H,  $J = 8.4$  Hz, H-7); 7.10 (d, 2H,  $J = 8.0$  Hz, aryl); 7.27 (d, 2H, aryl); 7.39 (d, 1H, H-6); 7.60 (s, 1H, H-4).  $^{13}\text{C}$  NMR (100 MHz,  $\text{CDCl}_3$ )  $\delta$  14.5 ( $\text{CH}_3$ ), 27.0 ( $\text{CH}_3$ ), 34.1 (C-5'), 41.7 ( $\text{CH}_2$ ), 63.1 ( $\text{CH}_2$ ), 64.5 (C-4'), 75.7 (C-2'), 110.1, 115.8, 127.8, 128.9, 129.2, 130.6, 132.9, 133.1, and 142.8 (aryl), 170.3, 174.3, and 177.8 (C=O). ESIMS *m/z* calcd for  $\text{C}_{22}\text{H}_{20}\text{BrClN}_2\text{O}_4\text{S}$ , 522.00; found 522.06.

**(2'S,4'R)-ethyl- 5-bromo-3'-benzoyl-1-methyl-2- oxospiro [indoline-3,2' thiazolidine]-4'-carboxylate. (13l)**

Overall yield 32%.  $[\alpha]^{25}_{\text{D}} -16.9^{\circ}$  (*c* 0.5, MeOH).  $^1\text{H}$  NMR (400 MHz,  $\text{CDCl}_3$ )  $\delta$  1.45 (t, 3H,  $\text{CH}_3$ ); 3.29(s, 3H,  $\text{CH}_3$ ); 3.36 (d, 1H,  $J = 12.4$  Hz, H-5'a); 3.96-4.01 (m, 1H, H-5'b); 4.37 (q, 2H,  $\text{CH}_2$ ); 4.91 (d, 1H,  $J = 6.2$  Hz, H-4'); 6.73 (d, 1H,  $J = 8.0$  Hz, H-7); 7.38-7.51 (m, 6H, H-6 and aryl); 7.91 (s, 1H, H-4).  $^{13}\text{C}$  NMR (100 MHz,  $\text{CDCl}_3$ )  $\delta$  14.5 ( $\text{CH}_3$ ), 25.6 ( $\text{CH}_3$ ), 35.4 (C-5'), 63.1 ( $\text{CH}_2$ ), 66.9 (C-4'), 73.1 (C-2'), 118.4, 127.5, 127.3, 128.2, 129.4, 133.5, 137.7, 139.2 (aryl), 168.8, 169.6, and 175.0 (C=O). ESIMS *m/z* calcd for  $\text{C}_{20}\text{H}_{17}\text{BrN}_2\text{O}_4\text{S}$ , 460.01; found, 460.09.

**(2'S,4'R)-ethyl-5-bromo-1-methyl-3'-(4-methylbenzoyl)-2-oxospiro[indoline-3,2'-thiazolidine]-4'-carboxylate. (13m)**

Overall yield 37%.  $[\alpha]^{25}_{\text{D}} -14.2^{\circ}$  (*c* 0.3, MeOH).  $^1\text{H}$  NMR (400 MHz,  $\text{CDCl}_3$ )  $\delta$  1.40 (t, 3H,  $\text{CH}_3$ ); 2.35 (s, 3H,  $\text{CH}_3$ ); 3.28 (s, 3H,  $\text{CH}_3$ ); 3.32 (d, 1H,  $J = 11.6$  Hz, H-5'a); 3.95 (dd, 1H,  $J = 6.0$  and 11.6 Hz H-5'b,); 4.39 (q, 2H,  $\text{CH}_2$ ); 4.91

(d, 1H,  $J = 5.6$  Hz, H-4'); 6.71 (d, 1H,  $J = 8.4$  Hz, H-7); 7.14 (d, 2H,  $J = 7.6$  Hz, aryl); 7.34 (d, 2H, aryl); 7.45 (d, 1H, H-6); 7.91 (s, 1H, H-4).  $^{13}\text{C}$  NMR (100 MHz,  $\text{CDCl}_3$ )  $\delta$  14.5 ( $\text{CH}_3$ ), 21.6 ( $\text{CH}_3$ ), 27.0 ( $\text{CH}_2$ ), 34.8 (C-5'), 62.8 ( $\text{CH}_2$ ), 66.8 (C-4'), 72.5 (C-2'), 109.9, 115.9, 126.9, 128.3, 128.4, 129.4, 133.0, 141.3, and 143.0 (aryl), 169.4, 170.6, and 175.2 (C=O). ESIMS  $m/z$  calcd for  $\text{C}_{22}\text{H}_{21}\text{BrN}_2\text{O}_4\text{S}$ , 488.04; found, 488.11.

**(2'S,4'R)-ethyl-5-bromo-3'-(cyclohexanecarbonyl)-1-methyl-2-oxospiro  
[indoline-3,2'-thiazolidine]-4'-carboxylate. (13n)**

Overall yield 49%.  $[\alpha]_{\text{D}}^{25} -37.3^\circ$  ( $c$  0.8, MeOH). **(A)** :  $^1\text{H}$  NMR (400 MHz,  $\text{CDCl}_3$ )  $\delta$  1.15-1.22 (m, 4H,  $\text{CH}_2$ ); 1.41 (t, 3H,  $\text{CH}_3$ ); 1.64-1.78 (m, 6H,  $\text{CH}_2$ ); 2.17 (t, 1H, CH); 3.20 (s, 3H,  $\text{CH}_3$ ); 3.47 (d, 1H,  $J = 12.0$  Hz, H-5'a); 3.97 (dd, 1H,  $J' = 6.0$  and 11.6 Hz, H-5'b); 4.41 (q, 2H,  $\text{CH}_2$ ); 5.13 (d, 1H,  $J = 5.6$  Hz, H-4'); 6.67 (d, 1H,  $J = 8.4$  Hz, H-7); 7.39 (d, 1H, H-6); 7.57 (s, 1H, H-4).  $^{13}\text{C}$  NMR (100 MHz,  $\text{CDCl}_3$ )  $\delta$  14.4 ( $\text{CH}_3$ ), 25.8 ( $\text{CH}_2$ ), 26.7 ( $\text{CH}_3$ ), 30.2 ( $\text{CH}_2$ ), 34.1 (C-5'), 44.1 (CH), 62.9 ( $\text{CH}_2$ ), 64.1 (C-4'), 75.7 (C-2'), 110.0, 115.8, 127.6, 128.9, and 132.7 (aryl); 170.3, 174.3, and 177.8 (C=O); **(B)** :  $^1\text{H}$  NMR (400 MHz,  $\text{CDCl}_3$ )  $\delta$  1.15-1.22 (m, 4H,  $\text{CH}_2$ ); 1.41 (t, 3H,  $\text{CH}_3$ ); 1.64-1.78 (m, 6H,  $\text{CH}_2$ ); 2.17 (t, 1H, CH); 3.26 (s, 3H,  $\text{CH}_3$ ); 3.34 (d, 1H,  $J = 12.0$  Hz, H-5'a); 3.92 (dd, 1H,  $J' = 6.0$  and 11.6 Hz, H-5'b); 4.37 (q, 2H,  $\text{CH}_2$ ); 5.52 (d, 1H,  $J = 5.2$  Hz, H-4'); 6.77 (d, 1H,  $J = 8.4$  Hz, H-7); 7.49 (d, 1H, H-6); 7.56 (s, 1H, H-4).  $^{13}\text{C}$  NMR (100 MHz,  $\text{CDCl}_3$ )  $\delta$  14.4 ( $\text{CH}_3$ ), 25.8 ( $\text{CH}_2$ ), 26.9 ( $\text{CH}_3$ ), 29.3 ( $\text{CH}_2$ ), 33.9 (C-5'), 43.8 (CH), 62.2 ( $\text{CH}_2$ ), 64.7 (C-4'), 75.7 (C-2'), 110.2, 115.9, 127.9, 129.0, and 132.7 (aryl); 170.1, 174.5, and 177.6 (C=O). ESIMS  $m/z$  calcd for  $\text{C}_{21}\text{H}_{25}\text{BrN}_2\text{O}_4\text{S}$ , 480.07; found, 480.15.

**(2'S,4'R)-ethyl-5-methyl-3'-(cyclohexanecarbonyl)-1-methyl-2 oxospiro  
[indoline-3,2'-thiazolidine]-4'-carboxylate. (13o)**

Overall yield 47%.  $[\alpha]_{\text{D}}^{25}$  -23.1° (c 0.5, MeOH). (A):  $^1\text{H}$  NMR (400 MHz,  $\text{CDCl}_3$ )  $\delta$  1.15-1.26 (m, 4H,  $\text{CH}_2$ ); 1.40 (t, 3H,  $\text{CH}_3$ ); 1.63-1.73 (m, 6H,  $\text{CH}_2$ ); 2.17 (t, 1H, CH); 2.30 (s, 3H,  $\text{CH}_3$ ); 3.21 (s, 3H,  $\text{CH}_3$ ); 3.45 (d, 1H,  $J = 12.0$  Hz, H-5'a); 4.00 (dd, 1H,  $J' = 6.0$  and 11.6 Hz, H-5'b); 4.40 (q, 2H,  $\text{CH}_2$ ); 5.13 (d, 1H,  $J = 5.6$  Hz, H-4'); 6.67 (d, 1H,  $J = 8.0$  Hz, H-7); 7.06 (d, 1H, H-6); 7.26 (s, 1H, H-4).  $^{13}\text{C}$  NMR (100 MHz,  $\text{CDCl}_3$ )  $\delta$  14.5 ( $\text{CH}_3$ ), 21.4 ( $\text{CH}_3$ ), 25.7 ( $\text{CH}_2$ ), 26.9 ( $\text{CH}_3$ ), 29.2 ( $\text{CH}_2$ ), 33.8 (C-5'), 44.2 (CH), 62.7 ( $\text{CH}_2$ ), 64.2 (C-4'), 75.7 (C-2'), 108.3, 125.0, 126.5, 130.3, 132.7 and 143.0 (aryl); 170.5, 174.2, and 177.8 (C=O); (B):  $^1\text{H}$  NMR (400 MHz,  $\text{CDCl}_3$ )  $\delta$  1.15-1.26 (m, 4H,  $\text{CH}_2$ ); 1.40 (t, 3H,  $\text{CH}_3$ ); 1.63-1.73 (m, 6H,  $\text{CH}_2$ ); 2.17 (t, 1H, CH); 2.35 (s, 3H,  $\text{CH}_3$ ); 3.25 (s, 3H,  $\text{CH}_3$ ); 3.30 (d, 1H,  $J = 12.0$  Hz, H-5'a); 3.94 (dd, 1H,  $J' = 6.0$  and 11.6 Hz, H-5'b); 4.36 (q, 2H,  $\text{CH}_2$ ); 5.52 (d, 1H,  $J = 6.0$  Hz, H-4'); 6.78 (d, 1H,  $J = 8.0$  Hz, H-7); 7.18 (d, 1H, H-6); 7.64 (s, 1H, H-4).  $^{13}\text{C}$  NMR (100 MHz,  $\text{CDCl}_3$ )  $\delta$  14.5 ( $\text{CH}_3$ ), 21.1 ( $\text{CH}_3$ ), 25.4 ( $\text{CH}_2$ ), 25.8 ( $\text{CH}_3$ ), 29.6 ( $\text{CH}_2$ ), 32.2 (C-5'), 43.8 (CH), 62.0 ( $\text{CH}_2$ ), 64.4 (C-4'), 75.8 (C-2'), 108.8, 126.4, 131.2, 132.9 and 143.2 (aryl); 170.7, 174.4, and 177.8 (C=O). ESIMS  $m/z$  calcd for  $\text{C}_{22}\text{H}_{28}\text{N}_2\text{O}_4\text{S}$ , 416.18; found, 416.24.

**(2'S,4'R)-ethyl-3'-(cyclohexanecarbonyl)-1-methyl-2 oxospiro[indoline-3,2'-  
thiazolidine]-4'-carboxylate. (13p)**

Overall yield 45%.  $[\alpha]_{\text{D}}^{25}$  -20.0° (c 0.4, MeOH). (A):  $^1\text{H}$  NMR (400 MHz,  $\text{CDCl}_3$ )  $\delta$  1.13-1.24 (m, 4H,  $\text{CH}_2$ ); 1.39 (t, 3H,  $\text{CH}_3$ ); 1.62-1.79 (m, 6H,  $\text{CH}_2$ ); 2.19 (t, 1H, CH); 3.23 (s, 3H,  $\text{CH}_3$ ); 3.45 (d, 1H,  $J = 12.0$  Hz, H-5'a); 3.99 (dd, 1H,  $J' = 6.0$  and 11.6 Hz, H-5'b); 4.38 (q, 2H,  $\text{CH}_2$ ); 5.13 (d, 1H,  $J = 5.6$  Hz, H-4'); 6.79 (d, 1H,  $J = 8.4$  Hz, H-7); 7.02 (t, 1H, H-6); 7.27 (t, 1H, H-5); 7.46 (d, 1H, H-4).  $^{13}\text{C}$  NMR (100 MHz,  $\text{CDCl}_3$ )  $\delta$  14.5 ( $\text{CH}_3$ ), 25.7 ( $\text{CH}_2$ ), 26.8 ( $\text{CH}_3$ ), 29.2 ( $\text{CH}_2$ ), 33.8 (C-5'), 44.1 (CH), 62.7 ( $\text{CH}_2$ ), 64.2 (C-4'), 75.9

(C-2'), 108.5, 123.2, 124.2, 126.1, 129.9, 131.0, and 143.5 (aryl); 170.5, 174.2, and 177.8 (C=O); (**B**): <sup>1</sup>H NMR (400 MHz, CDCl<sub>3</sub>) δ 1.13-1.24 (m, 4H, CH<sub>2</sub>); 1.39 (t, 3H, CH<sub>3</sub>); 1.62-1.79 (m, 6H, CH<sub>2</sub>); 2.19 (t, 1H, CH); 3.28 (s, 3H, CH<sub>3</sub>); 3.40 (d, 1H, *J* = 12.0 Hz, H-5'a); 3.95 (dd, 1H, *J*' = 6.0 and 11.6 Hz, H-5'b); 4.31 (q, 2H, CH<sub>2</sub>); 5.51 (d, 1H, *J* = 6.4 Hz, H-4'); 6.89 (d, 1H, *J* = 8.4 Hz, H-7); 7.14 (t, 1H, H-6); 7.38 (t, 1H, H-5); 7.46 (d, 1H, H-4). <sup>13</sup>C NMR (100 MHz, CDCl<sub>3</sub>) δ 14.5 (CH<sub>3</sub>), 25.7 (CH<sub>2</sub>), 27.0 (CH<sub>3</sub>), 29.3 (CH<sub>2</sub>), 32.1 (C-5'), 42.9 (CH), 62.1 (CH<sub>2</sub>), 65.3 (C-4'), 75.9 (C-2'), 109.0, 122.8, 125.1, 127.2, 128.2, 131.0, and 143.7 (aryl); 170.6, 174.0, and 177.6 (C=O). ESIMS *m/z* calcd for C<sub>21</sub>H<sub>26</sub>N<sub>2</sub>O<sub>4</sub>S, 402.16; found, 402.20.

**(2'S,4'R)-ethyl 5-bromo-3'-(cyclohexanecarbonyl)-2-oxospiro[indoline-3,2'-thiazolidine]-4'-carboxylate. (13q)**

Overall yield 42%. [ $\alpha$ ]<sub>D</sub><sup>25</sup> -27.0° (*c* 0.5, MeOH). <sup>1</sup>H NMR (400 MHz, CDCl<sub>3</sub>) δ 1.15-1.22 (m, 4H, CH<sub>2</sub>); 1.41 (t, 3H, CH<sub>3</sub>); 1.64-1.78 (m, 6H, CH<sub>2</sub>); 1.96 (t, 1H, CH); 3.43 (d, 1H, *J* = 12.0 Hz, H-5'a); 3.97 (dd, 1H, *J* = 6.0 and 11.6 Hz, H-5'b); 4.30 (q, 2H, CH<sub>2</sub>); 4.63 (d, 1H, *J* = 6.0 Hz, H-4'); 7.49 (d, 1H, *J* = 8.4 Hz, H-7'); 7.68 (s, 1H, H-4'); 8.10 (d, 1H, H-6'). <sup>13</sup>C NMR (100 MHz, CDCl<sub>3</sub>) δ 14.4 (CH<sub>3</sub>), 25.8 (CH<sub>2</sub>), 29.3 (CH<sub>2</sub>), 39.0 (C-1), 44.9 (CH), 62.6 (CH<sub>2</sub>), 65.0 (C-2), 75.7 (C-4), 118.8, 127.3, 128.0, 134.1, and 139.4 (aryl), 172.0, 175.9, and 177.4 (C=O). ESIMS *m/z* calcd for C<sub>20</sub>H<sub>23</sub>BrN<sub>2</sub>O<sub>4</sub>S, 466.06; found, 466.12.

**(2'S,4'R), (2'R,4'R)-5-bromo-3'-(cyclohexanecarbonyl)-1-methyl-2-oxospiro[indoline-3,2'-thiazolidine]-4'-carboxylic acid. (13r)**

Overall yield 37%. <sup>1</sup>H NMR (400 MHz, CDCl<sub>3</sub>) ( $\alpha$ ) δ 1.14-1.38 (m, 6H, CH<sub>2</sub>); 1.58-1.79 (m, 4H, CH<sub>2</sub>); 2.27 (t, 1H, CH); 3.19 (s, 3H, CH<sub>3</sub>); 3.54 (t, 1H, H-5'a); 3.88-3.91 (m, 1H, H-5'b); 5.11 (d, 1H, *J* = 6.8 Hz, H-4'); 6.64 (d, 1H, *J* = 8.0 Hz, H-7); 7.34 (d, 1H, H-6); 7.65 (s, 1H, H-4). ( $\beta$ ) δ 1.14-1.38 (m, 6H,

CH<sub>2</sub>); 1.58-1.79 (m, 4H, CH<sub>2</sub>); 2.27 (t, 1H, CH); 3.22 (s, 3H, CH<sub>3</sub>); 3.54 (t, 1H, H-5'a); 3.81-3.85 (m, 1H, H-5'b); 5.37 (d, 1H, *J* = 5.6 Hz, H-4'); 6.74 (d, 1H, *J* = 8.0 Hz, H-7); 7.47 (d, 1H, H-6); 8.00 (s, 1H, H-4). <sup>13</sup>C NMR (100 MHz, CDCl<sub>3</sub>) (α) δ 25.6 (CH<sub>2</sub>), 26.3 (CH<sub>2</sub>), 27.1 (CH<sub>2</sub>), 29.4 (CH<sub>2</sub>), 34.5 (C-5'), 43.3 (CH), 64.9 (C-4'), 71.4 (C-2'), 109.9, 115.6, 127.7, 129.2, 132.5 and 142.6 (aryl); 174.7, 175.3, and 176.9 (C=O). (β) δ 25.9 (CH<sub>2</sub>), 26.9 (CH<sub>2</sub>), 28.9 (CH<sub>2</sub>), 29.9 (CH<sub>2</sub>), 32.6 (C-5'), 43.7 (CH), 58.7 (C-4'), 69.8 (C-2'), 110.4, 116.7, 129.5, 129.9, 133.6 and 141.2 (aryl); 174.5, 175.2, and 176.7 (C=O). ESIMS *m/z* calcd for C<sub>18</sub>H<sub>19</sub>BrN<sub>2</sub>O<sub>4</sub>S, 438.02; found, 438.10.

***General Procedure for the Synthesis of the (2'S, 4'R)-ethyl 1-Substituted-2-oxospiro[indoline-3,2'-thiazolidine]-4'-carboxylate derivatives. (14a-c)***

To a solution of indol-2,3-dione derivatives (**1-3**, 300 mg, 1.5 mmol) in dichloromethane was added 4-chlorobenzoyl chloride (1.8 mmol) and TEA (1.8 mmol). The reaction mixture was stirred at room temperature for 1 h and water was then added. The organic solution was washed with water (3x 100 mL), dried over Na<sub>2</sub>SO<sub>4</sub>, and evaporated in vacuo. Flash chromatography on silica gel, using ethyl acetate/n-hexane as eluent, overall yielded the correspondent derivatives **16-18**. 1-substituted isatine **16-18** (150 mg, ~ 0,5 mmol) derivatives were dissolved in ethanol and cysteine ethyl ester and NaHCO<sub>3</sub> were added (0, 65 mmol). The mixture was stirred at room temperature for 12 h, then ethanol was filtrated and the surnatant was evaporated in vacuo. The crude was dissolved in dicholoromethane and washed with water (3 x 100 mL), the organic phase was dried over Na<sub>2</sub>SO<sub>4</sub>, and evaporated in vacuo. Flash chromatography on silica gel, using ethyl acetate/n-hexane as eluent, yielded the correspondent final derivatives **14a-c** as solid compounds.

**(2'S,4'R)-ethyl-1-(4-chlorobenzoyl)-2-oxospiro[indoline-3,2'-thiazolidine]-4'-carboxylate. (14a)**

Overall yield 32%.  $[\alpha]_{\text{D}}^{25} +2.29^{\circ}$  (c 0.5, MeOH).  $^1\text{H NMR}$  (400 MHz,  $\text{CDCl}_3$ )  $\delta$  1.32 (t, 3H,  $\text{CH}_3$ ); 3.34 (d, 2H,  $J = 5.6$  Hz, H-5'); 4.27 (q, 2H,  $\text{CH}_2$ ); 5.01 (dd, 1H,  $J = 5.5$  and 13.0 Hz, H-4'); 7.08 (t, 1H,  $J = 7.6$  Hz, H-6) 7.43 (d, 2H,  $J = 8.4$  Hz, aryl); 7.59 (t, 1H, H-5); 7.81 (d, 1H,  $J = 7.6$  Hz, H-7); 7.87 (d, 2H, aryl); 8.34 (d, 1H,  $J = 7.6$  Hz, H-4).  $^{13}\text{C NMR}$  (100 MHz,  $\text{CDCl}_3$ )  $\delta$  14.4 ( $\text{CH}_3$ ), 40.8 (C-5'), 52.3 (C-4'), 62.8 ( $\text{CH}_2$ ), 71.8 (C-2'), 120.9, 123.0, 129.1, 129.4, 131.7, 134.9, 137.5, 139.6, and 142.3 (aryl), 166.0, 172.1, and 190.6 (C=O). ESIMS  $m/z$  calcd for  $\text{C}_{20}\text{H}_{17}\text{ClN}_2\text{O}_4\text{S}$ , 416.06; found, 416.09.

**(2'S,4'R)-ethyl 1-(4-chlorobenzoyl)- 5-methyl-2-oxospiro[indoline-3,2'-thiazolidine]-4'-carboxylate. (14b)**

Overall yield 28%.  $[\alpha]_{\text{D}}^{25} +3.21^{\circ}$  (c 0.5, MeOH).  $^1\text{H NMR}$  (400 MHz,  $\text{CDCl}_3$ )  $\delta$  1.31 (t, 3H,  $\text{CH}_3$ ); 2.27 (s, 3H,  $\text{CH}_3$ ); 3.34 (d, 2H,  $J = 5.2$  Hz, H-5'); 4.28 (q, 2H,  $\text{CH}_2$ ); 5.02 (d, 1H,  $J = 6.0$  Hz, H-4'); 7.36-7.44 (m, 3H, H-7, aryl); 7.72 (m, 3H, H-6, aryl); 8.11 (s, 1H, H-4).  $^{13}\text{C NMR}$  (100 MHz,  $\text{CDCl}_3$ )  $\delta$  14.3 ( $\text{CH}_3$ ), 21.0 ( $\text{CH}_3$ ), 40.7 (C-5'), 52.8 (C-4'), 62.5 ( $\text{CH}_2$ ), 72.3 (C-2'), 120.8, 128.8, 128.9, 129.1, 129.3, 131.7, 132.0, 134.8, 138.4, and 140.5 (aryl), 166.2, 169.3, and 190.2 (C=O). ESIMS  $m/z$  calcd for  $\text{C}_{21}\text{H}_{19}\text{ClN}_2\text{O}_4\text{S}$ , 430.08; found, 430.15

**(2'R,4'R)-ethyl 5-bromo-1-(4-chlorobenzoyl)-2-oxospiro[indoline-3,2'-thiazolidine]-4'-carboxylate. (14c)**

Overall yield 36%.  $[\alpha]_{\text{D}}^{25} +2.2^{\circ}$  (c 0.4, MeOH).  $^1\text{H NMR}$  (400 MHz,  $\text{CDCl}_3$ )  $\delta$  1.31 (t, 3H,  $\text{CH}_3$ ); 3.68 (d, 2H,  $J = 5.2$  Hz, H-5'); 4.25 (q, 2H,  $\text{CH}_2$ ); 5.03 (dd, 1H,  $J = 5.2$  and 12.0 Hz, H-4'); 7.12 (d, 1H,  $J = 7.6$  Hz, NH); 7.37-7.43 (m, 3H, H-7, H-6, H4); 7.72 (d, 2H,  $J = 8.0$  Hz, aryl); 7.86 (m, 2H, aryl).  $^{13}\text{C NMR}$  (100 MHz,  $\text{CDCl}_3$ )  $\delta$  14.3 ( $\text{CH}_3$ ), 30.9 (C-5'), 53.3 (C-4'), 62.5 ( $\text{CH}_2$ ), 72.3 (C-

2'), 128.8, 128.9, 129.1, 129.3, 131.7, 132.0, 134.8, 138.4, and 140.7 (aryl), 166.3, 170.3, and 190.2 (C=O). ESIMS m/z calcd for C<sub>20</sub>H<sub>16</sub>BrClN<sub>2</sub>O<sub>4</sub>S, 493.97; found, 494.05.

***(2'S,4'R)- ethyl 5-bromo-1-(cyclohexanecarbonyl)-2-oxospiro[indoline-3,2'-thiazolidine]-4'-carboxylate. (14d)***

Overall yield 25%. [ $\alpha$ ]<sub>D</sub><sup>25</sup> -1.8° (c 0.1, MeOH). <sup>1</sup>H NMR (400 MHz, CDCl<sub>3</sub>)  $\delta$  1.35 (t, 3H, CH<sub>3</sub>); 1.39-1.48 (m, 4H, CH<sub>2</sub>); 1.73-1.97 (m, 7H, CH<sub>2</sub> and CH); 3.23 (d, 1H, NH); 3.46 (dd, 1H,  $J'$  = 5.2,  $J''$  = 10.8 Hz, H-5'a); 3.93 (dd, 1H,  $J'$  = 7.6,  $J''$  = 10.8 Hz, H-5'b); 4.31 (q, 2H, CH<sub>2</sub>); 4.63 (t, 1H, H-4'); 7.49 (d, 1H,  $J$  = 8.8 Hz, H-7); 7.67 (s, 1H, H-4); 8.10 (d, 1H, H-6). <sup>13</sup>C NMR (100 MHz, CDCl<sub>3</sub>)  $\delta$  14.4 (CH<sub>3</sub>), 25.8 (CH<sub>2</sub>), 26.0 (CH<sub>2</sub>), 29.2 (CH<sub>2</sub>), 39.1 (C-5'), 45.0 (CH), 62.5 (CH<sub>2</sub>), 65.0 (C-4'), 75.8 (C-2'), 118.8, 127.3, 128.0, 134.1 and 139.4 (aryl); 172.0, 175.9 and 177.4 (C=O). ESIMS m/z calcd for C<sub>20</sub>H<sub>23</sub>BrN<sub>2</sub>O<sub>5</sub>S, 466.06; found, 466.10.

***Ethyl 1-(4-chlorobenzoyl)-5-methyl-2-oxo-5'H-spiro[indoline-3,2'-thiazole]-4'-carboxylate. (15b)***

Overall yield 11%. <sup>1</sup>H NMR (400 MHz, CDCl<sub>3</sub>)  $\delta$  1.36 (t, 3H, CH<sub>3</sub>); 3.49 (s, 3H, CH<sub>3</sub>); 4.39 (q, 2H, CH<sub>2</sub>); 4.59 (dd, 2H,  $J'$  = 16.4 Hz,  $J''$  = 14.0 Hz, H-5); 7.26 (s, 1H, H-4); 7.32 (d, 1H,  $J$  = 8.0 Hz, H-7); 7.41-7.49 (m, 3H, aryl and H-6); 7.69 (d, 2H,  $J$  = 8.0 Hz, aryl). <sup>13</sup>C NMR (100 MHz, CDCl<sub>3</sub>)  $\delta$  29.9 (CH<sub>3</sub>), 45.5 (C-1), 53.8 (CH<sub>3</sub>), 74.8 (C-2), 115.7, 126.3, 128.9, 130.3, 131.0, 131.6 and 155.4 (aryl), 172.7, 176.9, and 179.3 (C=O). ESIMS m/z calcd for C<sub>21</sub>H<sub>19</sub>ClN<sub>2</sub>O<sub>4</sub>S, 430.08; found, 430.12.

***Ethyl 5-bromo-1-(4-chlorobenzoyl)-2-oxo-5'H-spiro[indoline-3,2'-thiazole]-4'-carboxylate. (15c)***

Overall yield 8%. <sup>1</sup>H NMR (400 MHz, CDCl<sub>3</sub>) δ 1.35 (t, 3H, CH<sub>3</sub>); 4.29-4.36 (m, 4H, CH<sub>2</sub> and H-5); 7.47-7.53 (m, 3H, aryl and H-7'); 7.63-7.70 (m, 3H, aryl and H-4'); 8.14 (d, 1H, *J* = 8.0 Hz, H-6'). <sup>13</sup>C NMR (100 MHz, CDCl<sub>3</sub>) δ 14.8 (CH<sub>3</sub>), 44.8 (C-1), 62.9 (CH<sub>2</sub>), 74.1 (C-2), 115.7, 119.3, 125.8, 127.7, 128.4, 129.9, 133.5, 139.3 and 156.6 (aryl), 173.1, 175.9, and 178.2 (C=O). ESIMS *m/z* calcd for C<sub>20</sub>H<sub>14</sub>BrClN<sub>2</sub>O<sub>4</sub>S, 491.95; found, 492.03.

***Ethyl 5-bromo-1-(cyclohexanecarbonyl)-2-oxo-5'H-spiro [indoline-3,2'-thiazole]-4'-carboxylate. (15d)***

Overall yield 12%. <sup>1</sup>H NMR (400 MHz, CDCl<sub>3</sub>) δ 1.18-1.26 (m, 4H, CH<sub>2</sub>); 1.39 (t, 3H, CH<sub>3</sub>); 1.48-1.53 (m, 2H, CH<sub>2</sub>); 1.62-1.70 (m, 4H, CH<sub>2</sub>); 1.96 (t, 1H, CH); 4.42 (q, 2H, CH<sub>2</sub>); 4.64 (dd, 2H, *J*' = 12.0 Hz, *J*'' < 1Hz, H-5); 7.52 (d, 1H, *J* = 8.0 Hz, H-7'); 7.58 (s, 1H, H-4'); 8.12 (d, 1H, H-6'). <sup>13</sup>C NMR (100 MHz, CDCl<sub>3</sub>) δ 14.8 (CH<sub>3</sub>), 25.6 (CH<sub>2</sub>), 30.1 (CH<sub>2</sub>), 44.4 (C-1), 45.6 (CH), 62.8 (CH<sub>2</sub>), 74.4 (C-2), 118.2, 127.9, 128.6, 133.7, 139.5 and 156.3 (aryl), 172.6, 176.9, and 178.3 (C=O). ESIMS *m/z* calcd for C<sub>20</sub>H<sub>21</sub>BrN<sub>2</sub>O<sub>4</sub>S, 464.04; found, 464.11.

## **4.2 Biology**

Dulbecco's modified Eagle medium (DMEM), fetal bovine serum (FBS), trypsin-EDTA solution (1×), penicillin and streptomycin, and phosphate buffered saline (PBS) were from Cambrex Biosciences. 3 (4,5-Dimethylthiazol-2-yl)-2,5-diphenyltetrazolium bromide (MTT), propidium iodide (PI), Triton X-100, sodium citrate, and formamide were purchased from Sigma (Milan, Italy). Rabbit polyclonal anti-caspase-3, anti-MDM2, anti-Bcl-xS/L, mouse monoclonal anti-actin, anti-p53, anti p21, anti p27, and anti cytochrome c were

purchased from Santa Cruz Biotechnology (DBA; Milan, Italy). ECL reagent was obtained from Amersham Pharmacia Biotech, U.K.

#### **4.2.1 Cell culture**

Human prostate cancer (PC3), human histiocytic lymphoma (U937), human lung adenocarcinoma (Calu), human hepatoma (HepG2), human anaplastic thyroid carcinoma (C643), and human breast cancer (MCF-7) cell lines and human primary gingival fibroblasts were grown at 37 °C in Dulbecco's modified Eagle medium containing 10 mM glucose (DMEMHG) supplemented with 10% fetal calf serum and 100 units/mL each of penicillin and streptomycin and 2 mmol/L glutamine. In each experiment, cells were placed in fresh medium, cultured in the presence of synthesized compounds (from 0.1 to 25 mM), and followed for further analyses.

#### **4.2.2 Cell viability assay**

Cell viability was determined using the 3[4,5- dimethylthiazol-2,5-diphenyl-2H-tetrazolium bromide (MTT) colorimetric assay. The test is based on the ability of mitochondrial dehydrogenase to convert, in viable cells, the yellow MTT reagent (Sigma Chemical Co., St. Louis, MO) into a soluble blue formazan dye. Cells were seeded into 96-well plates to a density of  $10^5$  cells/100  $\mu$ L well. After 24 h of growth to allow attachment to the wells, compounds were added at various concentrations (from 0.1 to 25 M). After 24 or 48 h of growth and after removal of the culture medium, 100  $\mu$ L/well medium containing 1 mg/mL MTT was added. Microplates were further incubated at 37 °C for 2 h in the dark. The solution was then gently aspirated from each well, and the formazan crystals within the cells were dissolved with 100  $\mu$ L of DMSO. Optical densities were read at 550 nm using a Multiskan Spectrum Thermo Electron Corporation reader. Results were expressed as percentage relative to vehicle-treated control (0.5% DMSO was added to untreated cells). IC<sub>50</sub> (concentration eliciting 50%

inhibition) values were determined by linear and polynomial regression. Experiments were performed in triplicate.

#### ***4.2.3 In vitro inhibition of p53-MDM2 interaction assay***

We performed an in vitro binding assay using ImmunoSet p53/MDM2 complex ELISA set (Enzo Life Sciences). The assay was performed according to the manufacturer's directions. Briefly, 96-multiwell was coated with p53 capture antibody and left overnight at room temperature. Then coating solution was removed and an amount of 200  $\mu$ L of blocking buffer was added to each wells. The plate was incubated for 1 h at room temperature. Blocking buffer was then removed, and an amount of 100  $\mu$ L of p53/MDM2 standards was added to wells (except blank) in the presence of 5  $\mu$ M indicated inhibitors. The plate was incubated for 1 h at room temperature on a plate shaker. Each well was washed 4 times with 200  $\mu$ L of wash buffer, and an amount of 100  $\mu$ L of MDM2 detection antibody was added to wells (except blank) for 1 h at room temperature. The plate was washed again, and an amount of 100  $\mu$ L of SA-HRP conjugated antibody was added to the wells (except blank). The plate was incubated for 30 min at room temperature on a plate shaker. The wells were washed again, and an amount of 100  $\mu$ L of TMB (3,3',5,5'-tetramethylbenzidine) was added to each well for 30 min at room temperature. To stop reaction, an amount of 100  $\mu$ L of 1 N HCl was added to the wells. After the plate reader was blanked against the substrate, optical density was read at 450 nm. Data were presented as % of inhibition referenced to control (only standards).

#### ***4.2.4 Cell cycle analysis***

Cells ( $1 \times 10^5$ ) were harvested when subconfluent, fixed in 70% ethanol for 1 h at -20 °C, rehydrated in PBS, and the pellet was resuspended in 300  $\mu$ L of PBS containing 250  $\mu$ g/mL RNaseA and 10  $\mu$ g/mL propidium iodide for 30 min in the dark. Samples were acquired with a CYAN flow cytometer (DAKO

Corporation, San Jose, CA, U.S.). The cell cycle distribution, expressed as percentage of cells in the G0/G1, S, and G2/M phases, was calculated using SUMMIT software.

#### ***4.2.5 Annexin V assay***

Cells were plated at  $1 \times 10^5$  in six-well plates and washed with  $1 \times$  PBS and then with annexin V binding buffer. After centrifugation at 2000 rpm for 5 min, the cells were resuspended in 100  $\mu$ L of annexin V binding buffer and incubated with 5  $\mu$ L of FITC annexin V (BioLegend) and 2  $\mu$ L of 500  $\mu$ g/mL propidium iodide for 15 min at 25 °C in the dark. Finally, an amount of 400  $\mu$ L of annexin V binding buffer was added to each test tube. Samples were acquired with a CYAN flow cytometer (DAKO Corporation, San Jose, CA, U.S.) and analyzed using SUMMIT software.

#### ***4.2.6 Western blotting and immunoprecipitation analysis***

MCF-7 cells were plated in Petri dishes ( $1 \times 10^6$  cells) in normal culture conditions and incubated with or without 4n and nutlin. At the indicated times, cells were lysed using an ice cold lysis buffer (50  $\mu$ M Tris, 150 mM NaCl, 10 mM EDTA, 1% Triton) supplemented with a mixture of protease inhibitors containing antipain, bestatin, chymostatin, leupeptin, pepstatin, phosphoramidon, Pefabloc, EDTA, and aprotinin (Boehringer, Mannheim, Germany). Equivalent amounts of protein were loaded on 8-12% sodium dodecyl sulfate (SDS)-polyacrylamide gels and electrophoresed followed by blotting onto nitrocellulose membranes (Bio-Rad, Germany). After blotting with 5% (w/v) fat-free milk powder and 0.1% Tween 20 in TBS, the membrane was incubated overnight at 4°C with specific antibodies at the concentrations indicated by the manufacturer's protocol (Santa Cruz Biotechnology). The antibody was diluted in Tris-buffered saline/ Tween 20 and 5% milk powder. Following incubation with horseradish peroxidase conjugated secondary

antibodies, bands were detected by enhanced chemiluminescence (ECL kit, Amersham, Germany). Each filter was then probed with mouse monoclonal anti-actin antibody. Level of expression of detected bands was quantified by NIH ImageJ 1.40 after normalization with  $\beta$ -actin. For immunoprecipitation, cells were lysed in immunoprecipitation buffer (0.05 mol/L Tris-HCl (pH 8.0), 0.005 mol/L EDTA, 0.15 mol/L NaCl, 1% Nonidet P-40, 0.5% sodium deoxycolate, 0.1% SDS, 0.01 mol/L NaF, 0.005 mol/L EGTA, 0.01 mol/L sodium pyrophosphate, and 0.001 mol/L phenylmethylsulfonyl fluoride). Rabbit polyclonal antibody reactive to MDM2 (Santa Cruz Biotechnology, Santa Cruz, CA, U.S.) and protein G plus/protein A agarose beads (Oncogene Science, Boston, MA, U.S.) were used to immunoprecipitate MDM2 from 1 mg total lysate. Mouse monoclonal antibodies to total p53 were from Santa Cruz Biotechnology.

#### **4.3 Molecular Modeling methods**

The new version of the docking program AutoDock2 as implemented through the graphical user interface called AutoDockTools (ADT) was used to dock into the MDM2 structure **13n** and the cocrystal ligand. The MDM2 structure was retrieved from the Protein Data Bank (PDB code 1LBL), and cocrystal waters and ligand were removed. **13n** was built using the builder in the Maestro package of the Schrodinger Suite 2007, and optimization using a version of MacroModel was also included. The constructed compounds and the receptor structure were converted to AD4 format files using ADT, automatically generating all other atom values. The docking area was centered around the putative binding site. Grids of 60 Å × 60 Å × 60 Å with 0.375 Å spacing were calculated around the docking area for the ligand atom types using AutoGrid4. For each ligand, 100 separate docking calculations were performed. Each docking calculation consisted of 10 million energy evaluations using the Lamarckian genetic algorithm local search (GALS) method. The GALS method

evaluates a population of possible docking solutions and propagates the most successful individuals from each generation into the subsequent generation of possible solutions. A low-frequency local search according to the method of Solis and Wets is applied to docking trials to ensure that the final solution represents a local minimum. All dockings described in this paper were performed with a population size of 250, and 300 rounds of Solis and Wets local search were applied with a probability of 0.06. A mutation rate of 0.02 and a crossover rate of 0.8 were used to generate new docking trials for subsequent generations, and the best individual from each generation was propagated over the next generation. The docking results from each of the 100 calculations were clustered on the basis of root-mean-square deviation (rmsd) (solutions differing by less than 2.0 Å) between the Cartesian coordinates of the atoms and were ranked on the basis of free energy of binding ( $\Delta G_{AD4}$ ). Because AD4 does not perform any structural optimization and energy minimization of the complexes found, a molecular mechanics/energy minimization (MM/EM) approach was applied to refine the AD4 output. The computational protocol applied consisted of the application of 100 000 steps of the Polak-Ribie re conjugate gradients (PRCG) or until the derivative convergence was 0.05 kJ/mol. The **13n**/MDM2 complex picture was rendered employing the UCSF Chimera software.

**CHAPTER V**  
**DESIGN, SYNTHESIS, RESULTS AND**  
**DISCUSSION OF POTENTIAL p53 MODULATORS**  
**(SERIES 3 AND SERIES 4)**

### 5.1 Background and design

Starting from the results obtained from the previous series and from the molecular modeling studies, the aim of my second year of PhD was to identify a new *lead compound* starting from the structure of **SM13**.

We designed and synthesized new derivatives bearing different and generally bulkier substituents, at the N-1 position for Series 3 and at the ester-group for Series 4, in order to explore the MDM2 wide pocket found to be partially occupied by in silico investigations. Similarly, the **SM13** enantiomer was synthesized in order to investigate the influence of the stereochemistry on the pharmacological activity. (Figure 27).

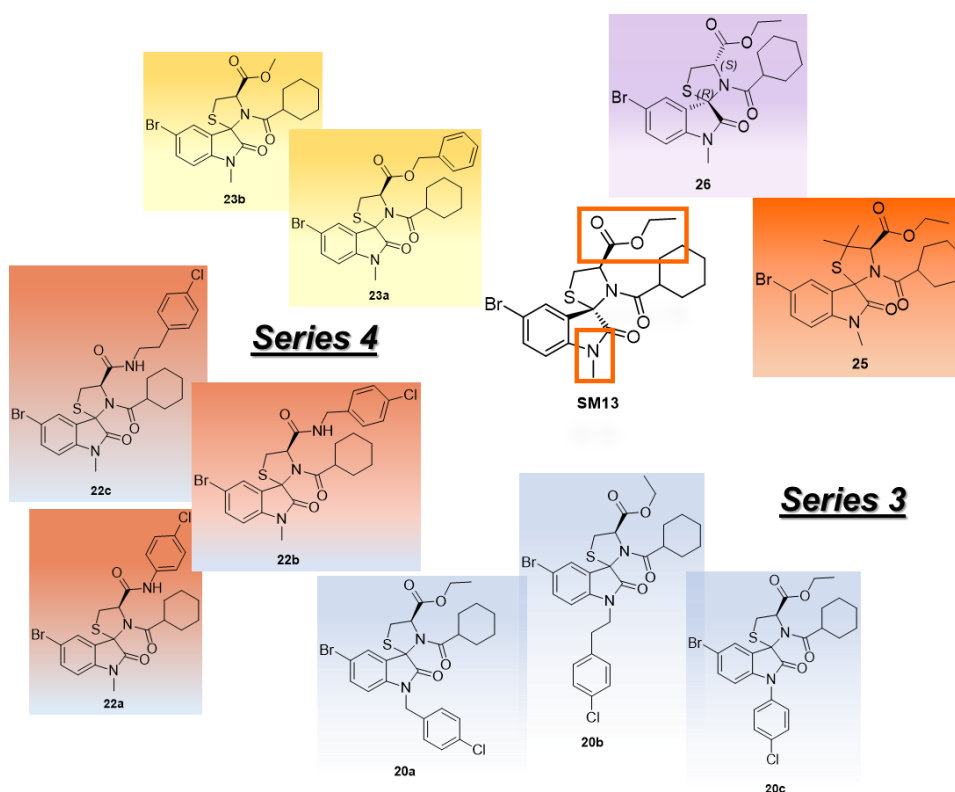


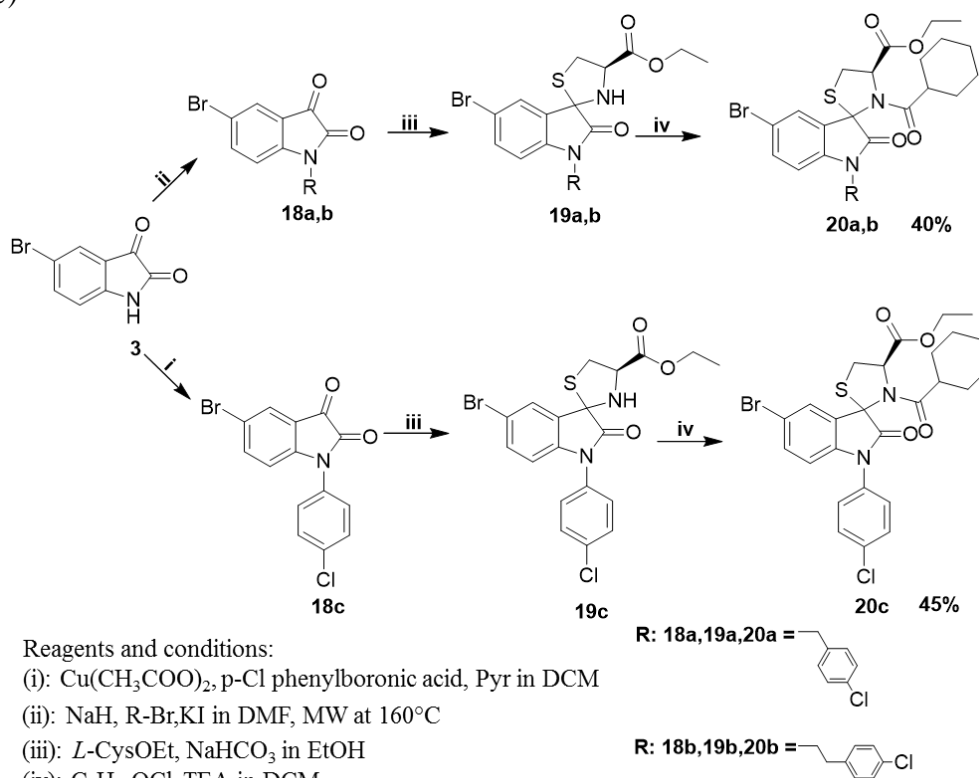
Figure 27. Synthesized compounds of series 3 and 4 starting from SM13

## 5.2 Chemistry

### 5.2.1 Chemistry 3<sup>rd</sup> series

The designed (4'*R*) –ethyl 5-bromo-1-(substituted)-2-oxospiro [indoline-3,2'-thiazolidine] -4'-carboxylate derivatives (**20a-c**) were prepared applying the synthetic route shown in Scheme 4.

**Scheme 4.** Alkylation and arylation reactions for the synthesis of (4'*R*)-ethyl 5-bromo-1-(substituted)-2-oxospiro[indoline-3,2'-thiazolidine]-4'-carboxylate derivatives (**20a-c**)



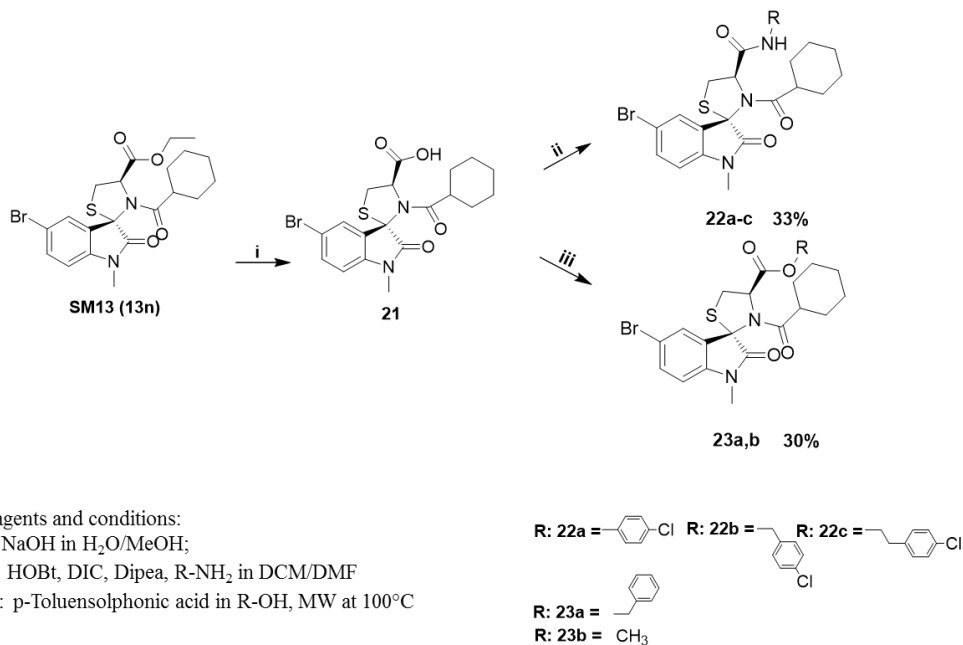
The starting 1-substituted-5-bromo-indoline-2, 3-dione intermediates (**18a-c**) were obtained through microwave assisted reaction, between the *N-1* of 5-bromine isatin and 1-(bromomethyl)-4-chlorobenzene or 1-(2-bromoethyl)-4-chlorobenzene for derivatives **18a** and **18b**, the reaction is conducted in strongly

basic conditions using DMF as solvent. While, for derivatives **18c**, p-Cl phenylboronic acid was used as reactants and Cu(CH<sub>3</sub>COO)<sub>2</sub> as catalyst. Then, all intermediates were transformed to the corresponding spirooxindolethiazolidines (**19a-c**) by condensation with *L*-cysteine ethyl ester in EtOH. These derivatives were obtained with 80-90% yields, as (2'*R*) / (2'*S*) epimeric mixtures ranging from 60/40 to 40/60 ratios as previously described [Paragraph 3.2.1]. The 3'-acyl derivatives were obtained as single diastereoisomers, by reaction of compounds **19a-c** with the corresponding cyclohexanecarbonyl chlorides in DCM using TEA as base.

### 5.2.2 Chemistry 4<sup>th</sup> series

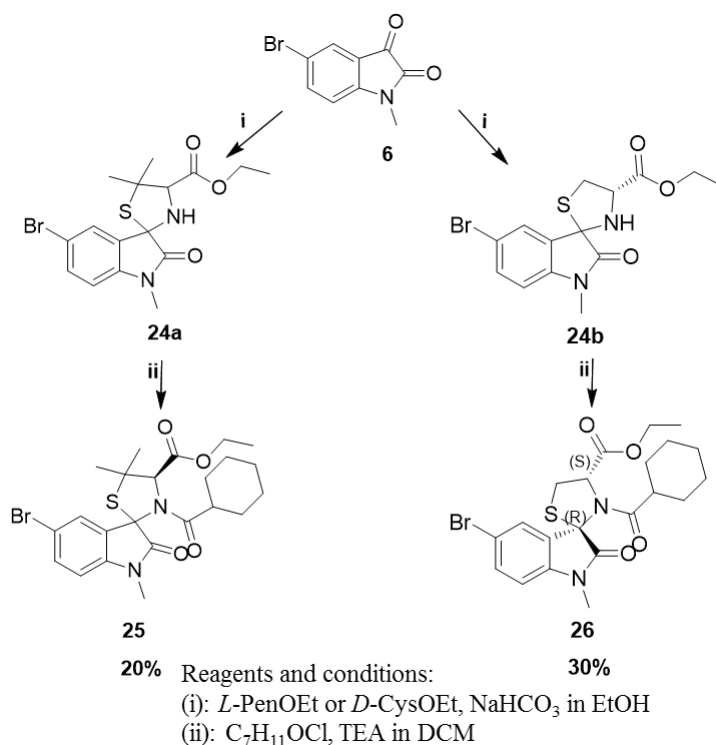
For the synthesis of **22a-c** and **23a-b** an alternative synthetic strategy was adopted (Scheme 5). The **SM13** compound, was subjected to hydrolysis of the ester group in alkaline conditions (**21**). The (2'*S*,4'*R*) -5-bromo-3'-(cyclohexanecarbonyl)-1-methyl-2-oxo-*N*-substituted-spiro[indoline-3,2'-thiazolidine]-4'carboxamide derivatives were obtained through a coupling reaction between the carboxyl group of the thiazolidine scaffold and several aliphatic and aromatic amines in DCM/DMF (9/1), using HOBt, HBTU as coupling agents and DIPEA as base. These derivatives were obtained with 33% yields, as single diastereoisomers. Differently, for compounds **23a,b** the carboxyl group in 4' was subjected to microwave assisted esterification, using p-toluenesulfonic acid as catalyst, methanol for compound **23a**, and benzil alcohol for **23b**. Also these derivatives were obtained as single diastereoisomers with 30% yields. Despite the different reaction conditions used racemization was always observed, as evidenced by NMR data.

**Scheme 5.** Synthesis of **22a-c** and **23a-b** derivatives



The final products **25** and **26** were obtained using the same procedure adopted for **SM13**, in this case is used for, using the *L*-Penicillamine-OEt and the *D*-Cysteine-OEt for the the construction of the thiazolidine scaffold of (4'*R*)-ethyl 5-bromo-3'-(cyclohexanecarbonyl)-1,5,5'-trimethyl-2-oxospiro [indoline-3,2'-thiazolidine]-4'-carboxylate (**25**) and of (2'*R*,4'*S*)-ethyl 5-bromo-3'-(cyclohexanecarbonyl)-1-methyl-2-oxospiro [indoline-3,2'-thiazolidine]-4' carboxylate (**26**), respectively. These derivatives were obtained with 20% and 30% yields respectively, as single diastereoisomers. (Scheme 6)

**Scheme 6.** Synthesis of (4*R*)-ethyl 5-bromo-3'-(cyclohexanecarbonyl)-1,5', 5'-trimethyl-2-oxospiro[indoline-3,2'-thiazolidine]-4'-carboxylate derivative (**25**) and (2'*R*,4'*S*)-ethyl 5-bromo-3'-(cyclohexanecarbonyl)-1-methyl-2-oxospiro[indoline-3,2'-thiazolidine]-4'-carboxylate (**26**) derivative



### 5.3 Biological effects of the spiro-indole-thiazolidine synthesized

#### 5.3.1 Antiproliferative activity

The synthesized compounds were examined, in the Department of Molecular and Cell Biology of the University of Naples “Federico II”, for their antiproliferative activity against two tumor cell lines: the human breast adenocarcinoma MCF-7 and human colon carcinoma HT-29 at 24 h. The IC<sub>50</sub> of the compounds was assessed both 24 and 48 hours, in order to verify if the mechanism of cytotoxicity was time dependent. The results are shown in Table 3.

**Table 3.** Antiproliferative activity of spiro [indoline-3,2'-thiazolidine] (series 3 and series 4)

COMPD	IC <sub>50</sub> (nM±SD) <sup>a</sup>	
	MCF-7	HT-29
<b>SM13</b>	<b>40±1.2</b>	<b>70±1.0</b>
<b>20a</b>	500±2.8	265±2.1
<b>20b</b>	535±2.1	210±1.4
<b>20c</b>	275±3.5	225±3.5
<b>22a</b>	195±7.0	480±1.4
<b>22b</b>	400±5.6	490±2.7
<b>22c</b>	150±8.9	190±4.4
<b>23a</b>	150±7.7	220±2.8
<b>23b</b>	135±2.2	490±1.4
<b>25</b>	300±1.2	278±2.0
<b>26</b>	660±8.4	165±2.1

<sup>a</sup>Data represent mean values (±SD) of three independent determinations

Despite the good results of cytotoxicity, by comparing the IC<sub>50</sub> values than **SM13** with all synthesized compounds, it is possible to observe a reduction of the biological activity. Despite the docking studies had indicated the existence of a large pocket on the surface of MDM2 corresponding to the binding region of the ester group of **SM13**, structural modification at this position did not lead to favorable biological activities. The compound **26**, (designed as **SM13** enantiomer), did not show improved biological properties, showing that the configurational inversion does not represent a convenient strategy for interacting with MDM2.

---

**CHAPTER VI**  
**EXPERIMENTAL SECTION FOR SERIES 3 AND 4**

### 6.1. Chemistry

Reactions were carried out with magnetic stirring in round-bottomed flasks unless otherwise noted. Moisture-sensitive reactions were conducted in oven-dried glassware under a positive pressure of dry nitrogen, using pre-dried, freshly distilled solvents. Microwave assisted reactions were performed in a Biotage Initiator<sup>+</sup> reactor. All solvents and reagent were purchased by Sigma-Aldrich. Analytical thin layer chromatography (TLC) was performed on pre-coated glass silica gel plates 60 (F254, 0.25 mm, VWR International). Purifications were performed by flash column chromatography on silica gel (230-400 mesh, Merck Millipore). Large scale purifications were conducted on the flash purification system apparatus Biotage Isolera One. NMR spectra were recorded on Varian Mercury-400 apparatus. <sup>1</sup>H and <sup>13</sup>C NMR spectra are reported in parts per million (ppm) referred to specific signals due to deuterated solvents as internal references. The following abbreviations are used to describe peaks: s (singlet), d (doublet), dd (double double), t (triplet), q (quadruplet) and m (multiplet). ESI-MS experiments were performed on an Applied Biosystem API 2000 triple-quadrupole spectrometer. Combustion microanalyses were performed on a Carlo Erba CNH 1106 analyzer, and were within 0.4% of calculated values. These elemental analysis results confirmed 95% purity for synthesized compounds. Unless otherwise specified, final products were converted to their chlorohydrate salts using HCl saturated diethyl ether, followed by filtration.

#### *General Procedure for the Synthesis of (4'R)-ethyl 5-bromo-1-(substituted)-2-oxospiro[indoline-3,2'-thiazolidine]-4' carboxylate derivatives. (20a-c)*

To a solution of 5-Br indol-2, 3-dione derivatives (1 mmol) in DMF (15 mL) was added NaH (1.5 mmol), KI (1.5 mmol) and 1-(bromomethyl)-4-chlorobenzene (1.5 mmol) or 1-(bromoethyl)-4-chlorobenzene (1.5 mmol) for obtained respectively **18a** and **18b**. While, for the **18c** intermediated to a solution

of 5-Br of indol-2, 3-dione derivatives (1 mmol) in DMF (15 mL) was added Cu(CH<sub>3</sub>COO)<sub>2</sub> (1.5 mmol), p-Cl phenylboronic acid (1.5 mmol) and Pyridine (1.5 mmol). Microwave assisted reactions were performed at 160 °C for 20 minutes. The solvent is evaporated in vacuo. The organic solution was dissolved in DCM and washed with water (3x 100 mL), dried over Na<sub>2</sub>SO<sub>4</sub>, and evaporated in vacuo. Flash chromatography on silica gel, using ethyl acetate/n-hexane as eluent, overall yielded the correspondent derivatives **18a-c**. The corresponding (4'R)-ethyl 5-bromo-1-(substituted)-2-oxospiro [indoline-3,2'-thiazolidine]-4' carboxylate derivatives (**20a-c**) are obtained as described previously<sup>101</sup> [Paragraph 4.1.1].

***(4'R)-ethyl 5-bromo-1-(4-chlorobenzyl)-3'-(cyclohexanecarbonyl)-2-oxospiro [indoline-3,2'-thiazolidine]-4'-carboxylate. (20a)***

yield 49%. <sup>1</sup>H NMR (400 MHz, CDCl<sub>3</sub>) δ 1.16-1.24 (m, 4H, CH<sub>2</sub>); 1.44 (t, 3H, CH<sub>3</sub>); 1.62-1.77 (m, 6H, CH<sub>2</sub>); 2.21 (t, 1H, CH); 3.27 (d, 1H, J = 15.0 Hz, H-5'a); 3.60 (d, 1H, H-5'b); 4.27 (q, 2H, CH<sub>2</sub>); 4.42 (d, 1H, J = 18.0 Hz, CH<sub>2</sub>); 4.95 (d, 1H, CH<sub>2</sub>); 6.00 (s, 1H, H-4'); 6.33 (d, 1H, J = 9.0 Hz, Aryl); 6.61 (d, 1H, J = 8.4 Hz, H-7); 6.79 (d, 1H, Aryl); 7.12 (d, 1H, J = 9.0 Hz, Aryl); 7.23 (d, 1H, Aryl); 7.31 (d, 1H, H-6); 7.52 (s, 1H, H-4). ESIMS m/z calcd for C<sub>27</sub>H<sub>28</sub>BrClN<sub>2</sub>O<sub>4</sub>S, 590.06; found, 590.15.

***(4'R)-ethyl 5-bromo-1-(4-chlorophenethyl)-3'-(cyclohexanecarbonyl)-2-oxospiro[indoline-3,2'-thiazolidine]-4'-carboxylate. (20b)***

yield 49%. <sup>1</sup>H NMR (400 MHz, CDCl<sub>3</sub>) δ 1.16-1.23 (m, 4H, CH<sub>2</sub>); 1.46 (t, 3H, CH<sub>3</sub>); 1.65-1.78 (m, 6H, CH<sub>2</sub>); 2.16 (t, 1H, CH); 2.94 (t, 2H, CH<sub>2</sub>); 3.46 (d, 1H, CH<sub>2</sub> Hz, H-5'a); 3.79-3.97 (m, 3H, H-5'b and CH<sub>2</sub>); 4.40 (q, 2H, CH<sub>2</sub>); 5.11 (d, 1H, J = 6.4 Hz, H-4'); 6.55 (d, 1H, J = 8.8 Hz, H-7); 7.22 (d, 2H, J = 9.0 Hz,

Aryl); 7.30 (d, 2H, Aryl); 7.33 (d, 1H, H-6); 7.57 (s, 1H, H-4). ESIMS m/z calcd for C<sub>28</sub>H<sub>30</sub>BrClN<sub>2</sub>O<sub>4</sub>S, 604.08; found, 604.16.

**(4'R)-ethyl 5-bromo-1-(4-chlorophenyl)-3'-(cyclohexanecarbonyl)-2-oxospiro[indoline-3,2'-thiazolidine]-4'-carboxylate. (20c)**

yield 49%. (A) : <sup>1</sup>H NMR (400 MHz, CDCl<sub>3</sub>) δ 1.16-1.24 (m, 4H, CH<sub>2</sub>); 1.44 (t, 3H, CH<sub>3</sub>); 1.62-1.77 (m, 6H, CH<sub>2</sub>); 2.21 (t, 1H, CH); 3.53 (d, 1H, J = 12.0 Hz, H-5'a); 4.03 (dd, 1H, J' = 6.0 and 11.6 Hz, H-5'b); 4.48 (q, 2H, CH<sub>2</sub>); 5.20 (d, 1H, J = 5.6 Hz, H-4'); 6.64 (d, 1H, J = 8.4 Hz, H-7); 7.37 (d, 1H, H-6); 7.41 (d, 2H, J = 8.0 Hz, Aryl); 7.44 (d, 2H, Aryl); 7.70 (s, 1H, H-4). (B) : <sup>1</sup>H NMR (400 MHz, CDCl<sub>3</sub>) δ 1.15-1.22 (m, 4H, CH<sub>2</sub>); 1.41 (t, 3H, CH<sub>3</sub>); 1.64-1.78 (m, 6H, CH<sub>2</sub>); 2.06 (t, 1H, CH); 3.34 (d, 1H, J = 12.0 Hz, H-5'a); 3.92 (dd, 1H, J' = 6.0 and 11.6 Hz, H-5'b); 4.37 (q, 2H, CH<sub>2</sub>); 5.52 (d, 1H, J = 5.2 Hz, H-4'); 6.77 (d, 1H, J = 8.4 Hz, H-7); 7.49 (d, 1H, H-6); 7.56 (s, 1H, H-4). ESIMS m/z calcd for C<sub>26</sub>H<sub>26</sub>BrClN<sub>2</sub>O<sub>4</sub>S, 576.05; found, 576.15.

**Synthesis of (2'S,4'R)-5-bromo-N-(4-chlorophenyl), N-(4-chlorobenzyl) e N-(4-chlorophenethyl) -3'-(cyclohexanecarbonyl)-1-methyl-2-oxospiro[indoline-3,2'-thiazolidine]-4'-carboxamide derivatives. (22a-c)**

SM13<sup>101</sup> [Paragraph 4.1.1] (1 mmol) was added to a H<sub>2</sub>O/CH<sub>3</sub>OH solution in 9/1 ratio and 3 mmol of NaOH. The reaction is was stirring for 3 hours at room temperature and monitored by TLC (ethyl acetate / methanol, 9/1) Subsequently, the solvent is evaporated under reduced pressure and the crude of reaction dissolved in ethyl acetate and the organic solvent is washed with a bicarbonate solution (3x100mL). The acetate was dried with Na<sub>2</sub>SO<sub>4</sub> and evaporated in vacuo, obtaining a quantitative yield. The intermediate **21** was presented as an orange oil. From 5 mmol of the derivative **21**, dissolved in dichloromethane and DMF, (9/1) (50 mL) HOBt (6.0 mmol), DIC (6.0 mmol), DIPEA (12.0 mmol) and 4-Cl aniline, or 4-Cl benzylamine, or 4-Cl phenethylamine (6.0 mmol) were added. After 12 hours the reaction was

stopped; the dichloromethane was washed with water (3 x 150 mL). The organic solvent was then dried over anhydrous sodium sulfate and evaporated under vacuum. The final product were obtained by purification through column chromatography using silica gel as stationary phase and as eluent a suitable mixture of ethyl acetate / n-hexane. The product **22a-c** were isolated as single diastereomers with a yield ranging between 32 and 44% and characterized by NMR spectroscopy and mass spectrometry.

***(2'S,4'R)-5-bromo-N-(4-chlorophenyl)-3'-(cyclohexanecarbonyl)-1-methyl-2-oxospiro[indoline-3,2'-thiazolidine]-4'-carboxamide. (22a)***

Overall yield 44%. (A) : <sup>1</sup>H NMR (400 MHz, CDCl<sub>3</sub>) δ 1.15-1.18 (m, 4H, CH<sub>2</sub>); 1.56-1.87 (m, 6H, CH<sub>2</sub>); 2.34 (t, 1H, CH); 3.24 (s, 3H, CH<sub>3</sub>); 3.62 (d, 1H, J = 12.0 Hz, H-5'a); 4.18 (dd, 1H, J' = 6.0 and 11.6 Hz, H-5'b); 5.21 (d, 1H, J = 6.8 Hz, H-4'); 6.68 (d, 1H, J = 8.4 Hz, H-7); 7.27-7.70 (m, 6H, H-6, H-4 and aryl); (B) : <sup>1</sup>H NMR (400 MHz, CDCl<sub>3</sub>) δ 1.15-1.22 (m, 4H, CH<sub>2</sub>); 1.64-1.78 (m, 6H, CH<sub>2</sub>); 2.17 (t, 1H, CH); 3.26 (s, 3H, CH<sub>3</sub>); 3.64 (d, 1H, J = 12.0 Hz, H-5'a); 4.24-4.27 (m, 1H, H-5'b); 4.51-4.54 (m, 1H, CH<sub>2a</sub>); 4.74-4.76 (m, 1H, CH<sub>2b</sub>); 5.77 (d, 1H, J = 5.2 Hz, H-4'); 6.68 (d, 1H, J = 8.4 Hz, H-7); 7.26-7.35 (m, 6H, H-6, H-4 and aryl). ESIMS m/z calcd for C<sub>25</sub>H<sub>27</sub>BrClN<sub>3</sub>O<sub>2</sub>S, 547,07; found, 548,92.

***(2'S,4'R)-5-bromo-N-(4-chlorobenzyl)-3'-(cyclohexanecarbonyl)-1-methyl-spiro[indoline-3,2'-thiazolidine]-4'-carboxamide. (22b)***

Overall yield 32%. (A). <sup>1</sup>H NMR (400 MHz, CDCl<sub>3</sub>) δ 1.12-1.30 (m, 4H, CH<sub>2</sub>); 1.57-1.82 (m, 6H, CH<sub>2</sub>); 2.22 (t, 1H, CH); 3.21 (s, 3H, CH<sub>3</sub>); 3.56 (d, 1H, J = 12.0 Hz, H-5'a); 4.02 (dd, 1H, J' = 6.0 and 11.6 Hz, H-5'b); 4.51 (dd, 1H, CH<sub>2a</sub> J' = 6.8, J'' = 14.8 Hz); 4.73 (dd, 1H, CH<sub>2b</sub> J' = 6.8, J'' = 14.8 Hz); 5.04 (d, 1H, J = 6.8 Hz, H-4'); 6.68 (d, 1H, J = 8.4 Hz, H-7); 6.76-6.79 (m, 2H, H-6 and aryl); 7.02 (s, 1H, H-4); 7.26-7.40 (m, 3H, aryl); (B): <sup>1</sup>H NMR (400 MHz,

CDCl<sub>3</sub>)  $\delta$  1.15-1.22 (m, 4H, CH<sub>2</sub>); 1.64-1.78 (m, 6H, CH<sub>2</sub>); 2.17 (t, 1H, CH); 3.25 (s, 3H, CH<sub>3</sub>); 3.64 (d, 1H,  $J = 12.0$  Hz, H-5'a); 4.24-4.27 (m, 1H, H-5'b); 4.51-4.54 (m, 1H, CH<sub>2a</sub>); 4.74-4.76 (m, 1H, CH<sub>2b</sub>); 5.49 (d, 1H,  $J = 5.2$  Hz, H-4'); 6.68 (d, 1H,  $J = 8.4$  Hz, H-7); 7.26-7.35 (m, 6H, H-6, H-4 and aryl). ESIMS  $m/z$  calcd for C<sub>26</sub>H<sub>29</sub>BrClN<sub>3</sub>O<sub>2</sub>S, 561.09; found, 562.95.

***(2'S,4'R)-5-bromo-N-(4-chlorophenethyl)-3'-(cyclohexanecarbonyl)-1-methyl-2-oxospiro [indoline-3,2'-thiazolidine]-4'-carboxamide. (22c)***

Overall yield 44%. (A) : <sup>1</sup>H NMR (400 MHz, CDCl<sub>3</sub>)  $\delta$  1.13-1.34 (m, 4H, CH<sub>2</sub>); 1.56-1.84 (m, 6H, CH<sub>2</sub>); 2.11 (t, 1H, CH); 2.93-3.12 (m, 2H, CH<sub>2</sub>); 3.23 (s, 3H, CH<sub>3</sub>); 3.51 (d, 1H,  $J = 12.0$  Hz, H-5'a); 3.72-3.79 (m, 2H, CH<sub>2</sub>); 4.01 (dd, 1H,  $J' = 6.0$  and  $11.6$  Hz, H-5'b); 5.01 (d, 1H,  $J = 6.8$  Hz, H-4'); 6.49 (s, 1H, NH); 6.72 (d, 1H,  $J = 8.4$  Hz, H-7); 7.24-7.69 (m, 5H, H-4, H-6 and aryl); 7.48 (d, 1H, aryl); (B): <sup>1</sup>H NMR (400 MHz, CDCl<sub>3</sub>)  $\delta$  1.13-1.19 (m, 7H, CH<sub>2</sub> and CH<sub>3</sub>); 1.62-1.75 (m, 6H, CH<sub>2</sub>); 2.16 (t, 1H, CH); 2.95-3.13 (m, 2H, CH<sub>2</sub>); 3.26 (s, 3H, CH<sub>3</sub>); 3.62 (d, 1H,  $J = 12.0$  Hz, H-5'a); 3.74-3.77 (m, 2H, CH<sub>2</sub>); 4.23-4.25 (m, 1H, H-5'b); 5.49 (d, 1H,  $J = 5.2$  Hz, H-4'); 6.67 (d, 1H,  $J = 8.4$  Hz, H-7); 7.25-7.59 (m, 6H, H-6, H-4 and aryl). ESIMS  $m/z$  calcd for C<sub>27</sub>H<sub>29</sub>BrClN<sub>3</sub>O<sub>3</sub>S; 589.08 found, 590.06.

***Synthesis of (2'S,4'R)-benzyl 5-bromo-3'-(cyclohexanecarbonyl)-1-methyl-2-oxospiro[indoline-3,2'-thiazolidine]-4'-carboxylate derivative (23a) and (2'S,4'R)-methyl 5-bromo-3'-(cyclohexanecarbonyl)-1-methyl-2-oxospiro[indoline-3,2'-thiazolidine]-4'-carboxylate derivative. (23b)***

The intermediate **21** (1 mmol), synthesized as described previously, was solubilized in a toluene and methyl alcohol solution (1/1) (for the compound **23b**) or toluene and benzyl alcohol (1/1) (for the compound **23a**), (1 mmol) of *p*-toluene sulfonic acid was added. The reaction is stirring at reflux temperature for 16 h. Subsequently, the solvent was evaporated under reduced pressure and

the crude is solubilized in dichloromethane and extracted with water (3 x 100 mL), the organic phase is dried on anhydrous sodium sulphate and evaporated in vacuo. The final products (**23a,b**) are obtained by purification through column chromatography using silica gel as stationary phase and as eluent a suitable mixture of ethyl acetate / n-hexane as single diastereoisomer.

**(2'S,4'R)-benzyl 5-bromo-3'-(cyclohexanecarbonyl)-1-methyl-2-oxospiro[indoline-3,2'-thiazolidine]-4'-carboxylate derivative. (23a)**

Overall yield 38%. (**A**): <sup>1</sup>H NMR (400 MHz, CDCl<sub>3</sub>) δ 1.14-1.75 (m, 10H, CH<sub>2</sub>); 2.19 (t, 1H, CH); 3.22 (s, 3H, CH<sub>3</sub>); 3.48 (d, 1H, J = 12.0 Hz, H-5'a); 3.96-3.99 (m, 1H, H-5'b); 5.15 (d, 1H, J = 8.0 Hz, H-4'); 5.37 (dd, 2H, CH<sub>2</sub>, J' = 8.0 Hz, J'' = 32.0 Hz); 6.66 (d, 1H, J = 8.4 Hz, H-7); 7.26-7.55 (m, 6H, H-6 and aryl); 7.60 (s, 1H, H-4). (**B**): <sup>1</sup>H NMR (400 MHz, CDCl<sub>3</sub>) δ 1.14-1.75 (m, 10H, CH<sub>2</sub>); 2.18 (t, 1H, CH); 3.25 (s, 3H, CH<sub>3</sub>); 3.49 (d, 1H, J = 12.0 Hz, H-5'a); 4.30 (dd, 1H, J' = 6.0 and 11.6 Hz, H-5'b); 5.21-5.23 (d, 2H, CH<sub>2</sub>, J = 8.0 Hz); 5.58 (d, 1H, J = 5.2 Hz, H-4'); 6.79 (d, 1H, J = 8.0 Hz, H-7); 7.48 (d, 1H, H-6); 7.54 (s, 1H, H-4). ESIMS m/z calcd for C<sub>26</sub>H<sub>27</sub>BrN<sub>2</sub>O<sub>4</sub>S, 542.09; found, 543.47.

**(2'S,4'R)-methyl 5-bromo-3'-(cyclohexanecarbonyl)-1-methyl-2-oxospiro[indoline-3,2'-thiazolidine]-4'-carboxylate derivative. (23b)**

Overall yield 41%. (**A**): <sup>1</sup>H NMR (400 MHz, CDCl<sub>3</sub>) δ 1.18-1.81 (m, 10H, CH<sub>2</sub>); 2.18 (t, 1H, CH); 3.23 (s, 3H, CH<sub>3</sub>); 3.49 (d, 1H, J = 12.0 Hz, H-5'a); 3.98 (s, 3H, CH<sub>3</sub>); 4.02 (dd, 1H, J' = 6.0 and 11.6 Hz, H-5'b); 5.18 (d, 1H, J = 8.0 Hz, H-4'); 6.70 (d, 1H, J = 8.4 Hz, H-7); 7.43 (d, 1H, H-6); 7.60 (s, 1H, H-4). (**B**): <sup>1</sup>H NMR (400 MHz, CDCl<sub>3</sub>) δ 1.14-1.80 (m, 10H, CH<sub>2</sub>); 2.16 (t, 1H, CH); 3.48 (s, 3H, CH<sub>3</sub>); 3.73 (d, 1H, J = 12.0 Hz, H-5'a); 3.90 (s, 3H, CH<sub>3</sub>); 4.46 (dd, 1H, J' = 6.0 and 11.6 Hz, H-5'b); 5.55 (d, 1H, J = 5.2 Hz, H-4'); 6.77

(d, 1H,  $J = 8.4$  Hz, H-7); 7.49 (d, 1H, H-6); 7.56 (s, 1H, H-4). ESIMS  $m/z$  calcd for  $C_{20}H_{23}BrN_2O_4S$ , 466.06; found, 467.38.

***Synthesis of (4'R)-ethyl 5-bromo-3'-(cyclohexanecarbonyl)-1,5',5'-trimethyl-2-oxospiro[indoline-3,2'-thiazolidine]-4'-carboxylate derivative (25) and (2'R,4'S)-ethyl 5-bromo-3'-(cyclohexanecarbonyl)-1-methyl-2-oxospiro[indoline-3,2'-thiazolidine]-4'-carboxylate derivative. (26)***

$NaHCO_3$  (1.0 g, 12 mmol) and 5-bromo-1-methyl isatin (6, 2.4 g, 10 mmol) were added to a solution of *L*-Pen-OEt (2.3 g, 12 mmol) for compound **24a**, or *D*-Cys-OEt (2.3 g, 12 mmol) for compound **24b**, in ethanol (100 mL), and the suspension was stirred at room temperature for 12 h. Then the suspension was filtered, and the filtrate was concentrated. Spiro(oxoindolethiazolidine) ethyl ester residue was dissolved in DCM and washed with water ( $3 \times 50$  mL). The combined organic layer was dried over anhydrous sodium sulfate, filtered, and concentrated. A 5:1 diastereoisomeric mixture of the title's compound was obtained as an oil with 73% yield. The compound were used in the next reaction without further purification. To a solution of **24a** and **24b** derivatives (5 mmol) in THF (50 mL) was added a solution of cyclohexanecarbonyl chlorides (5.5 mmol) in THF (10 mL) and TEA (10 mmol). The reaction mixture was stirred at room temperature for 2 h, and water was then added. The organic solution was washed with water ( $3 \times 100$  mL), dried over  $Na_2SO_4$ , and evaporated in vacuo. Flash chromatography on silica gel, using ethyl acetate/*n*-hexane as eluent, overall yielded the corresponding final derivatives as oil.

***(4'R)-ethyl 5-bromo-3'-(cyclohexanecarbonyl)-1,5',5'-trimethyl-2-oxospiro[indoline-3,2'-thiazolidine]-4'-carboxylate derivative. (25)***

Overall yield 37%. **(A)**:  $^1\text{H}$  NMR (400 MHz,  $\text{CDCl}_3$ )  $\delta$  1.18-1.24 (m, 4H,  $\text{CH}_2$ ); 1.40 (t, 3H,  $\text{CH}_3$ ); 1.60-1.71 (m, 6H,  $\text{CH}_2$ ); 1.77 (s, 6H,  $\text{CH}_3$ ); 2.15 (t, 1H,  $\text{CH}$ ); 3.24 (s, 3H,  $\text{CH}_3$ ); 4.41 (q, 2H,  $\text{CH}_2$ ); 5.03 (d, 1H,  $J = 4.2$  Hz, H-4'); 6.74 (d, 1H,  $J = 8.0$  Hz, H-7); 7.35 (d, 1H, H-6); 7.59 (s, 1H, H-4). **(B)**:  $^1\text{H}$  NMR (400 MHz,  $\text{CDCl}_3$ )  $\delta$  1.18-1.24 (m, 4H,  $\text{CH}_2$ ); 1.40 (t, 3H,  $\text{CH}_3$ ); 1.60-1.73 (m, 6H,  $\text{CH}_2$ ); 1.80 (s, 6H,  $\text{CH}_3$ ); 2.21 (t, 1H,  $\text{CH}$ ); 3.29 (s, 3H,  $\text{CH}_3$ ); 4.35 (q, 2H,  $\text{CH}_2$ ); 5.12 (d, 1H,  $J = 5.2$  Hz, H-4'); 6.69 (d, 1H,  $J = 8.4$  Hz, H-7); 7.49 (d, 1H, H-6); 7.55 (s, 1H, H-4). ESIMS  $m/z$  calcd for  $\text{C}_{23}\text{H}_{29}\text{BrN}_2\text{O}_4\text{S}$ , 508.10; found, 508.18.

**(2'R,4'S)-ethyl 5-bromo-3'-(cyclohexanecarbonyl)-1-methyl-2-oxospiro[indoline-3,2'-thiazolidine]-4'-carboxylate derivative. (26)**

Overall yield 49%.  $[\alpha]^{25}_{\text{D}} +40.5^\circ$  ( $c$  0.8, MeOH). **(A)**:  $^1\text{H}$  NMR (400 MHz,  $\text{CDCl}_3$ )  $\delta$  1.15-1.22 (m, 4H,  $\text{CH}_2$ ); 1.41 (t, 3H,  $\text{CH}_3$ ); 1.64-1.78 (m, 6H,  $\text{CH}_2$ ); 2.17 (t, 1H,  $\text{CH}$ ); 3.20 (s, 3H,  $\text{CH}_3$ ); 3.47 (d, 1H,  $J = 12.0$  Hz, H-5'a); 3.97 (dd, 1H,  $J' = 6.0$  and 11.6 Hz, H-5'b); 4.41 (q, 2H,  $\text{CH}_2$ ); 5.13 (d, 1H,  $J = 5.6$  Hz, H-4'); 6.67 (d, 1H,  $J = 8.4$  Hz, H-7); 7.39 (d, 1H, H-6); 7.57 (s, 1H, H-4). **(B)**:  $^1\text{H}$  NMR (400 MHz,  $\text{CDCl}_3$ )  $\delta$  1.15-1.22 (m, 4H,  $\text{CH}_2$ ); 1.41 (t, 3H,  $\text{CH}_3$ ); 1.64-1.78 (m, 6H,  $\text{CH}_2$ ); 2.17 (t, 1H,  $\text{CH}$ ); 3.26 (s, 3H,  $\text{CH}_3$ ); 3.34 (d, 1H,  $J = 12.0$  Hz, H-5'a); 3.92 (dd, 1H,  $J' = 6.0$  and 11.6 Hz, H-5'b); 4.37 (q, 2H,  $\text{CH}_2$ ); 5.52 (d, 1H,  $J = 5.2$  Hz, H-4'); 6.77 (d, 1H,  $J = 8.4$  Hz, H-7); 7.49 (d, 1H, H-6); 7.56 (s, 1H, H-4). ESIMS  $m/z$  calcd for  $\text{C}_{21}\text{H}_{25}\text{BrN}_2\text{O}_4\text{S}$ , 480.07; found, 480.15.

## 6.2 Biology

Dulbecco's modified Eagle medium (DMEM), fetal bovine serum (FBS), trypsin-EDTA solution (1 $\times$ ), penicillin and streptomycin, and phosphate buffered saline (PBS) were from Cambrex Biosciences. 3 (4,5-Dimethylthiazol-2-yl)-2,5-diphenyltetrazolium bromide (MTT), propidium iodide (PI), Triton X-100, sodium citrate, and formamide were purchased from Sigma (Milan, Italy).

### **6.2.1 Cell culture**

Human breast cancer (MCF-7) cell lines and human colorectal adenocarcinoma cell lines (HT-29) were grown at 37 °C in Dulbecco's modified Eagle medium containing 10 mM glucose (DMEMHG) supplemented with 10% fetal calf serum and 100 units/mL each of penicillin and streptomycin and 2 mmol/L glutamine. In each experiment, cells were placed in fresh medium, cultured in the presence of synthesized compounds (from 0.1 to 25 mM), and followed for further analyses.

### **6.2.2 Cell viability assay**

Cell viability was determined using the 3[4,5- dimethylthiazol-2,5-diphenyl-2H-tetrazolium bromide (MTT) colorimetric assay. The test is based on the ability of mitochondrial dehydrogenase to convert, in viable cells, the yellow MTT reagent (Sigma Chemical Co., St. Louis, MO) into a soluble blue formazan dye. Cells were seeded into 96-well plates to a density of  $10^5$  cells/100  $\mu$ L well. After 24 h of growth to allow attachment to the wells, compounds were added at various concentrations (from 0.1 to 25 M). After 24 or 48 h of growth and after removal of the culture medium, 100  $\mu$ L/well medium containing 1 mg/mL MTT was added. Microplates were further incubated at 37 °C for 2 h in the dark. The solution was then gently aspirated from each well, and the formazan crystals within the cells were dissolved with 100  $\mu$ L of DMSO. Optical densities were read at 550 nm using a Multiskan Spectrum Thermo Electron Corporation reader. Results were expressed as percentage relative to vehicle-treated control (0.5% DMSO was added to untreated cells). IC<sub>50</sub> (concentration eliciting 50% inhibition) values were determined by linear and polynomial regression. Experiments were performed in triplicate.

**CHAPTER VII**  
**BIOLOGICAL BASES FOR SM13 TUMOR**  
**GROWTH INHIBITION**

### **7.1 Background**

Since the chemical modification on the structure of the lead compound **SM13** did not allow the identification of more potent derivatives, further investigations about the biochemical mechanism of action of **SM13** were conducted using some focused biological assays.

### **7.2 Effects of SM13 on KAT-4 cell proliferation in vitro**

The effectiveness of the spiro[indoline-3,2'-thiazolidine] derivate compound, **SM13**, in the regulation of apoptotic signalling in a several p53 WT tumour cells lines has already been demonstrated [Paragraph 3.3.1, Table 1 and Table 2]. Thus, in the Department of Advanced Biochemical Sciences, of the University of Naples, 'Federico II', the effect of **SM13** in a p53 mutant cell line (KAT-4) was evaluated. It was found that **SM13** reduces KAT-4 cell proliferation both at 24 and 48h after treatment (Figure 28A).<sup>121</sup>

Giving the mutation of p53 gene in KAT-4 cells, which inhibits its transcriptional activity, we evaluated the effect of **SM13** on mitochondrial-dependent apoptotic signalling. Indeed, recent studies have shown that interactions of p53 with various members of the Bcl-2 family cause mitochondrial-mediated apoptosis in a transcription-independent manner.<sup>122</sup> Accordingly, our data showed that **SM13** induced p53 levels, increased the expression of the proapoptotic protein Bax, leading to the release of cytochrome-c. This event leads to the activation of both Caspase 9 and Caspase 3, thus, inducing cell death (Figure 28B).<sup>106</sup>

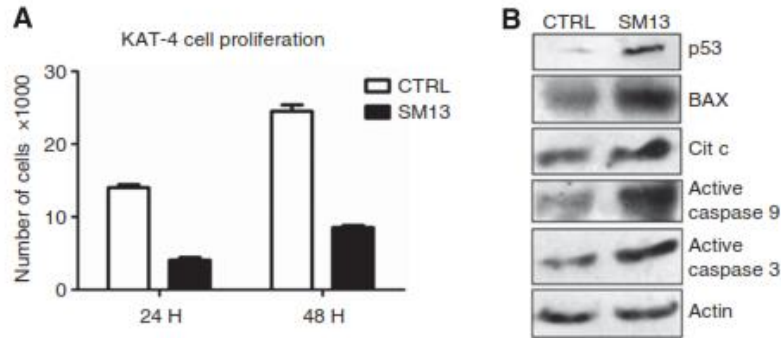


**Figure 28.** Effects of SM13 on tumour cell growth in vitro. (A) KAT-4 cells were treated with SM13 for 24 and 48 h, and cell proliferation was analyzed. (\* $P < 0.05$  vs control 24H; \*\* $P < 0.05$  vs control 48H). Results are representative of five independent experiments and are presented as mean  $\pm$  s.e.m. (B) To evaluate the mechanism of action of SM13, we analyzed its effect on mitochondrial-dependent apoptotic signalling by western blot. Images are the mean of three independent experiments

Accordingly, also the levels of Cyt-c in cytosolic extracts were increased (Figure 29A). Moreover SM13 does not modify gene expression of p53 (Figure 29B), thus confirming that SM13 rather inhibits p53 degradation.

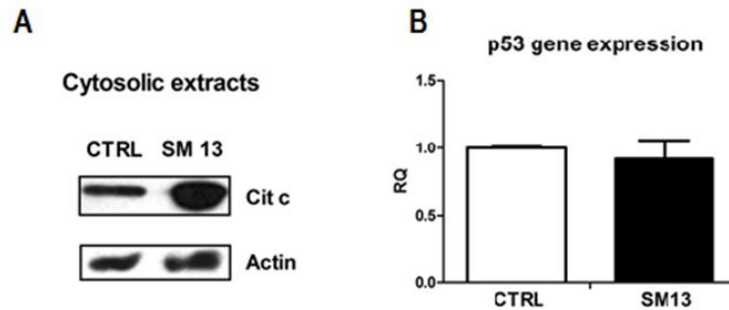


**Figure 29.** (A) To confirm the pro-apoptotic effect of SM13 we evaluated cytochrome c release from mitochondria towards cytosol by western blot. In cytosolic extracts, Cyt c levels were increased in treated cells respect to control. Images are representative of 3 independent experiments (\* $p < 0.05$  vs control). (B) To demonstrate the specificity of SM13 mechanism action to inhibit p53 degradation rather than regulate p53 gene expression, we performed a Real Time PCR to evaluate the effect of SM13 on p53 gene expression. Data show that there are no significant difference between control and treated cells. Results are the mean of 5 independent experiments (\* $p < 0.05$  vs control)

To confirm the apoptotic effect of **SM13**, we evaluated DNA fragmentation through a TUNEL assay. Figure 30 shows that treatment with **SM13** induced apoptotic events in tumour cells. All together, these data suggest that **SM13** is able to induce apoptosis in tumour cells by activating mitochondrial apoptotic signalling.

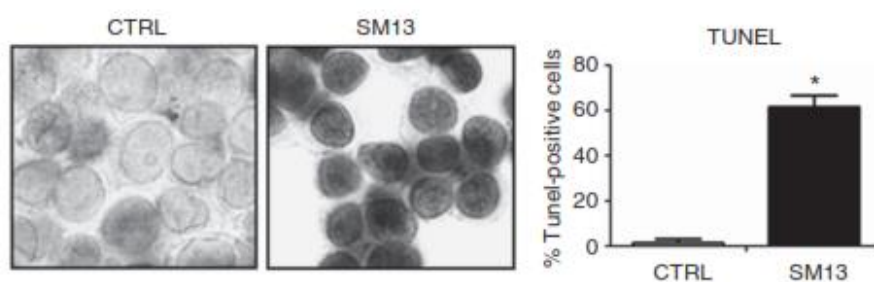


**Figure 30.** TUNEL assay. Positive nuclei were counted and results were expressed in graph as mean  $\pm$  s.d. SM13 is able to induce apoptotic events in tumour cells. Images are representative of three independent experiments

Moreover, to confirm the p53 transcription independent effect of **SM13**, gene expression of p53 target genes, p21 and Gadd45, was assessed. In a p53 WT tumour cell line (MCF7) the treatment with SM13 induced p21 and Gadd45 gene expression, whereas in p53-mutant cell type (KAT-4) such phenomenon was reduced. These data suggest that the effects of SM13 are strictly dependent on p53, and given the lack of transcriptional activity of p53 (Figure 31), they are due to the activation of p53-dependent mitochondrial apoptotic pathway.<sup>106</sup>

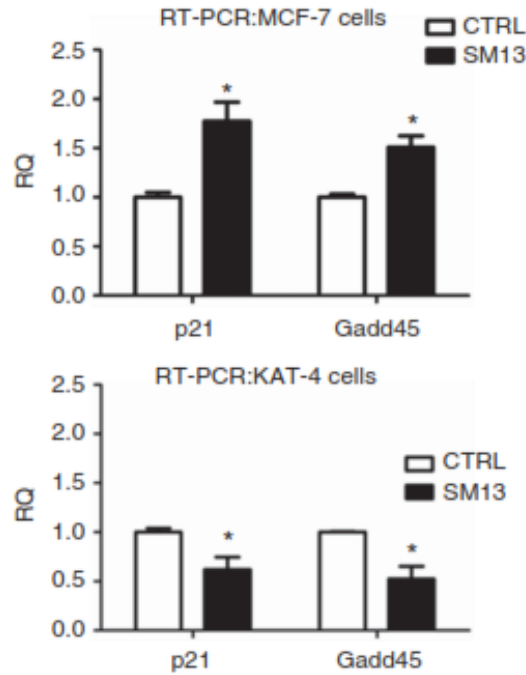


**Figure 31.** To confirm the p53 transcription-independent effect of SM13, we evaluated gene expression of p53 target genes, p21 and Gadd45. In a p53 WT tumour cell line, MCF7, the treatment with SM13 induced p21 and Gadd45 gene expression, whereas in p53-mutant cell type, KAT-4, such phenomenon was reduced (\* $P < 0.05$  vs control). Results are the mean of five independent experiments and are presented as mean  $\pm$  s.e.m.

### 7.3 Effects of SM13 on FRO cell proliferation in vitro

To assess the specificity of SM13 effectiveness in the regulation of p53-dependent apoptosis, we evaluated its effects in FRO cells, a tumour cell line which does not express p53.<sup>123</sup> Figure 32 shows that SM13 increased cleaved caspase 3 levels in KAT-4, but not in FRO cells; thus, suggesting that the ability of SM13 to induce apoptosis strictly depends on p53.<sup>106</sup>

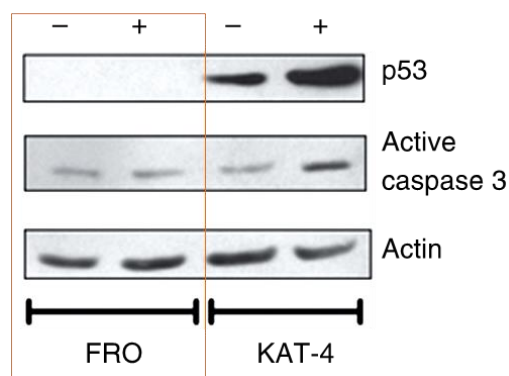


**Figure 32.** The ability of SM13 to induce apoptosis was evaluated in FRO cells, a tumour cell line, which do not express p53. p53 and cleaved caspase 3 levels were evaluated by western blot. SM13 was not able to regulate cleaved caspase 3 levels in FRO cells with respect to KAT-4 cells. Results are representative of three independent experiments

#### 7.4 Effects of SM13 on KAT-4 cell growth in vivo

To confirm in vitro data, we evaluated the effect of **SM13** on tumour growth in vivo. Experiments were carried out, in 6-week-old BALB/c nude mice. For tumour formation, a suspension containing  $2 \times 10^6$  KAT-4 cells in 200 ml of DMEM were injected subcutaneously in the dorsal side of nude mice, as previously described by Sorriento's research group.<sup>124</sup> Mice were divided into four groups (5 mice per group) and administered twice a week for 2 weeks with intra-tumour or intraperitoneal injections (IP) of the specific treatment of **SM13**. In particular, two groups received intra-tumour injection of **SM13** at low (low:  $1 \text{ mg kg}^{-1}$ ) or high dosage (high:  $3 \text{ mg kg}^{-1}$ ); another group received IP of  $5 \text{ mg kg}^{-1}$  of the compound and; the control group received intra-tumour or IP of DMSO. The IP of DMSO did not modify tumour growth with respect to intra-tumour injection. Tumour growth was measured by caliper twice a week and expressed as tumour volumes in  $\text{mm}^3$ . Data show that **SM13** is a potent inhibitor of tumour growth in a dose-dependent manner. Indeed, the intra-tumour injection of **SM13** inhibited tumour growth at low dosages and was more

efficient at high dosages. Also the intra-peritoneal treatment strongly delayed tumour growth. (Figure 33)

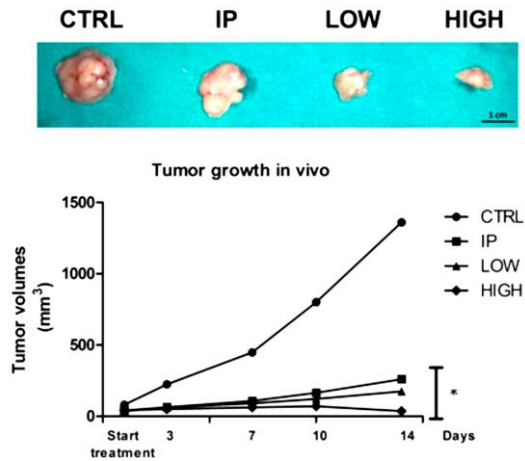


**Figure 33.** Effects of SM13 on tumour growth in vivo. To validate *in vitro* results, we studied the effects of SM13 *in vivo* in Balb/c nude mice. Tumour growth was measured twice a week by a caliper during all the treatment long (14 days of treatment). SM13 retard tumour growth compared with controls. Results are the mean of measurements from five mice per group (\* $P < 0.05$  vs control). Figure also shows a representative image of tumours at the end of the treatment

To confirm the mechanism by which SM13 induced apoptosis, we evaluated its effect on mitochondrial signalling in tumours from treated and control mice. According to *in vitro* data, intra-tumour injection of low and high doses of SM13 significantly increased p53, Bax, Cit-C, active caspase 9 and active caspase 3 levels in a dose-dependent manner. (Figure 34)<sup>106</sup>

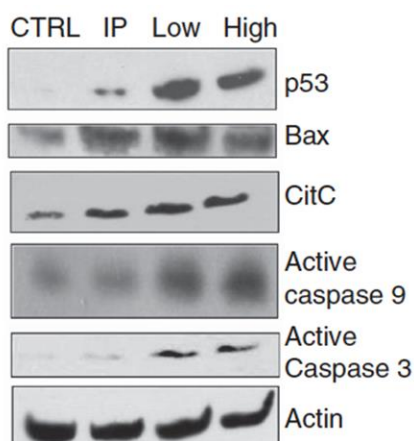


**Figure 34.** Tumours were homogenized to confirm by western blot analysis the effect of SM13 on mitochondrial-dependent apoptotic signalling. In treated tumours, SM13 increases protein levels of Bax and cytochrome c, and activates both caspase 9 and caspase 3. Images are the mean of five independent experiments

#### 7.4.1 Evaluation of side effects after treatment with SM13

Finally, we tested the safety of in vivo administration of our compound in healthy nude mice. There were no significant changes in body weight among treated and control groups of mice. No morphological differences were found in tissues from treated mice compared with controls (Figure 35). These data indicate that the treatments with **SM13** had no effects on mice health at the doses and time of treatment that were used in this study.

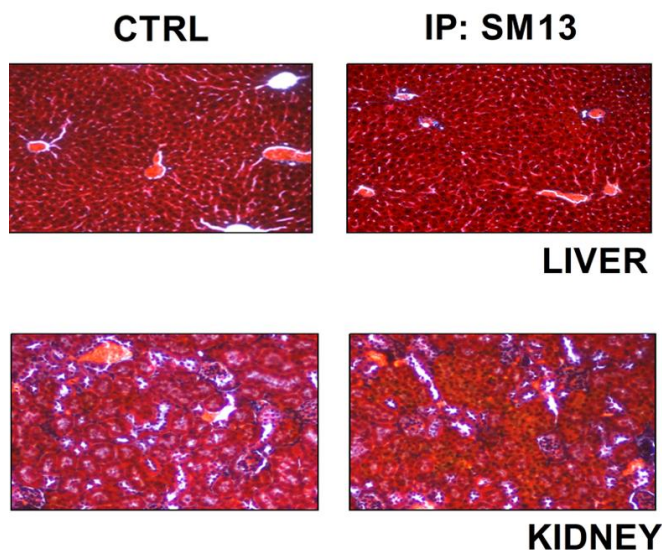


**Figure 35.** We tested the safety of *in vivo* administration of our compounds in healthy nude mice. Internal organs (liver and kidney) from mice treated with intra-peritoneal injection (IP) of SM13 (5mg/kg) were analyzed by Masson trichrome staining. No morphological differences were found in treated mice compared to controls. Images are the mean of 5 independent experiments

### 7.5 Discussion

Examining in depth the biochemical properties of SM13, it has been demonstrated how this molecule, at low doses, is capable of inducing the accumulation of p53 protein, simultaneously inducing significant apoptotic cell death also. Moreover, **SM13** proved to be a potent inhibitor of tumour growth in cells carrying a mutated p53 gene, being effective also at low dosages. It is known that p53 induces apoptotic events through the regulation of gene transcription in the nucleus. [Paragraph 1.6.1] Recently, it has been shown that p53 is also able to induce apoptosis in a transcription independent manner (Figure 36A) by the activation of the mitochondrial apoptotic signalling.<sup>125</sup> Indeed, it directly induces permeabilisation of the outer mitochondrial membrane by forming complexes with antiapoptotic proteins Bcl-x and Bcl-2, resulting in the release of cytochrome c in the cytosol. Moreover, it has been shown that p53 translocation to mitochondria occurs earlier after TPA

stimulation, leading to mitochondrial dysfunction.<sup>126</sup> The specific signalling involved in this transcriptional-independent effect of p53 on apoptosis is still unclear. What is known is that the transcriptional blockade of p53 by  $\alpha$ -amanitin induces p53 mitochondrial localization and Bax accumulation, and activation in mitochondria. Accordingly, here we show that SM13 induces apoptosis of KAT-4 cells, which express a mutated p53 protein lacking the transcriptional activity, by targeting p53-dependent mitochondrial signalling (Figure 36B). Indeed, the SM13-dependent increase of p53 levels, in KAT-4 cells is associated with the increase of BAX, release of cytochrome c, increase of cleaved caspase 3 levels and, finally, cell death. The confirmation that such mechanism strictly depends on p53, either WT or transcription activity deficient, derives from the finding that **SM13** has no effect on FRO cells, a cell line that does not express p53. It could be a compensatory response in those conditions, like cancer, in which p53 cannot activate gene transcription, but must induce cell death to block a pathological increase of cell growth. In conclusion, it has been evidenced that **SM13** is an effective regulator of p53 in KAT-4 cells. It is well known that the treatment of human tumours by a combination of selected drugs with different mechanisms of action decrease toxicity in comparison with monotherapy. In this context, **SM13** could be considered a good anticancer drug to be used in combination chemotherapy, as it is selective and does not generate side effects. **SM13**, in fact, has strong pro-apoptotic effects by regulating p53 turnover within the cell and it could be used as a prototype *small molecule* for cancer therapy.

In conclusion, during my PhD programme I contributed in the identification of **SM13** as a feasible anticancer agents, which could be used alone or in combination with other drugs to ameliorate the response to chemotherapy in a wide set of tumour types characterised by elevated levels of MDM2 and low levels of p53.<sup>106</sup>

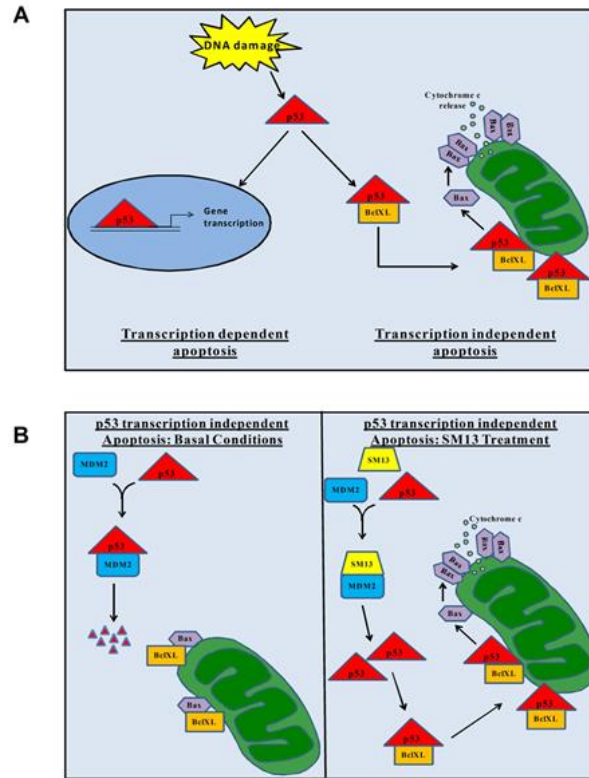


**Figure 36.** p53 transcription-dependent and -independent activation of apoptotic pathway. (A) p53 is activated in response to DNA damage and induces the apoptotic pathway through two alternative mechanisms, one dependent on transcriptional activity of p53 and one independent from transcriptional activity of p53. Indeed, activated p53 can move towards nucleus to activate the transcription of pro-apoptotic genes or move towards mitochondria to induce the release of cytochrome c. (B) Under basal conditions, MDM2 binds p53, thus leading to the degradation of the protein. SM13 inhibits MDM2/p53 binding by competing with p53 for binding to MDM2. SM13 therefore leads to the inhibition of MDM2dependent degradation of p53 and to the increase of p53 levels. p53 binds and inhibits antiapoptotic proteins (BclXL); thus, inducing Bax levels on mitochondrial membrane, which leads to the release of cytochrome c from mitochondria that on turn activates apoptotic events



**CHAPTER VIII**  
**EXPERIMENTAL SECTION OF BIOLOGICAL**  
**BASES FOR SM13**

### ***8.1 Cell culture***

MCF7, which express a WT variant of p53, KAT-4, which bears a p53 variant mutated at codon 273 (CGT-CAT; Arg-His), BHT101, which expresses a p53 mutant at codon 251 (ATC-ACC; Ile-Thr) and FRO cells, which do not express p53 at all, were cultured in Dulbecco's minimal essential medium (DMEM) supplemented with 10% foetal bovine serum (FBS) at 37 °C in 95% air – 5% CO<sub>2</sub>

### ***8.2 Compound***

SM13 was dissolved in absolute DMSO. Intra-peritoneal and intra-tumour injections of absolute DMSO were used for the treatment of control mice.

### ***8.3 Immunoprecipitation and Western Blot***

Immunoprecipitation and western blot analysis were performed as described in REF 110. Anti-p53, MDM2, Bax, Cytochrome c, Caspase 9 and Actin antibodies were from Santa Cruz Biotechnology, Inc. (Heidelberg, Germany); anti-cleaved caspase 3 antibody was from Cell Signalling (Danvers, MA, USA).

### ***8.4 Tunel assay***

Apoptosis was evaluated in KAT-4 cells after treatment with SM13, using the DeadEnd Colorimetric Tunel System from Promega (Madison, WI, USA), following the manufacturer's instructions. Results are expressed as mean ± s.d. of apoptotic nuclei.

### ***8.5 In vivo study design***

Experiments were carried out, in accordance to NIH guidelines for Animal Investigation, in 6-week-old BALB/c nude mice (Charles River Italia, Calco, Italy), which had access to food and water ad libitum. For tumour formation, a suspension containing  $2 \times 10^6$  KAT-4 cells in 200 µl of DMEM were injected

subcutaneously in the dorsal side of nude mice, as previously described.<sup>110</sup> Animals were anesthetised using isoflurane 2%. We used mice that developed tumours of B6 mm in diameter by 2 weeks. Mice were divided into four groups (5 mice per group) and administered twice a week for 2 weeks with intra-tumour or intraperitoneal injections (IP) of the specific treatment of **SM13**. In particular, two groups received intra-tumour injection of **SM13** at low (low: 1 mg kg<sup>-1</sup>) or high dosages (high: 3 mg kg<sup>-1</sup>); another group received IP of 5 mg kg compounds and; the control group received intra-tumour or IP of DMSO. The IP of DMSO did not modify tumour growth with respect to intra-tumour injection, thus in figures we include intratumour injection of DMSO as control for treated tumours. Tumour growth was measured by caliper twice a week and expressed as tumour volumes in mm<sup>3</sup> according to the formula 'Volume = ¼ (width)<sup>2</sup> x length/2'. At the end of the treatment, mice were killed by cervical dislocation and tumours were processed for biochemical or histological analysis. The 'Federico II' University Ethical Committed for Animal Studies approved all in vivo experimental protocols.



**CHAPTER IX**  
**DESIGN AND SYNTHESIS OF THIAZOLIDINE**  
**AND DIKETOPIPERAZINE BASED DERIVATIVES**  
**AS POTENTIAL p53 MODULATORS**

### 9.1 Background and design

In the search for structural modifications able in increasing the efficacy of **SM13** as p53 modulators, also different templates have been investigated during my Phd work. Considering the minimal structural requirements necessary to inhibit p53-MDM2 protein-protein interaction, evidenced in the previous chapters. two *privileged scaffolds*, namely thiazolidine and diketopiperazine nucleus were selected for the synthesis of new inhibitors. (Figure 37)

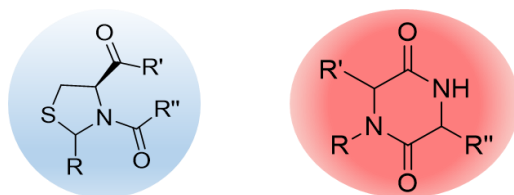


**Figure 37.** Thiazolidine and diketopiperazine nucleus selected

Both scaffolds, in fact, provide several derivatization groups. Moreover, the thiazolidine can be considered as a structural simplification of the previous libraries,<sup>99,100</sup> maintaining unchanged the portion of thiazolidine and substituting the indole nucleus by an aryl group. This modification increases *scaffold* flexibility and, therefore, may allow an optimal orientation of the substituents to the binding site. Similarly, the diketopiperazine nucleus is obtainable from reactions between different amino acids, being a particularly suitable *template* for the spatial orientation of the substituents. Thus, the diketopiperazine derivatives were designed using as aminoacidic building blocks the ones bringing the same substituents in the side chain of the amino acids involved in p53-MDM2 interaction. Hence, for my last year of PhD, I worked on the synthesis of two new libraries of thiazolidine and diketopiperazine based molecules designed as modulators of p53 activity. (Figure 38)

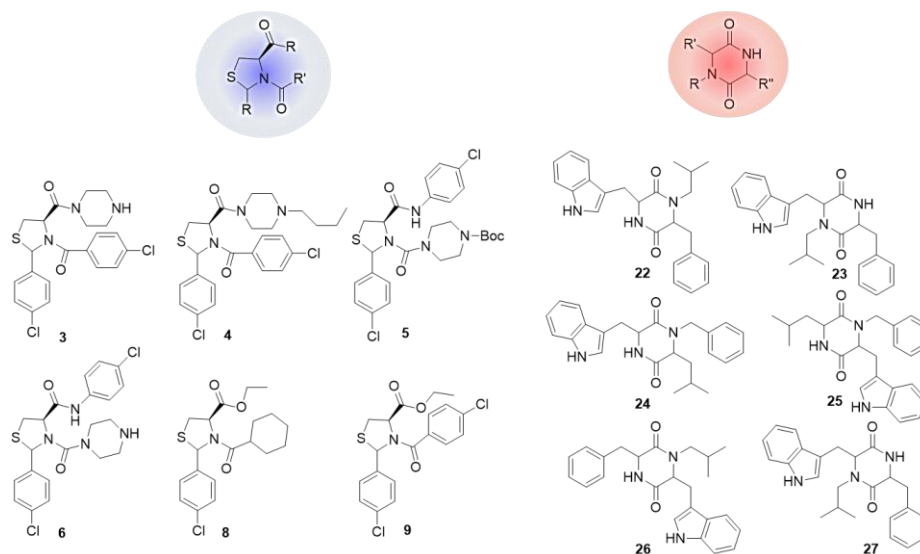


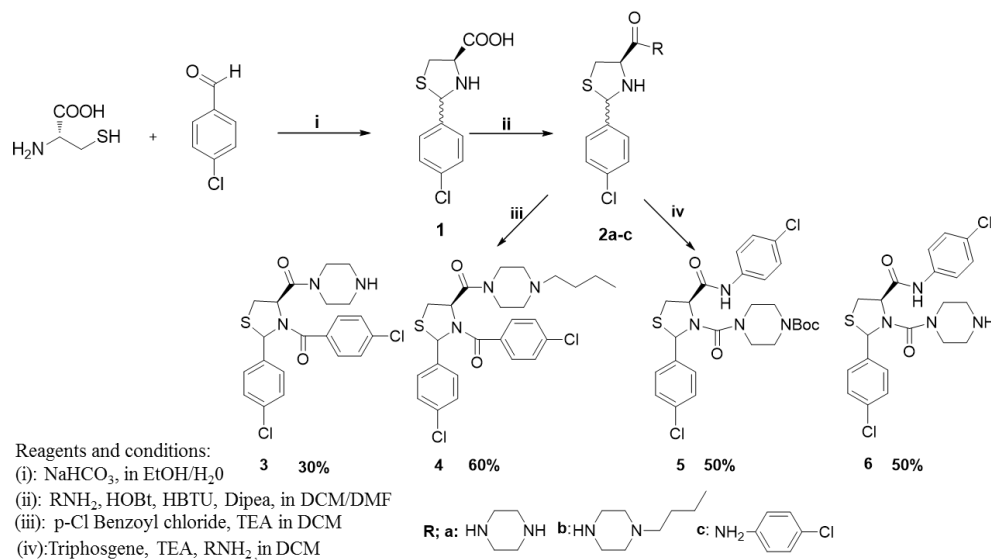
Figure 38. Synthesized compounds

## 9.2 Chemistry

### 9.2.1 Chemistry of Thiazolidine based derivatives

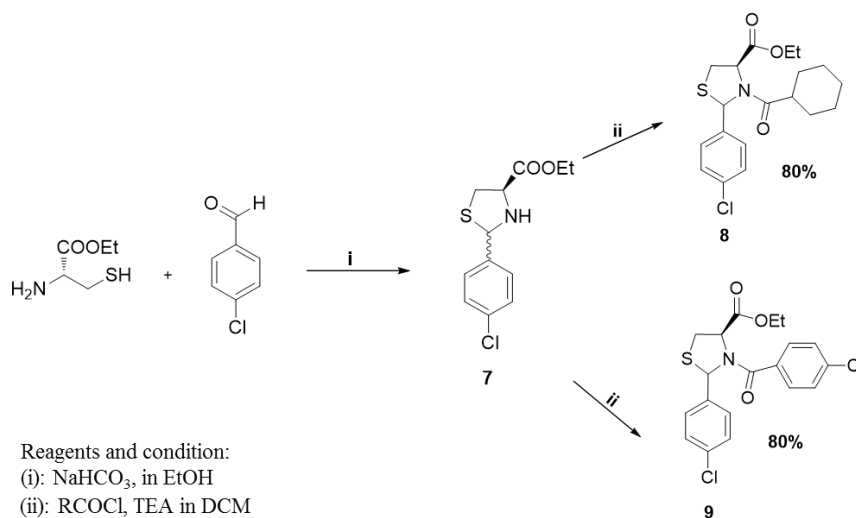
The new (4*R*)-2-(4-chlorophenyl)-*N*-(substituted)-3-substituted-4-carboxamide derivatives (**3-6**) were obtained starting from the synthesis of the thiazolidine **1** which was, subsequently, functionalized at the carboxyl using with different aromatic and alifatic amines as widely described previously.<sup>102</sup> (Scheme 7). The isomeric mixture of intermediate **2a-c** was then subjected to an acylation reaction of the *N*-3 by *p*-Cl benzoyl chloride in DCM with TEA used as base. The derivatives (**3, 4**) were obtained with a yield of 30% and 60% and as a pure diastereoisomer. Contrarily, the compounds **5** and **6** were synthesized as *N*-3 ureido analogues of the previously described intermediates by reaction with triphosgene and various aliphatic amines. Also in this case the final compounds were isolated as pure diastereomers with a yield around 50%.

**Scheme 7.** Synthesis of derivatives 3-6



The (4*R*)-ethyl 2-(4-chlorophenyl)-3-(cyclohexanecarbonyl) thiazolidine-4-carboxylate (**8**) and (4*R*)-ethyl 3-(4-chlorobenzoyl)-2-(4-chlorophenyl) thiazolidine-4-carboxylate (**9**) derivatives were prepared applying the synthetic route shown in Scheme 8. The thiazolidine ethyl ester derivative **7** was prepared as previously described and then derivatized at the N-3- thiazolidine by cyclohexanecarbonyl chloride or p-Cl benzoyl chloride in DCM and TEA as base leading to derivatives **8** and **9**, respectively. Final products were obtained with a yield of 80% and isolated as a pure diastereoisomer.

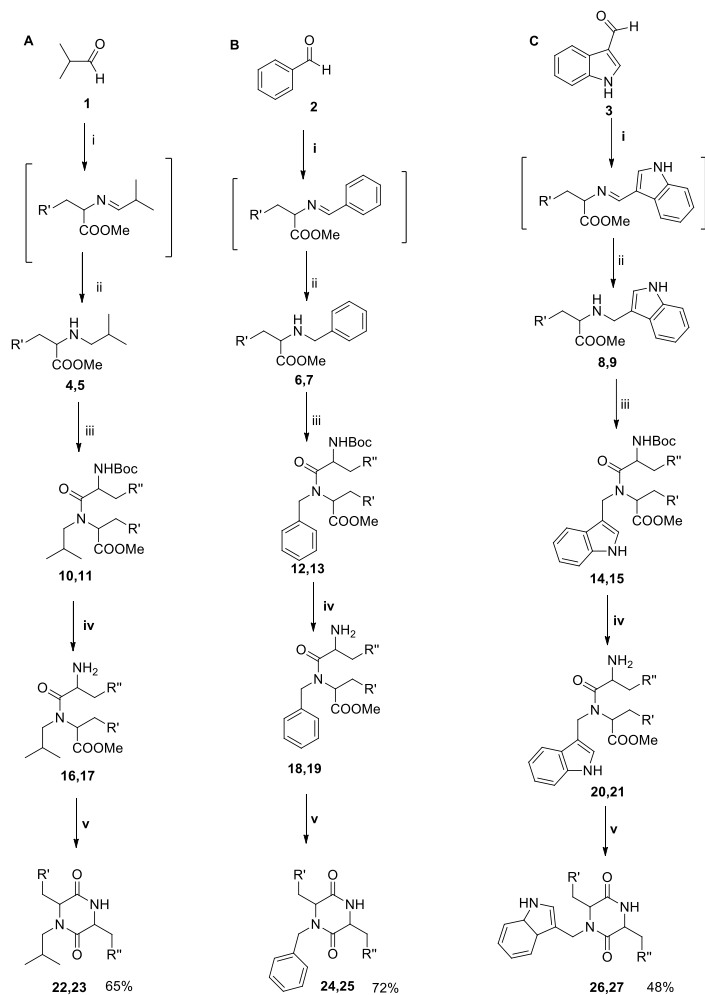
**Scheme 8.** Synthesis of (4*R*)-ethyl 2-(4-chlorophenyl)-3-(cyclohexanecarbonyl)thiazolidine-4-carboxylate (8) and (4*R*)-ethyl 3-(4-chlorobenzoyl)-2-(4-chlorophenyl)thiazolidine-4-carboxylate (9) derivatives



### 9.2.2 Chemistry of diketopiperazine based derivatives

The designed diketopiperazine derivatives (22-27) were prepared applying the general synthetic route shown in Scheme 9. All compounds were obtained by a reaction of reductive amination, between aldehydes properly selected amino acids. Followed by a coupling reaction with other aminoacids and intramolecular cyclization to the desired products. The final products maintained the starting chirality since racemization was not observed.

**Scheme 9.** General synthesis of diketopiperazine derivatives



A:

(i): R' = PheOMe  
or R' = TrpOMe

DCM/acetic acid in ratio 4:1

(ii): sodium triacetoxyborohydride

(iii): R'' = BocTrp  
or R'' = BocPhe

DCM/DMF 9:1; PyBop; HOAt and Dipea

(iv): DCM/TFA in ratio 3:1

(v): DCM/TEA under reflux temperature

B:

(i): R' = LeuOMe  
or R' = TrpOMe

DCM/acetic acid in ratio 4:1

(ii): sodium triacetoxyborohydride

(iii): R'' = BocTrp  
or R'' = BocLeu

DCM/DMF 9:1; PyBop; HOAt and Dipea

(iv): DCM/TFA in ratio 3:1

(v): DCM/TEA under reflux temperature

C:

(i): R' = PheOMe  
or R' = LeuOMe

DCM/acetic acid in ratio 4:1

(ii): 2,8 sodium triacetoxyborohydride

(iii): R'' = BocLeu  
or R'' = BocPhe

DCM/DMF 9:1; PyBop; HOAt and Dipea

(iv): DCM/TFA in ratio 3:1

(v): DCM/TEA under reflux temperature

### **9.3 Biological effects**

All synthesized derivatives are current in the process of biological assays to test their cytotoxic activity.



**CHAPTER X**  
**EXPERIMENTAL SECTION FOR THIAZOLIDINE**  
**AND DIKETOPIPERAZINE DERIVATIVES**

### 10.1 Chemistry

**Synthesis of ((4R)-3-(4-chlorobenzoyl)-2-(4-chlorophenyl)thiazolidin-4-yl)(piperazin-1-yl)methanone derivative (3) and (4-butylpiperazin-1-yl)((4R)-3-(4-chlorobenzoyl)-2-(4-chlorophenyl)thiazolidin-4-yl)methanone derivatives. (4)**

2-(4-chlorophenyl) thiazolidine-4-carboxylic acid <sup>102</sup> (**1**, 1.0 g, 4.11 mmol, 1.0 eq.) was dissolved in 30 ml of DCM/DMF (1/1 v/v). Then, HOBt (0.72 g, 5.34 mmol, 1.3 eq.), HBTU (2.02 g, 5.34 mmol, 1.3 eq.), DIPEA (1.86 ml, 10.7 mmol, 2.6 eq.) and piperazine (0.65 ml, 5.34 mmol, 1.2 eq.) (**2a**) or 1-butylpiperazine (0.65 ml, 5.34 mmol, 1.2 eq.) (**2b**) were added. The mixture was stirred at room temperature for 24h, then the organic phase was dried, crude product was dissolved in DCM, washed with water (2 x 30 mL), dried over Na<sub>2</sub>SO<sub>4</sub> and concentrated. Derivative **2a,b** were purified by Isolera One using a gradient from n-hexane to ethyl acetate/n-hexane 2:1 (v:v) and obtained as a colourless oil in around 65% of yield. Both the intermediates (**2a,b**) were derivatized with p-Clbenzoyl chloride in conditions previously described for obtaining **3** and **4** derivatives. They were purified by Isolera One using a gradient from n-hexane to ethyl acetate/n-hexane 2:1 with a yield 30% and 60% respectively.

**((4R)-3-(4-chlorobenzoyl)-2-(4-chlorophenyl)thiazolidin-4-yl)(piperazin-1-yl)methanone derivative. (3)**

Overall yield 67%. <sup>1</sup>H NMR (400 MHz, CDCl<sub>3</sub>) δ 2.65 (t, 1H, CH<sub>2</sub>); 2.77-2.81 (m, 4H, CH<sub>2</sub>); 2.99 (dd, 1H, CH<sub>2</sub>, J'=4.6, J''= 11.0 Hz); 3.40-3.44(m, 4H, CH<sub>2</sub>); 4.87 (t, 1H, CH); 5.99 (s, 1H, CH); 7.27-7.33 (m, 6H, aryl) 7.66 (d, 2H, J= 8.2 Hz). ESIMS m/z calcd for C<sub>21</sub>H<sub>21</sub>N<sub>3</sub>Cl<sub>2</sub>O<sub>2</sub>S, 449.07; found 449.13.

**(4-butylpiperazin-1-yl)((4R)-3-(4-chlorobenzoyl)-2-(4-chlorophenyl)thiazolidin-4-yl)methanone derivatives. (4)**

Overall yield 63%. <sup>1</sup>H NMR (400 MHz, CDCl<sub>3</sub>) δ 0.95 (t, 3H, CH<sub>3</sub>); 1.33-1.39(m, 2H, CH<sub>2</sub>); 1.50-1.61 (m, 2H, CH<sub>2</sub>); 3.11-3.17 (m, 2H, CH<sub>2</sub>); 2.55-2.68 (m, 4H, CH<sub>2</sub>); 2.81-2.85 (m, 1H, CH); 3.30-3.39 (m, 1H, CH); 3.77-3.89 (m, 4H, CH<sub>2</sub>); 5.19 (t, 1H, CH); 6.05 (s, 1H, CH); 7.18-7.39 (m, 6H, aryl) 7.92 (d, 2H, J= 8.2 Hz). ESIMS m/z calcd for C<sub>25</sub>H<sub>29</sub>N<sub>3</sub>ClO<sub>2</sub>S, 505.14; found 505.21.

*Synthesis of the tert-butyl 4-((4R)-2-(4-chlorophenyl)-4-((4-chlorophenyl)carbamoyl)thiazolidine-3-carbonyl)piperazine-1-carboxylate (5) and (4R)-N,2-bis(4-chlorophenyl)-3-(piperazine-1-carbonyl)thiazolidine-4-carboxamide derivatives. (6)*

2-(4-chlorophenyl) thiazolidine-4-carboxylic acid <sup>102</sup> (**1**, 1.0 g, 4.11 mmol, 1.0 eq.) was dissolved in 30 ml of DCM/DMF (1/1 v/v). Then, HOBT (0.72 g, 5.34 mmol, 1.3 eq.), HBTU (2.02 g, 5.34 mmol, 1.3 eq.), DIPEA (1.86 ml, 10.7 mmol, 2.6 eq.) p-Cl aniline (0.65 ml, 5.34 mmol, 1.2 eq.) were added. The mixture was stirred at room temperature for 24h, then the organic phase was dried, crude product was dissolved in DCM, washed with water (2 x 30 mL), dried over Na<sub>2</sub>SO<sub>4</sub> and concentrated. Derivative **2c** was purified by Isolera One using a gradient from n-exhane to ethyl acetate/n-exane 2:1 (v:v) and obtained as a colourless oil in 65%. Subsequently, A solution of **2c** (1 mmol) in DCM (10 ml) was treated with triphosgene ( 0.4 eq.), TEA ( 1.2 eq.) and piperazine for obtained derivatives **5** and 1-butyl piperazine for derivatives **6**. The reaction was stirred at room temperature for 10 minutes, then the organic phase was washed with distilled water (3x15 mL), dried over Na<sub>2</sub>SO<sub>4</sub> and evaporated. Derivative **5** and **6** were purified by Isolera One using a gradient from n-exhane to ethyl acetate/n-exane 2:1 (v:v) and obtained as a colourless oil in 50%.

***4-((4R)-2-(4-chlorophenyl)-4-((4-chlorophenyl)carbamoyl)thiazolidine-3-carbonyl)piperazine-1-carboxylate. (5)***

Overall yield 62%. <sup>1</sup>H NMR (400 MHz, CDCl<sub>3</sub>) δ 1.41(s, 9H, Boc); 3.11-3.22 (m, 5H, CH<sub>2</sub> and CH); 3.28-3.32 (m, 4H, CH<sub>2</sub>); 3.59 (t, 1H, CH<sub>2</sub>); 5.12(t, 1H, CH); 6.09 (s, 1H, CH); 7.26-7.30 (m, 4H, aryl); 7.39-7.44 (m, 4H, aryl); 9.02 (s, 1NH). ESIMS m/z calcd for C<sub>26</sub>H<sub>30</sub>N<sub>4</sub>Cl<sub>2</sub>O<sub>4</sub>S, 564.14; found 564.22.

***(4R)-N,2-bis(4-chlorophenyl)-3-(piperazine-1-carbonyl)thiazolidine-4-carboxamide derivatives. (6)***

Overall yield 59%. <sup>1</sup>H NMR (400 MHz, CDCl<sub>3</sub>) δ 2.73-2.77 (m, 1H, CH<sub>2</sub>); 2.80-2.88 (m, 5H, CH<sub>2</sub> and CH); 3.39-3.45 (m, 4H, CH<sub>2</sub>); 4.51(t, 1H, CH); 5.48 (s, 1H, CH); 7.22-7.29 (m, 6H, aryl) 7.54 (d, 2H, J= 8.2 Hz). ESIMS m/z calcd for C<sub>21</sub>H<sub>22</sub>N<sub>4</sub>Cl<sub>2</sub>O<sub>2</sub>S, 464.08; found 464.12.

***Synthesis of the (4R)-ethyl 2-(4-chlorophenyl)-3-(cyclohexanecarbonyl)thiazolidine-4-carboxylate (8) derivative and (4R)-ethyl 3-(4-chlorobenzoyl)-2-(4-chlorophenyl)thiazolidine-4-carboxylate derivative. (9)***

To a solution of (4R, 2S,R)-ethyl 2-(4-chlorophenyl)thiazolidine-4-carboxylate (**7**) (1 mmol) in DCM (10 ml) TEA (1.2 eq.) and cyclohexanecarbonyl chloride (1.2 eq) for derivatives **8** or pCl-benzoyl chloride for derivatives **9** were added. The reaction were stirred at room temperature for 10 minutes, then the organic phase was washed with distilled water (3x15 mL), dried over Na<sub>2</sub>SO<sub>4</sub> and evaporated. Derivative **8** and **9** were purified by Isolera One using a gradient of n-exhane/ethyl acetate/n-exane 2:1 (v:v) and obtained as a colourless oil in 80%.

***(4R)-ethyl 2-(4-chlorophenyl)-3-(cyclohexanecarbonyl) thiazolidine-4-carboxylate. (8)***

Overall yield 66%. <sup>1</sup>H NMR (400 MHz, CDCl<sub>3</sub>) δ 1.18-1.24 (m, 4H, CH<sub>2</sub>); 1.40 (t, 3H, CH<sub>3</sub>); 1.66-1.79 (m, 6H, CH<sub>2</sub>); 2.15 (t, 1H, CH); 2.80 (d, 1H, CH, J =

12.0 Hz); 3.61 (dd, 1H, CH,  $J' = 6.0$  and  $11.6$  Hz); 4.38 (q, 2H, CH<sub>2</sub>); 5.41 (d, 1H, CH,  $J = 5.6$  Hz); 6.11 (s, 1H, CH); 7.28-7.35 (m, 4H, aryl); 7.42-7.50 (m, 4H, aryl). ESIMS m/z calcd for C<sub>19</sub>H<sub>24</sub>NClO<sub>3</sub>S, 381.12; found 381.19.

***(4R)-ethyl 3-(4-chlorobenzoyl)-2-(4-chlorophenyl)thiazolidine-4-carboxylate derivative. (9)***

Overall yield 60%. <sup>1</sup>H NMR (400 MHz, CDCl<sub>3</sub>) δ 1.38 (t, 3H, CH<sub>3</sub>); 2.85 (dd, 1H, CH<sub>2</sub>,  $J' = 6.2$ ,  $J'' = 11.4$  Hz); 3.52-3.56 (m, 1H, CH), 4.93 (t, 1H, CH); 6.03 (s, 1H, CH); 7.15-7.28 (m, 4H, aryl) 7.42-7.50 (m, 4H, aryl). ESIMS m/z calcd for C<sub>19</sub>H<sub>17</sub>NCl<sub>2</sub>O<sub>3</sub>S, 409.03; found 409.12.

***General Procedure for the Synthesis of the diketopiperazine derivatives. (22-27)***

Aldehyde derivatives **1** (500 μl) was added to a solution of *L*-Trp-OMe or *L*-Phe-OMe, or *L*-Leu-OMe (**2**) in dichlorometane/acetic acid in ratio 4:1 (20/5 ml) at reflux temperature to obtain compounds **3**. After 2 hours to the solution were added 2,8 equivalents of sodium triacetoxyborohydride maintaining reflux temperature for 3 hours to obtain derivatives **4** (yield 73%). Then the solution was brought to neutral pH and washed with water (3 x 20 mL). The combined organic layer was dried over anhydrous sodium sulfate, filtered, concentrated and purified with flash chromatography in 8:2 n-Exane/AcOEt. To a solution of Boc-Phe-COOH, or Boc-Trp-COOH, or Boc-Leu-COOH dissolved in DCM/DMF in ratio 9:1 were added 1,2 eq of PyBop, 1,2 eq of HOAt and 2,4 eq of Dipea (were added Boc-aminoacid) at room temperature over night, to obtain compounds **5**. Then the solution was washed with neutral, acid and basic water (3 x 50 mL). The combined organic layer was dried over anhydrous sodium sulfate, filtered, concentrated and purified with flash chromatography in 5:5 n-Exane/AcOEt (yield: 65%). To obtain derivatives **6** was prepared a solution of DCM/TFA in ratio 3:1 (9:3 mL) to remove the protecting group Boc.

Trifluoroacetic acid was removed with diethyl ether under pressure. Final compounds **7a-e** were obtained with DCM/TEA under reflux temperature for 30 minutes, washed with water, dried over anhydrous sodium sulfate, filtered, concentrated and purified with flash chromatography in 30:20 n-Exane/AcOEt (yield 41-50%).

**(36,6S)-3 -[(1H-indol-3-yl)methyl ]-6-benzyl-1-isobutylpiperazine -2,5-dione.**  
**(22)**

Overall yield 47%. <sup>1</sup>H NMR (400 MHz, CDCl<sub>3</sub>) δ 0.95 (d, 3H, CH<sub>3</sub>, J= 4.0 Hz); 1.01 (d, 3H, CH<sub>3</sub>, J= 4.0 Hz); 1.24 (t, 2H, CH<sub>2</sub>); 2.15 (m, 1H, CH); 2.68 (q, 1H, CH<sub>2</sub>); 3.18 (d, 1H, CH<sub>2</sub> J=3.0 Hz); 3.53 (d, 1H, CH<sub>2</sub> J=6.0 Hz); 4.10 (d, 1H, CH<sub>2</sub> J=12.2 Hz); 4.18 (q, 1H, H-6); 4.25 (t, 1H, H-3); 6.78-7.42 (m, 10H, aryl). <sup>13</sup>C NMR (100 MHz, CDCl<sub>3</sub>) δ 20.6 (2CH<sub>3</sub>), 26.3 (CH); 30.9 (CH<sub>2</sub>), 37.2 (CH<sub>2</sub>), 51.7 (CH<sub>2</sub>); 55.7 (C-6); 61.3 (C-3); 110.5, 111.7, 119.1, 120.2, 122.9, 123.8, 126.8, 128.1, 129.3, 130.9, 135.5 and 136.9 (aryl); 166.4 and 166.5 (CO). ESIMS m/z calcd for C<sub>24</sub>H<sub>27</sub>N<sub>3</sub>O<sub>2</sub>, 389,21; found 390.21.

**(36,6S)-6-[(1H-indol-3-yl) methyl]-3-benzyl-1-isobutylpiperazine-2,5-dione.**  
**(23)**

Overall yield 41%. <sup>1</sup>H NMR (400 MHz, CDCl<sub>3</sub>) δ 0.97 (d, 3H, CH<sub>3</sub> J= 6.0 Hz); 1.02 (d, 3H, CH<sub>3</sub> J= 6.0 Hz); 2.17 (m, 1H, CH); 2.81 (m, 2H, CH<sub>2</sub>); 3.33 (dd, 1H, CH<sub>2</sub>, J'=6.2, J''=12.4 Hz); 3.65 (dd, 1H, CH<sub>2</sub> J'=3.6, J''=6.4 Hz); 3.75 (d, 1H, CH<sub>2</sub> J=6.2 Hz); 4.25 (q, 1H, CH<sub>2</sub>); 4.32 (t, 1H, H-3); 5.35 (d, 1H, H-6 J=18.0 Hz); 6.11-7.79 (m, 10H, aryl). <sup>13</sup>C NMR (100 MHz, CDCl<sub>3</sub>) δ 20.31 (1CH<sub>3</sub>); 20.74 (1CH<sub>3</sub>); 26.3 (CH); 27.1 (CH<sub>2</sub>), 40.42 (CH<sub>2</sub>), 51.42 (CH<sub>2</sub>); 57.46 (C-3); 61.04 (C-6); 109.07, 111.90, 119.90, 120.83, 123.04, 127.06, 129.05, 129.39, 135.96 and 135.97 (aryl); 166.45 and 167.43 (CO). ESIMS m/z calcd for C<sub>24</sub>H<sub>27</sub>N<sub>3</sub>O<sub>2</sub>, 389,21; found 390.21.

**(36,6S)-3-[(1H-indol-3-yl)methyl]-1-benzyl-6-isobutylpiperazine-2,5-dione.**

**(24)**

Overall yield 45%. <sup>1</sup>H NMR (400 MHz, CDCl<sub>3</sub>) δ 0.97 (d, 3H, CH<sub>3</sub>, J= 6.2 Hz); 1.03 (d, 3H, CH<sub>3</sub>, J= 6.2 Hz); 2.17 (m, 1H, CH); 2.8 (m, 2H, CH<sub>2</sub>); 3.33 (dd, 1H, CH<sub>2</sub>, J'=6.4, J''=12.2 Hz); 3.65 (dd, 1H, CH<sub>2</sub>, J'=3.6, J''=6.4 Hz); 3.75 (d, 1H, CH<sub>2</sub>, J=6.2 Hz); 4.25 (q, 1H, CH<sub>2</sub>); 4.32 (t, 1H, H-3); 5.35 (d, 1H, H-6, J=17.8 Hz); 6.11-7.67 (m, 10H, aryl). <sup>13</sup>C NMR (100 MHz, CDCl<sub>3</sub>) δ 20.31 (1CH<sub>3</sub>); 20.74 (1CH<sub>3</sub>); 26.3 (CH); 27.1 (CH<sub>2</sub>), 40.42 (CH<sub>2</sub>), 51.42 (CH<sub>2</sub>); 57.46 (C-3); 61.04 (C-6); 109.07, 111.90, 119.90, 120.83, 123.04, 127.06, 129.05, 129.39, 135.96 and 135.97 (aryl); 166.45 and 167.43 (CO). ESIMS m/z calcd for C<sub>24</sub>H<sub>27</sub>N<sub>3</sub>O<sub>2</sub>, 389,21; found 390.21.

**(36,6S)-6-[(1H-indol-3-yl)methyl]-1-benzyl-3-isobutylpiperazine-2,5-dione.**

**(25)**

Overall yield 50%. <sup>1</sup>H NMR (400 MHz, CDCl<sub>3</sub>) δ 0.96 (d, 3H, CH<sub>3</sub>, J= 4.4 Hz); 0.97 (d, 3H, CH<sub>3</sub>, J= 4.2 Hz); 1.03 (m, 3H, CH, CH<sub>2</sub>); 3.37 (dd, 1H, CH<sub>2</sub>, J'=4, J''=8.2 Hz); 3.52 (dd, 1H, CH<sub>2</sub>, J'=4.4, J''=8.0 Hz); 3.80 (m, 1H, H-6); 3.95 (d, 1H, CH<sub>2</sub>, J=16.0 Hz); 4.15 (t, 1H, H-3); 5.62 (d, 1H, CH<sub>2</sub>, J=16.0 Hz); 6.78 (s, 1H, NH); 6.92 (s, 1H, H-2'); 7.03 (t, 1H, H-6'); 7.20 (t, 1H, H-5'); 7.22-7.36 (m, 6H, H-7' and aryl); 7.58 (d, 1H, H-4', J=8.2 Hz). <sup>13</sup>C NMR (100 MHz, CDCl<sub>3</sub>) δ 22.5 (2CH<sub>3</sub>), 24.4 (CH); 33.9 (CH<sub>2</sub>), 41.2 (CH<sub>2</sub>), 50.4 (CH<sub>2</sub>); 57.3 (C-6); 72.2 (C-3); 109.7, 111.1, 118.8, 119.8, 121.7, 123.0, 127.0, 127.9, 128.5, 136.4 and 136.5 (aryl); 165.0 and 165.3 (CO). ESIMS m/z calcd for C<sub>24</sub>H<sub>27</sub>N<sub>3</sub>O<sub>2</sub>, 389,21; found 390.21.

**(3*S*,6*S*)-6-[(1*H*-indol-3-yl)methyl]-3-benzyl-1-isobutylpiperazine-2,5-dione (26).**

Overall yield 43%. <sup>1</sup>H NMR (400 MHz, CDCl<sub>3</sub>) δ 0.88 (d, 3H, CH<sub>3</sub>, J= 4.0 Hz); 0.98 (d, 3H, CH<sub>3</sub>, J= 4.2 Hz); 1.54 (m, 3H, CH, CH<sub>2</sub>); 3.41 (dd, 1H, CH<sub>2</sub> J'=4.6, J''=8.2 Hz); 3.63 (dd, 1H, CH<sub>2</sub> J'=4.4, J''=8.0 Hz); 3.95 (m, 1H, H-6); 4.02 (d, 1H, CH<sub>2</sub>, J=16.0 Hz); 4.17 (t, 1H, H-3); 5.40 (d, 1H, CH<sub>2</sub>, J=16.4 Hz); 6.83 (s, 1H, NH); 6.95 (s, 1H, H-2'); 7.09 (t, 1H, H-6'); 7.24 (t, 1H, H-5'); 7.28-7.39 (m, 6H, H-7' and aryl); 7.66 (d, 1H, H-4' J=8 Hz). <sup>13</sup>C NMR (100 MHz, CDCl<sub>3</sub>) δ 22.8 (2CH<sub>3</sub>), 24.6 (CH); 33.7 (CH<sub>2</sub>), 41.5 (CH<sub>2</sub>), 50.2 (CH<sub>2</sub>); 57.6 (C-6); 71.2 (C-3); 109.4, 111.3, 118.5, 119.7, 121.1, 123.3, 127.2, 127.9, 128.4, 136.3 and 136.8 (aryl); 165.5 and 165.9 (CO). ESIMS m/z calcd for C<sub>24</sub>H<sub>27</sub>N<sub>3</sub>O<sub>2</sub>, 389,21; found 390.21.

**(3*S*,6*S*)-1-((1*H*-indol-3-yl)methyl)-3-benzyl-6-isobutylpiperazine-2,5-dione (27).**

Overall yield 45%. <sup>1</sup>H NMR (400 MHz, CDCl<sub>3</sub>) δ 0.98 (d, 3H, CH<sub>3</sub>, J= 6.2 Hz); 1.06 (d, 3H, CH<sub>3</sub>, J= 6.2 Hz); 2.18 (m, 1H, CH); 2.85 (m, 2H, CH<sub>2</sub>); 3.36 (dd, 1H, CH<sub>2</sub>, J'=6.4, J''=12.2 Hz); 3.71 (dd, 1H, CH<sub>2</sub>, J'=3.6, J''=6.4 Hz); 3.78 (d, 1H, CH<sub>2</sub> J=6.2 Hz); 4.24 (q, 1H, CH<sub>2</sub>); 4.39 (t, 1H, H-3); 5.50 (d, 1H, H-6, J=17.8 Hz); 6.13-7.41 (m, 10H, aryl). <sup>13</sup>C NMR (100 MHz, CDCl<sub>3</sub>) δ 20.4 (1CH<sub>3</sub>); 20.5 (1CH<sub>3</sub>); 26.7 (CH); 27.2 (CH<sub>2</sub>), 40.4 (CH<sub>2</sub>), 51.6 (CH<sub>2</sub>); 57.4 (C-3); 61.0 (C-6); 109.2, 112.5, 119.0, 120.6, 123.0, 127.1, 129.3, 129.5, 136.3 and 136.9 (aryl); 166.5 and 168.0 (CO). ESIMS m/z calcd for C<sub>24</sub>H<sub>27</sub>N<sub>3</sub>O<sub>2</sub>, 389,21; found 390.21.

**CHAPTER XI**  
**DIHYDRITHIENO [2,3-b]NAPHTO-4,9-DIONE**  
**ANALOGUES AS ANTICANCER AGENTS:**  
**SYNTHESIS AND IN CELL PHARMACOLOGICAL**  
**STUDIES**

### **11.1 Introduction**

Quinones are a widely diffused group of natural products with wide-ranging properties that are involved in many biological processes.<sup>127</sup> The most intensely investigated biological property of this class of compounds is cytotoxicity against tumour cells. Several quinone-based compounds, particularly those belonging to the anthracycline group, are widely used to treat liquid tumours (leukaemia and lymphomas), and, in combination with chemotherapy, they are also used in the treatment of solid tumours.<sup>128,129</sup> Given the rapid onset of drug resistance mechanisms<sup>130,131</sup> and such severe side-effects as myelosuppression and cardiotoxicity,<sup>132,133</sup> the clinical use of quinone-based anti-cancer drugs is much debated. Nevertheless, scientific interest in this class of compounds has not abated thanks to their positive risk-benefit ratio, especially when combined with anti-tumour therapies, and to their recently demonstrated synergy with biotechnological drugs.<sup>134,135</sup> Indeed, interest in the quinone-based scaffold and its derivatives, either as modulators or as pharmacological tools, has even increased consequent to their involvement in such metabolic pathways as purinergic signalling,<sup>136</sup> inhibition of human monoamine oxidase,<sup>137</sup> telomerase<sup>138</sup> and vasorelaxation.<sup>139</sup>

### **11.2 Background and design**

In the last part of my PhD work I focused my research work in the design and synthesis of dihydrithieno [2,3-b] naphto-4,9-dione analogues as anticancer agents. In the last years, the research group in which I spend my PhD programme has deeply investigate the potential use of the dihydrithieno[2,3-b] naphto-4,9-dione scaffold (**DTNQ**) and its derivatives as anti-tumour agents.<sup>140</sup> Five different series of compounds have been synthesized and investigated (Figure 39, series **A-E**), and their structure-activity relationship studied. The cytotoxicity of synthesized derivatives against several tumour cell lines was

comparable to that of leading reference compounds, in both wild type and resistant cell lines. Moreover, biological studies revealed mechanisms of action other than typical ROS and NO production, namely, modulation of heat shock protein<sup>140b</sup> and, particularly for the most planar chromophores (Figure 39, series E), topoisomerase-II inhibition.<sup>140a</sup>

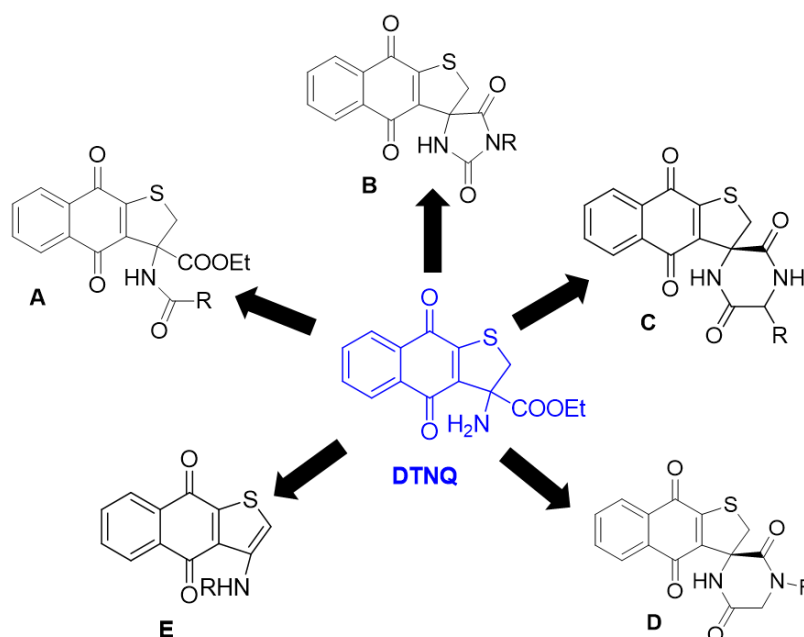


**Figure 39.** Molecular structures of the previously synthesized derivatives (A-E)

**DTNQ-Pro** (Figure 40) resulted as the most potent derivative towards the different series, with an  $IC_{50}$  in the nanomolar range in different solid and liquid tumors.<sup>140d</sup> Hence, starting from this lead-compound (**DTNQ-Pro**) and in the attempt to shed further light on the structure-activity relationship of this class of compounds, I've been involved in the design and synthesis of DTNQ derivatives bearing modifications of the ester group at position 3. The first modification consisted in the reduction of the ethyl carboxylate leading to more hydrophilic derivatives (Figure 40, series **F**). Derivatization of the same carboxylic group to

amide was performed to obtain highly functionalized compounds (Figure 40, series **G**), designed as open analogues of the diketopiperazine series previously described (series **C** and **D**, figure 39). The main biochemical events correlated to the activity of these compounds was also explored using a range of cell-based approaches.<sup>141</sup>

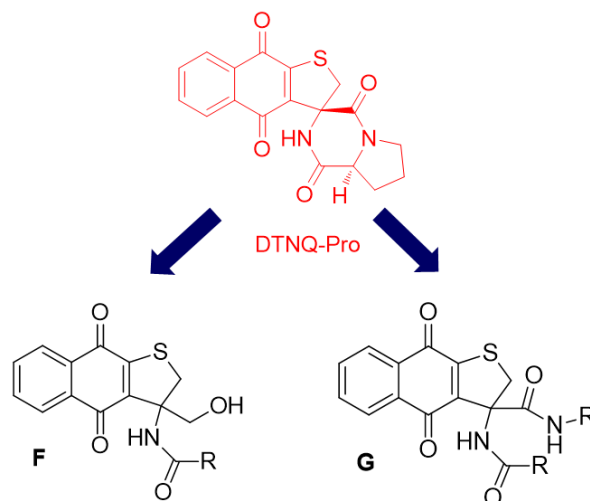


**Figure 40.** Molecular structures of the proposed analogues (*F* and *G*)

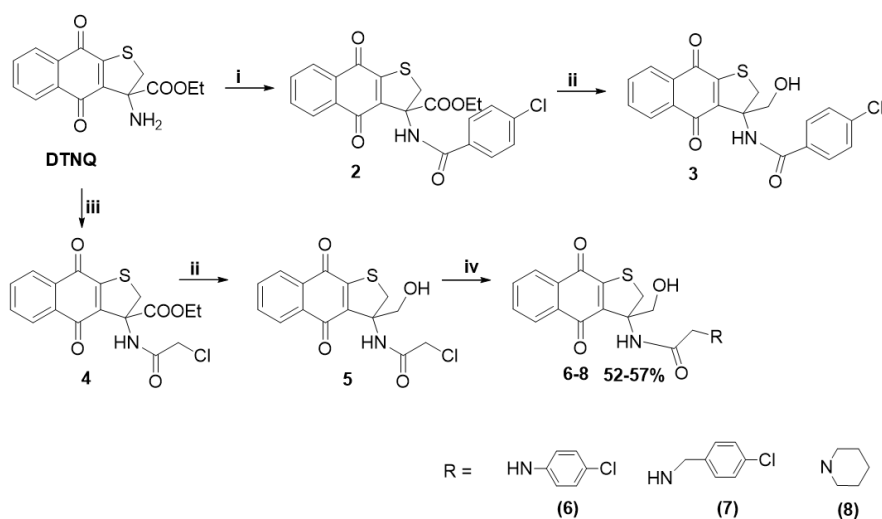
### 11.3 Chemistry

#### 11.3.1. Chemistry of series *F*

The first series of compounds was prepared starting from DTNQ, according to the pathway depicted in Scheme 10.<sup>141</sup> Acylation of the starting compound with a slight excess of 4-chlorobenzoyl chloride or 2-chloroacetyl chloride led to the corresponding 4chlorobenzamido (**2**) and (2'-chloro) acetamide (**4**) intermediates with 65% and 95% yields, respectively. Reduction of the ester group at position 3 of derivatives **2** and **4** was achieved with sodium borohydride (3 eq.) in methanol. Fast and almost quantitative conversion to hydroxymethyl derivatives **3** and **5** was obtained after minimal work-up of crude products. Finally, nucleophilic displacement of the chlorine atom of **5** using the

appropriate aromatic or aliphatic amines in dichloromethane and triethylamine at reflux readily provided the corresponding acetamide analogues (**6-8**, 52-57% yield).

**Scheme 10.** Synthesis of 3-(Hydroxymethyl)-4,9-dioxo-2,3,4,9-tetrahydronaphtho [2,3-b]thiophen-3-yl derivatives, (**6-8**)



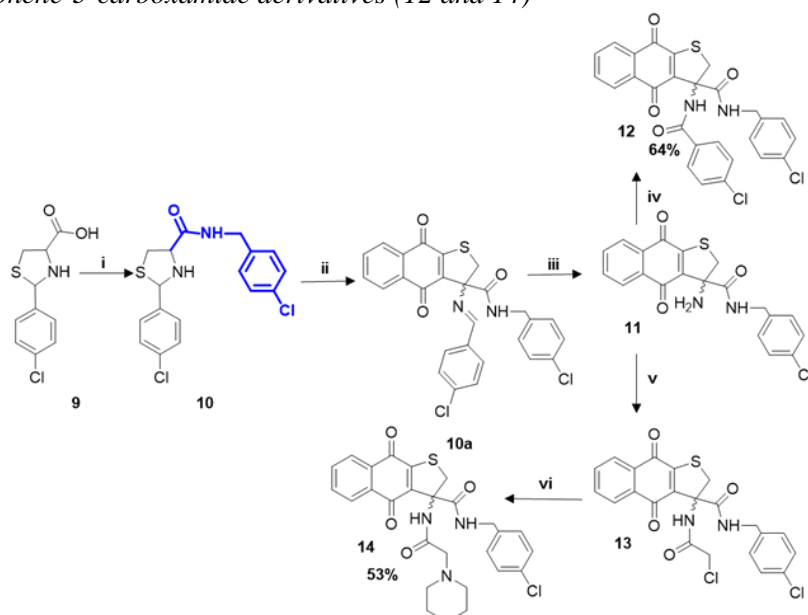
Reagents and conditions:(i): DCM, ClCO(4-Cl)C<sub>6</sub>H<sub>4</sub>,TEA; (ii): MeOH, NaBH<sub>4</sub>; (iii): DCM, ClCOCH<sub>2</sub>Cl, TEA; (iv): DCM, RNH<sub>2</sub>, TEA, cat. NaI

### 11.3.2 Chemistry of series G

The products of series G were synthesized by replacing the 3- ester group with an amide group followed by functionalization of the 3-amino group of the DTNQ system.<sup>141</sup> Initially, direct amidation using the Curtius rearrangement upon derivatization of the ester to acylazide and sodium methoxide catalyzed transamidation<sup>142</sup> was unsuccessful. On the other hand, hydrolysis of the ester prior to amidation was not feasible due to rapid decarboxylation in both acidic and alkaline media, as previously described.<sup>143</sup> Consequently, we used a different synthetic route given the feasibility of a solid phase catalysed double Michael addition to quinone systems, previously reported.<sup>144</sup> Our synthetic

strategy implies the condensation of naphthoquinone with an appropriately **4** modified thiazolidine derivative. As shown in Scheme 11, the starting thiazolidine derivative **10** was obtained by reaction of 2-phenyl-1,3-thiazolidine-4-carboxylic acid with 4-chlorobenzylamine using HOBt/HBTU as coupling agent in a dichloromethane/dimethylformamide mixture with 57% yield. Condensation of compound **10** with naphthoquinone, in MeOH, over Al<sub>2</sub>O<sub>3</sub>, gave, after acid hydrolysis of Schiff base intermediate (**10a**), the 3-(*N*-4-chlorophenyl)-carboxamide DTNQ derivative **11** in a 44% yield. Acylation of the 3-amino group of **11** with the same reagents and under the conditions described above for the *N*-acylated DTNQ derivatives, yielded the 3-(4-chlorobenzamido)-3-*N*-(4chlorophenyl) carboxamide derivative **12** as final product and the 3-(2-chloro) acetamide intermediate **13** with yields of 64 and 78%, respectively. Reacting compound **13** with piperidine under the conditions previously described led to the final compound **14** (yield 53%).

**Scheme 11.** Synthesis of *N*-3-disubstituted 4,9-dioxo-2,3,4,9-tetrahydronaphtho[2,3-*b*]thiophene-3-carboxamide derivatives (**12** and **14**)



Reagents and conditions: (i): DCM/DMF, HOBt, HBTU, DIPEA; (ii): MeOH, Napthoquinone, Alumina; (iii): HCl 2N; (iv): DCM, (4-Cl)COC<sub>6</sub>H<sub>5</sub>, TEA; (v): DCM, ClCOCH<sub>2</sub>Cl, TEA; (vi): piperidine, TEA, cat. NaI

## 11.4 Biological effects

### 11.4.1 In vitro cytotoxicity

The synthesized compounds were examined, in the Department of Molecular and Cell Biology of the Second University of Naples “Sun”, for their antiproliferative activity against the HuH7 (human hepatocarcinoma), MCF7 (human breast adenocarcinoma), LN229 (glioblastoma) and BxPC3 (human pancreas adenocarcinoma) cell lines, some of which are characterized by a reduced response to doxorubicin.<sup>145</sup> Cell viability was assessed 48 h after treatment with the tested compounds using the MTT assay. The IC<sub>50</sub> values are summarized in Table 4. For comparative purposes, doxorubicin was included in the assay. Doxorubicin exerted marked cytotoxicity against the breast cancer cell line; it was less effective against the glioblastoma, liver and pancreatic cell lines. DTNQ analogues **6** and **7**, which belong to the F series, retained micromolar activity against all tested cell lines, whereas derivative **8** was the most potent analogue; indeed, its cytotoxic effect was 4.4-fold higher versus doxorubicin in LN229 cells.<sup>126</sup>

**Table 4.** Cytotoxic activity of DTNQ derivatives on selected tumour cell lines. Values were calculated 48 h after compound administration and are expressed as mean ± SEM

Compounds	IC <sub>50</sub> (μM±SD)			
	HuH7 liver	MCF7 breast	LN229 glioblastoma	BxPC3 pancreas
<b>3</b>	> 10	> 10	> 10	> 10
<b>6</b>	3.51±0.12	2.12±0.09	1.23±0.19	2.18±0.10
<b>7</b>	3.90±0.21	1.72±0.08	1.25±0.11	1.68±0.09
<b>8</b>	0.96±0.07	1.26±0.13	0.51±0.11	2.51±0.16
<b>12</b>	0.44±0.07	0.47±0.09	0.32±0.13	0.66±0.10
<b>14</b>	1.02±0.14	0.82±0.07	0.61±0.07	0.83±0.10
<b>Doxorubicin</b>	1.11±0.32	0.13 ±0.04	2.25±0.30	1.78±0.17

The most interesting results were obtained with derivatives **12** and **14**, which belong to the G series and were designed as open analogues of previously synthesized spirodiketopiperazine derivatives. The cytotoxicity of these compounds was higher than that of doxorubicin in all tested cells, except breast cancer cells.

#### **11.4.2 Cardiotoxicity**

It is well known that the clinical use of anthracyclines, especially doxorubicin, in the treatment of many neoplastic diseases is limited by cumulative cardiotoxicity.<sup>116,117</sup> This effect has been attributed to the redox process involving the quinone system that results in the formation of reactive oxygen species and ultimately in myocyte death. Thus, we evaluated the cardiotoxicity of the most potent synthesized compounds by means of proliferation and lipid peroxidation (TBARS) assays in cardiac-derived H9C2 myocytes. The H9C2 cells were treated for 48 h with 2.5  $\mu$ M of compounds **8**, **12**, **14**, and doxorubicin. This concentration was selected because it was the highest IC<sub>50</sub> value found in MTT assays of LN299 cells. As shown in Figure 41A, treatment with compound **14** did not affect H9C2 proliferation, whereas cardiomyocyte proliferation was significantly lower in cells treated with compounds **8**, **12** and doxorubicin (83, 61, and 53%, respectively) than in untreated cells. Concomitantly, lipid peroxidation was significantly higher after administration of these compounds, as evidenced by the values of the lipid peroxidation marker TBARS (Figure 41B). Compound **14** did not affect TBARS values in treated cells, which explains at least one of the reasons for its lack of toxicity in the cell line used in the assay.

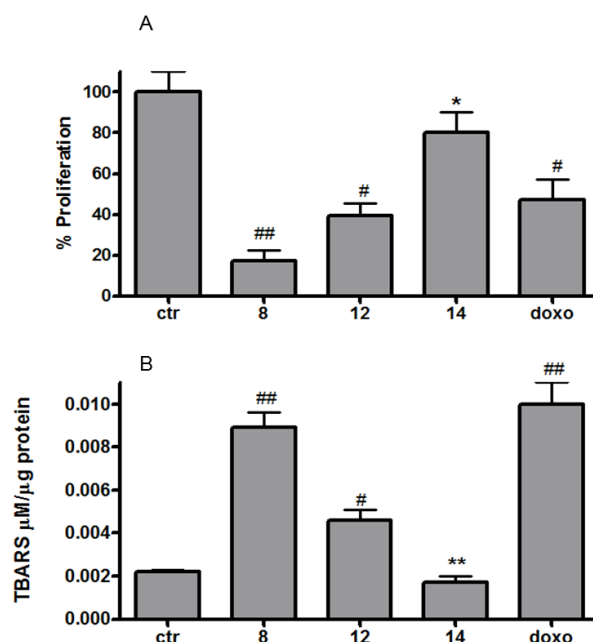
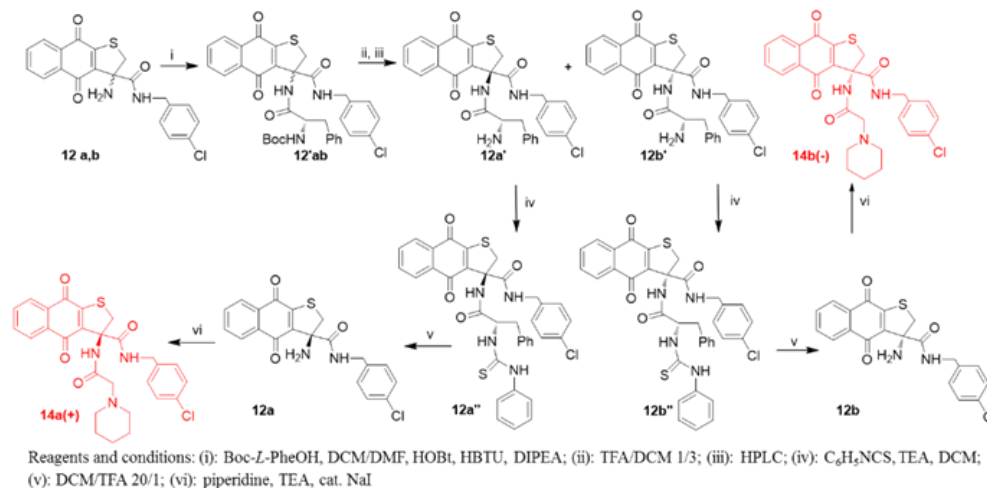


**Figure 41.** Effects of the treatment of H9C2 cells with 2,5  $\mu\text{M}$  of compounds 8, 12, 14, and doxorubicin for 48 h on cell growth and lipid peroxidation. Proliferation is expressed as percentage with respect to the untreated cells (control). Cell growth was evaluated by the MTT assay as described in the Experimental section. In the panel B is reported the TBARS value in treated and untreated (control) H9C2 cells. The bars represent means  $\pm$  SEM of three independent experiments. \*  $p < 0.05$ , \*\* $p < 0.01$  values significantly different from doxorubicin #  $p < 0.05$ , ##  $p < 0.01$  values significantly different from control

#### 11.4.3 Biological effects of compound 14 on LN299 cells

The preliminary results regarding the cytotoxicity and cardiotoxicity after treatment with compound **14** prompted us to study the mechanism of action of this compound on the LN299 glioblastoma cell line. To this aim, we first verified the effect of the stereochemistry of the chiral centre at C-3 on the activity of **14**. The two enantiomerically pure compounds, **14(+R)** and **14(-S)** were prepared as reported elsewhere <sup>125c-g</sup> by the method of Evans (Scheme 12).

Scheme 12. Resolution of enantiomers by Evans' method



Treatment of LN299 cells with 0.6  $\mu$ M of **14**, **14(+)** and **14(-)** induced a cytotoxic effect resulting in 50, 48, 50% cell death, respectively.<sup>126</sup> These data suggest that the stereochemistry of C-3 in these derivatives does not influence the cytotoxic activity, as previously observed for other DTNQ analogues.<sup>125c-g</sup> In the attempt to explain the differences observed in the behaviour of compound **14** and doxorubicin against glioblastoma cells [Table 4], we verified the site of action of both compounds. Accordingly, the intracellular localization of the molecules was investigated by confocal microscopy of LN229 cells treated with 0.6  $\mu$ M of compound **14** and doxorubicin (Figure 42). Compound **14** clearly induced cell differentiation by vimentin remodelling and was prevalently located in the cytoplasm.<sup>146</sup> Doxorubicin was mainly located in the nucleus of the survived undifferentiated cells, which suggests its mechanism of action differs from that of compound **14**.

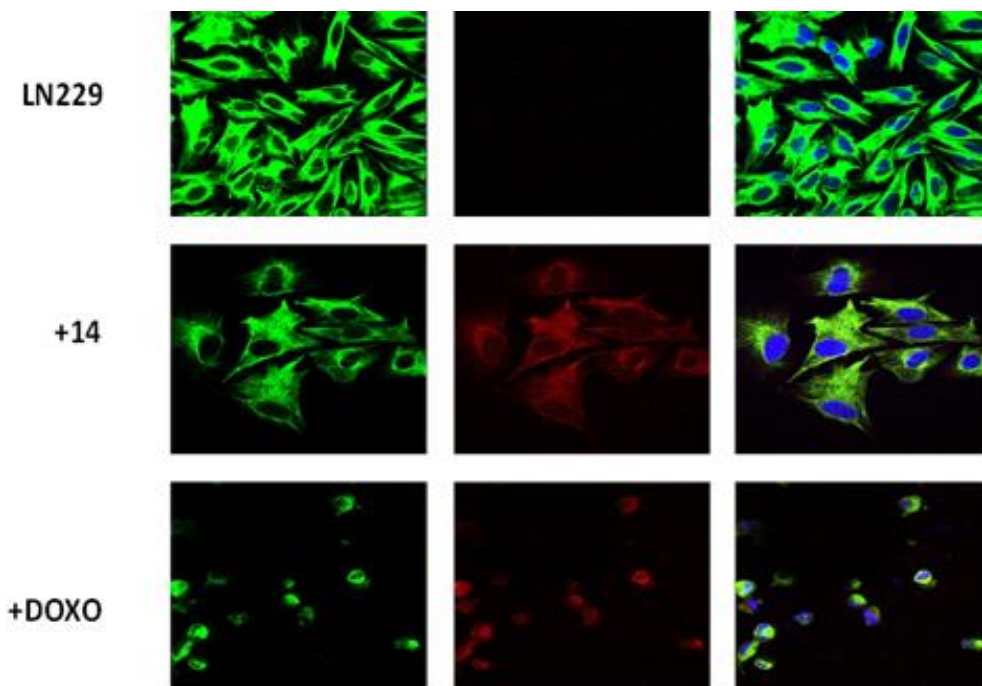


**Figure 42.** Subcellular localization of compound 14 and doxorubicin in LN229 cells. LN229 cells were cultured as described in Methods, and treated for 48 h with and without 0.6  $\mu\text{M}$  of compound 14 and doxorubicin (red) and visualized by confocal microscopy. The cells were fixed in paraformaldehyde and vimentin and nuclei were stained with anti-vimentin antibody (green) and DAPI (blue), respectively. The merged images show the localization of the tested compound (red), vimentin filaments (green) and nuclei (blue)

Human glioblastoma tissues display metabolic abnormality as reflected by increased uptake of glucose compared with normal brain tissue.<sup>147</sup> Consistent with the importance of glucose for tumour growth, many studies have shown that tumour suppressors and oncogenes influence the metabolism of this nutrient. The phosphatidylinositol 3-kinase/AKT pathway, which is activated in a large fraction of human tumours, positively regulates glucose uptake and glycolysis.<sup>148</sup> Therefore, we analysed the effects of compound **14** on glucose uptake and serine/threonine kinase AKT expression. Incubation of LN229 cells with 0.6  $\mu\text{M}$  of compound **14** for 48 h (Table 5) induced a strong increase of glucose content in the medium of LN229 cells (about 2.2-fold versus untreated

cells). This effect was negligible after treatment with the same concentration of doxorubicin.

**Table 5.** Glucose concentration in the medium of LN299 cells after incubation for 48 h with 0.6  $\mu$ M of compound 14 and doxorubicin. Values are expressed as glucose concentration per mg of protein  $\pm$  SEM.

LN299 CELLS	GLUCOSE (mg/dL)/ $\mu$ g protein
Untreated	98 $\pm$ 8
+14	215 $\pm$ 22
+Doxorubicin	120 $\pm$ 15

Moreover, as shown in the western blot of Figure 43, AKT expression was 2-fold lower in treated than in untreated LN299 cells. Concomitantly, a decrease in the expression of full length caspase 9 was observed.<sup>149</sup>

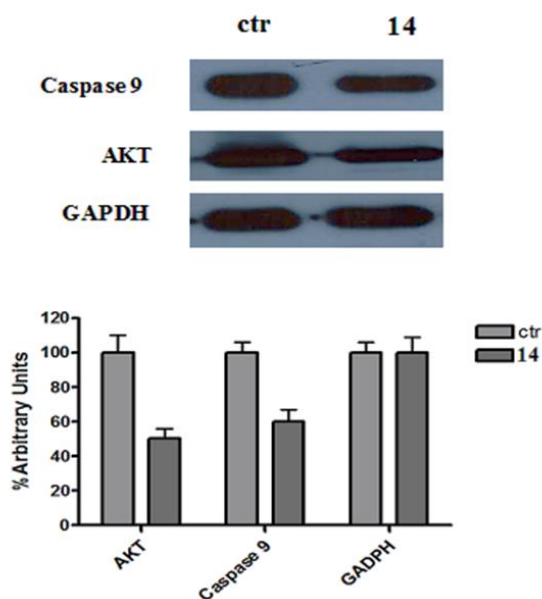


**Figure 43.** Western blot analysis of cytoplasmatic AKT and inactive caspase-9 levels in LN299 cells untreated (ctr) and treated with 0.6  $\mu$ M of compound 14 for 48 h

A decrease of glucose concentration and AKT expression in LN299 cells could switch energy metabolism towards fatty acid degradation and thus increase membrane lipid peroxidation.<sup>150</sup> To determine if one of the cytotoxic effects of compound **14** was to induce apoptosis by lipid peroxidation we evaluated TBARS production and caspase 3 activity in these cells (Figure 43). After 48 h treatment with 0.6  $\mu\text{M}$  **14**, there was a dramatic increase (five-fold) in membrane lipid peroxidation evaluated by TBARS assay (Figure 44A). Moreover, caspase-3 activity was three fold higher in treated cells (Figure 44B), which indicates that cell death was induced via an apoptotic pathway.<sup>151</sup>

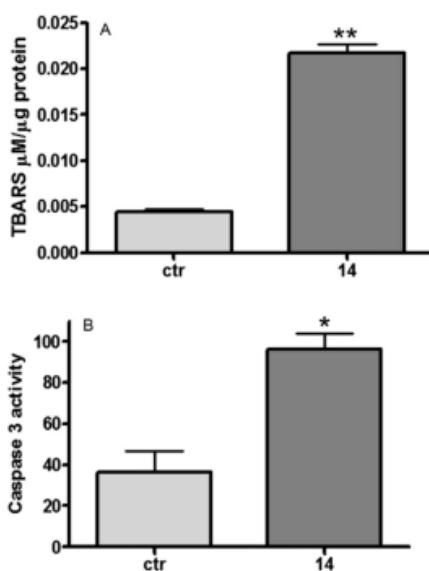


**Figure 44.** (A) TBARS levels in LN299 cells after 48 h of incubation with 0.6  $\mu\text{M}$  **14**. (B) LN299 cells were treated with 0.6  $\mu\text{M}$  for 48 h and then evaluated for cell-free caspase3 activity as described in the Experimental protocols. Data are expressed as mean  $\pm$  SEM \*\* $P < 0.003$ ; \* $P < 0.05$

---

**CHAPTER XII**  
**EXPERIMENTAL SECTION FOR SERIES F AND**  
**SERIES H (DTNQ DERIVATIVES)**

### **12.1. Chemistry**

Reactions were carried out with magnetic stirring in round-bottomed flasks unless otherwise noted. Moisture-sensitive reactions were conducted in oven-dried glassware under a positive pressure of dry nitrogen, using pre-dried, freshly distilled solvents. Microwave assisted reactions were performed in a Biotage Initiator<sup>+</sup> reactor. All solvents and reagent were purchased by Sigma-Aldrich. Analytical thin layer chromatography (TLC) was performed on pre-coated glass silica gel plates 60 (F254, 0.25 mm, VWR International). Purifications were performed by flash column chromatography on silica gel (230-400 mesh, Merck Millipore). Large scale purifications were conducted on the flash purification system apparatus Biotage Isolera One. NMR spectra were recorded on Varian Mercury-400 apparatus. <sup>1</sup>H and <sup>13</sup>C NMR spectra are reported in parts per million (ppm) referred to specific signals due to deuterated solvents as internal references. The following abbreviations are used to describe peaks: s (singlet), d (doublet), dd (double double), t (triplet), q (quadruplet) and m (multiplet). ESI-MS experiments were performed on an Applied Biosystem API 2000 triple-quadrupole spectrometer. Combustion microanalyses were performed on a Carlo Erba CNH 1106 analyzer, and were within 0.4% of calculated values. These elemental analysis results confirmed 95% purity for synthesized compounds. Unless otherwise specified, final products were converted to their chlorohydrate salts using HCl saturated diethyl ether, followed by filtration.

#### ***Ethyl-3-(4-chlorobenzamido)-4,9-dioxo-2,3,4,9 tetrahydronaphtho[2,3-b]thiophen-3-carboxylate. (2)***

4-chlorobenzoyl chloride (0.073 ml, 0.57 mmol, 1.2 eq.) and triethylamine (0.08 ml, 0.57 mmol, 1.2 eq.) were added to a solution of **DTNQ** (0.48 mmol, 0.14 g, 1.0 eq.) in 10 ml of dichloromethane and the mixture was stirred at room temperature during 30 minutes. The solution was treated with distilled water (3

x 20 mL), and the organic phase was extracted, dried over Na<sub>2</sub>SO<sub>4</sub> and evaporated *in vacuo*. Crude product was purified by flash chromatography using diethyl ether: n-hexane 3:2 (v:v) as eluent. Intermediate **6** was isolated as a yellowish solid with 65% yield. <sup>1</sup>H NMR (400 MHz, CDCl<sub>3</sub>) δ 1.23 (t, 3H, CH<sub>3</sub>); 3.84 (d, 1H, *J* = 12.8 Hz, H-2'); 3.97 (d, 1H, H-2''); 4.35 (q, 2H, CH<sub>2</sub>); 7.44 (d, 2H, *J* = 8.6 Hz, aryl); 7.72-7.77 (m, 2H, H-6 and H-7); 7.80 (d, 2H); 8.04 (s, 1H, NH); 8.06-8.11 (m, 2H, H-8 and H-5). ESI-MS *m/z* calcd for C<sub>22</sub>H<sub>16</sub>ClNO<sub>5</sub>S 441.04, found 441.13.

**4'-chloro-N-(3-(hydroxymethyl)-4,9-dioxo-2,3,4,9-tetrahydronaphtho[2,3-b]thiophen-3-yl)benzamide. (3)**

Intermediate **2** (0.1 g, 0.23 mmol) was dissolved in methanol (10 mL), and the resulting solution was cooled to 0°C in an ice bath. After addition of NaBH<sub>4</sub> (26.1 mg, 0.69 mmol, 3 eq.) the reaction was allowed to warm at room temperature and was stirred for 3h. After quenching with citric acid (10% w/w), resulting solution was concentrated *in vacuo* and extracted in DCM (2x15 ml). The organic solvent was dried over Na<sub>2</sub>SO<sub>4</sub>, evaporated and the crude product purified by flash chromatography using diethyl ether: n-hexane 3:1 (v:v) as eluent. The final compound **7** was obtained as yellow solid (yield 87%). <sup>1</sup>H NMR (400 MHz, CDCl<sub>3</sub>) δ 3.71 (d, 1H, *J* = 14.2 Hz, CH<sub>2</sub>'); 3.80 (d, 1H, CH<sub>2</sub>''); 3.92 (d, 1H, *J* = 12.8 Hz, H-2'); 4.14 (d, 1H, H-2''); 7.09 (d, 2H, *J* = 8.8 Hz, aryl); 7.42 (d, 2H, aryl); 7.73-7.77 (m, 2 H, aryl); 7.95-7.99 (m, 2H, H-6 and H-7); 8.05-8.10 (m, 3H, H-8, H-5, NH). <sup>13</sup>C NMR (100 MHz, CDCl<sub>3</sub>) δ 39.2 (C-2); 66.5 (CH<sub>2</sub>OH); 72.9 (C-3); 126.9; 127.2; 127.4; 128.9; 129.2; 129.5; 132.3; 133.4; 133.8; 134.8; 137.2; 138.6. (aryl); 159.6, 166.6, 180.6, (C=O). (C=O). ESI-MS *m/z* calcd for C<sub>20</sub>H<sub>14</sub>ClNO<sub>4</sub>S 399.03, found 399.11.

***Ethyl 3-(2'-chloroacetamido)-4,9-dioxo-2,3,4,9-tetrahydronaphtho[2,3-b]thiophen-3-carboxylate. (4)***

A solution of **DTNQ** (0.1 g, 0.33 mmol) in DCM (10 ml) was treated with chloroacetyl chloride (0.031 ml, 0.40 mmol, 1.2 eq.) and TEA (0.56 ml, 0.40 mmol, 1.2 eq.). The reaction was stirred at room temperature for 30 minutes, then the organic phase was washed with distilled water (15 mL), saturated NaHCO<sub>3</sub> (15 ml) and HCl 2N (15 ml), dried over Na<sub>2</sub>SO<sub>4</sub> and evaporated. Crude product was characterized by high purity, as evidenced by NMR spectra, hence was used in the following step without further purification. Spectral data were in accordance with literature.<sup>125c</sup>

***2'-chloro-N-(3-(hydroxymethyl)-4,9-dioxo-2,3,4,9-tetrahydronaphtho[2,3-b]thiophen-3-yl)-acetamide. (5)***

Reduction of the ester **4** to its hydroxymethyl derivative was achieved as previously described for the synthesis of compound **3**. Product was obtained as a yellowish solid in 78% yield. <sup>1</sup>H NMR (400 MHz, CDCl<sub>3</sub>) δ 3.61-3.70 (m, 2H, CH<sub>2</sub>); 3.91 (d, 1H, *J* = 11.6 Hz, H-2'); 4.08 (s, 2H, CH<sub>2</sub>); 4.12 (d, 1H, H-2''); 7.63-7.72 (m, 2H, H-6 and H-7); 8.07-8.18 (m, 3H, H-8, H-5 and NH). ESI-MS *m/z* calcd for C<sub>15</sub>H<sub>12</sub>ClNO<sub>4</sub>S 337.02, found 337.08.

***General procedure for the synthesis of compounds 6-8***

Intermediate **5** (0.12 g, 0.35 mmol, 1.0 eq.) was dissolved in 12 ml of DCM together with TEA (0.059 ml, 0.42 mmol, 1.2 eq.) and catalytic amount of NaI. Then, 1.2 equivalents of 4-chloroaniline, 4-chlorobenzylamine or piperidine were added to the solution, refluxing at 80°C for 4h. Hence, the organic solvent was washed with HCl 2N (10 ml) and brine (2 x 15 mL), dried over Na<sub>2</sub>SO<sub>4</sub> and concentrated. Compounds **6-8** were isolated by flash chromatography using DCM:MeOH 9:1 (v:v) as eluent.

**2-(4-chlorophenylamino)-N-(3-(hydroxymethyl)-4,9-dioxo-2,3,4,9-tetrahydronaphtho[2,3-b]thiophen-3-yl)acetamide. (6)**

Orange solid (53% yield)  $^1\text{H}$  NMR (400 MHz,  $\text{CD}_3\text{OD}$ )  $\delta$  3.60-3.65 (m, 2H,  $\text{CH}_2$ ); 3.72 (s, 2H,  $\text{CH}_2$ ); 3.82 (d, 1H,  $J = 12.8$  Hz, H-2'); 3.89 (d, 1H, H-2''); 6.61 (d, 2H,  $J = 8.8$  Hz, aryl); 7.09 (d, 2H, aryl); 7.68-7.83 (m, 2H, H-6 and H-7); 8.02 (d, 2H,  $J = 7.2$  Hz; H-8 and H-5).  $^{13}\text{C}$  NMR (100 MHz,  $\text{CD}_3\text{OD}$ )  $\delta$  37.1 (C-2); 49.5 ( $\text{CH}_2$ ); 62.7 ( $\text{CH}_2$ ); 72.3 (C-3); 118.5; 125.9; 126.3; 130.1; 132.2; 138.9; 139.7; 140.0, 142.5 (aryl); 161.3, 175.1 (C=O). ESI-MS  $m/z$  calcd for  $\text{C}_{21}\text{H}_{17}\text{ClN}_2\text{O}_4\text{S}$  428.06, found 428.11

**2-(4-chlorobenzylamino)-N-(3-(hydroxymethyl)-4,9-dioxo-2,3,4,9-tetrahydronaphtho[2,3-b]thiophen-3-yl)acetamide. (7)**

Yellowish solid (57% yield).  $^1\text{H}$  NMR (400 MHz,  $\text{CD}_3\text{OD}$ )  $\delta$  3.35 s, 2H,  $\text{CH}_2$ ); 3.62-3.69 (m, 2H,  $\text{CH}_2$ ); 3.84 (d, 1H,  $J = 10.8$  Hz, H-2'); 3.99 (m, 3H H-2'',  $\text{CH}_2$ ); 6.97 (d, 2H,  $J = 7.5$ , aryl) 7.24 (d, 2H, aryl); 7.65-7.80 (m, 2H, H-6 and H-7); 7.98-8.06 (m, 2H, H-8 and H-5).  $^{13}\text{C}$  NMR (100 MHz,  $\text{CD}_3\text{OD}$ )  $\delta$  38.4 (C-2); 48.4 ( $\text{CH}_2$ ); 49.9 ( $\text{CH}_2$ ); 62.8 ( $\text{CH}_2$ ); 72.6 (C-3); 125.7; 126.2; 129.3; 131.8; 133.5; 134.7; 136.0; 138.8; 139.5 (aryl); 161.1, 175.8, 180.3 (C=O). ESI-MS  $m/z$  calcd for  $\text{C}_{22}\text{H}_{19}\text{ClN}_2\text{O}_4\text{S}$  442.08, found 442.13

**N-(3-(hydroxymethyl)-4,9-dioxo-2,3,4,9-tetrahydronaphtho[2,3-b]thiophen-3-yl)-2-(piperidin-1-yl)acetamide. (8)**

Yellow solid (52% yield).  $^1\text{H}$  NMR (400 MHz,  $\text{CDCl}_3$ )  $\delta$  1.43-1.47 (m, 2H, piperidine); 1.60-1.65 (m, 4H, piperidine); 2.42-2.49 (m, 4H, piperidine); 2.88-3.00 (m, 2H,  $\text{CH}_2\text{OH}$ ); 3.66 (s, 2H,  $\text{CH}_2$ ); 3.86 (d, 1H,  $J = 11.2$  Hz, H-2'); 4.13 (d, 1H, H-2''); 7.69-7.84 (m, 2 H, H-6 and H-7); 8.06-8.09 (m, 2H, H-8 and H-5); 8.64 (s, 1H, NH).  $^{13}\text{C}$  NMR (100 MHz,  $\text{CDCl}_3$ )  $\delta$  23.9 ( $\text{CH}_2$ ); 26.3 ( $\text{CH}_2$ ); 39.2 (C-2); 55.1 ( $\text{CH}_2$ ); 62.6 ( $\text{CH}_2$ ); 66.7 ( $\text{CH}_2$ ); 72.6 (C-3); 126.8; 127.1; 132.3;

133.5; 133.6; 134.7; 137.9 (aryl); 159.2, 171.9, 181.0 (C=O). ESI-MS  $m/z$  calcd for  $C_{20}H_{22}N_2O_4S$  386.13, found 386.19.

**(2R,4R) and (2S,4R) -N-(4-chlorobenzyl)-2-(4-chlorophenyl)thiazolidine-4-carboxamide. (10)**

2-(4-chlorophenyl) thiazolidine-4-carboxylic acid (**9**, 1.0 g, 4.11 mmol, 1.0 eq.) was dissolved in 30 ml of DCM/DMF (1/1 v/v). Then, HOBT (0.72 g, 5.34 mmol, 1.3 eq.), HBTU (2.02 g, 5.34 mmol, 1.3 eq.), DIPEA (1.86 ml, 10.7 mmol, 2.6 eq.) and 4-chlorobenzylamine (0.65 ml, 5.34 mmol, 1.2 eq.) were added. The mixture was stirred at room temperature for 24h, then the organic phase was dried, crude product was dissolved in DCM, washed with water (2 x 30 mL), dried over  $Na_2SO_4$  and concentrated. Derivative **10** was purified by Isolera One using a gradient from n-hexane to ethyl acetate/n-hexane 2:1 (v:v) and obtained as a colourless oil in 57% yield.  $^1H$  NMR (400 MHz,  $CDCl_3$ )  $\delta$  3.09-3.14 (dd, 1H,  $J = 6.0$  and  $3.0$  Hz, H-5<sub>b</sub>) 3.24-3.30 (m, 2H, H-5<sub>b</sub> and H-6<sub>a</sub>); 3.33-3.41 (dd, 1H,  $J = 6.0 = 3.0$  Hz, H-5<sub>a</sub>); 3.89 (t, 1H, H-4<sub>b</sub>); 4.26-4.30 (dd, 1H,  $J = 6.0$  and  $3.0$  Hz, H-4<sub>a</sub>); 4.32-4.35 (m, 2H,  $CH_2$ ); 5.45 (s, 1H, H-2<sub>a</sub>); 5.49 (s, 1H, H-2<sub>b</sub>); 7.18-7.29 (m, 6H, Aryl); 7.41-7.47 (t, 2H, Aryl). ESI-MS  $m/z$  calcd for  $C_{17}H_{16}Cl_2N_2OS$  366.04, found 366.08

**3-amino-N-(4-chlorobenzyl)-4,9-dioxo-2,3,4,9-tetrahydronaphtho[2,3-b]thiophene-3-carboxamide. (11)**

Compound **11** was synthesized using the synthetic procedure elsewhere described starting from 0.5 g of **10** (1.37 mmol). Purification was achieved in purification system apparatus Biotage Isolera One using a gradient elution from n-hexane to diethyl ether/n-hexane 2/1. The desired compound was obtained in 44% yield as an orange solid.  $^1H$  NMR (400 MHz,  $CDCl_3$ )  $\delta$  3.17 (d, 1H,  $J = 12.0$  Hz, H-2'); 3.95 (d, 1H, H-2''); 4.41-4.48 (dd, 1H,  $J = 5.8$  and  $14.6$  Hz,  $CH_2$ ); 4.64-4.71 (dd, 1H,  $CH_2''$ ); 7.38-7.42 (m, 4H, aryl); 7.70-7.79 (m, 2H, H-

6 and H-7); 7.90 (s, 1H, NH); 8.07-8.13 (m, 2H, H-8 and H-5). ESI-MS  $m/z$  calcd for  $C_{20}H_{15}ClN_2O_3S$  398.05, found 398.12.

***3-(4-chlorobenzamido)-N-(4-chlorobenzyl)-4,9-dioxo-2,3,4,9-tetrahydronaphtho[2,3-b]thiophene-3-carboxamide. (12)***

Derivative **12** was obtained from **11** using the same protocol previously described for **2**. Final product was isolated as a yellowish solid by flash chromatography using diethyl ether:n-hexane 1:1. Yield 64%.  $^1H$  NMR (400 MHz,  $CDCl_3$ )  $\delta$  3.91 (d, 1H,  $J = 12.4$  Hz, H-2'); 4.21 (d, 1H, H-2''); 4.38-4.42 (dd, 1H,  $J = 5.6$  and 15.2 Hz,  $CH_2'$ ); 4.48-4.52 (dd, 1H,  $CH_2''$ ); 6.87 (s, 1H, NH); 7.11 (d, 2H,  $J = 7.6$  Hz, aryl); 7.22 (d, 2H, aryl); 7.43 (d, 2H;  $J = 7.6$  Hz, aryl); 7.69-7.76 (m, 4 H, H-6, H-7, and aryl); 8.00-8.05 (m, 2H, H-8 and H-5); 8.37 (s, 1H, NH).  $^{13}C$  NMR (100 MHz,  $CDCl_3$ )  $\delta$  42.9 (C-2); 44.5 ( $CH_2$ ); 82.7 (C-3); 125.9; 128.2; 128.5; 131.8; 132.1; 134.0; 134.3; 134.4; 136.2; 159.9 (aryl); 160.3, 162.9, 172.0, 180.0 (C=O). ESI-MS  $m/z$  calcd for  $C_{27}H_{18}Cl_2N_2O_4S$ : 536.04, found 536.12.

***3-(2-chloroacetamido)-N-(4-chlorobenzyl)-4,9-dioxo-2,3,4,9-tetrahydronaphtho[2,3-b]thiophene-3-carboxamide. (13)***

Intermediate **13** was obtained from **11** using the protocol described above for **4**. Crude product was purified by flash chromatography using diethyl ether:n-hexane 3:1 (v:v) as eluent. A yellowish solid was obtained in 78% yield.  $^1H$  NMR (400 MHz,  $CDCl_3$ )  $\delta$  3.50 (d, 1H,  $J = 12.6$  Hz, H-2'); 4.02-4.12 (dd, 2H,  $J' < 1$  and 15.2 Hz,  $CH_2$ ); 4.24 (d, 1H, H-2''); 4.37-4.44 (dd, 1H,  $J = 6.0$  and 15.2 Hz,  $CH_2$ ); 4.49-4.56 (dd, 1H,  $CH_2$ ); 6.68 (s, 1H, NH); 7.15 (d, 2H,  $J = 8.8$  Hz, aryl); 7.27 (d, 2H, aryl); 7.71-7.78 (m, 2H, H-6 and H-7); 7.92 (s, 1H, NH); 8.05 (t, 2H, H-8 and H-5). ESI-MS  $m/z$  calcd for  $C_{22}H_{16}Cl_2N_2O_4S$  474.02, found 474.09.

***N*-(4-chlorobenzyl)-4,9-dioxo-3-(2-(piperidin-1-yl)acetamido)-2,3,4,9-tetrahydronaphtho[2,3-*b*]thiophene-3-carboxamide. (14)**

Compound **14** was obtained from **13** as described for **8**. Purification by flash chromatography, using diethyl ether as eluent, led to a yellow solid in 53% yield.  $^1\text{H}$  NMR (400 MHz,  $\text{CDCl}_3$ )  $\delta$  1.43-1.46 (m, 2H, piperidine); 1.54-1.63 (m, 4H, piperidine); 2.41-2.47 (m, 4H, piperidine); 2.86-2.98 (d, 2H,  $J = 4.8$  Hz,  $\text{CH}_2$ ); 3.76 (d, 1H,  $J = 12.4$  Hz, H-2'); 4.35-4.39 (m, 2H, H-2'' and  $\text{CH}_2'$ ); 4.45-4.51 (dd, 1H,  $\text{CH}_2''$ ,  $J = 5.6$  and 15.2 Hz); 6.80 (s, 1H, NH); 7.13 (d, 2H,  $J = 7.6$  Hz, aryl); 7.24 (d, 2H, aryl); 7.69-7.77 (m, 2 H, H-6 and H-7); 8.05-8.09 (m, 2H, H-8 and H-5); 8.97 (s, 1H, NH).  $^{13}\text{C}$  NMR (100 MHz,  $\text{CDCl}_3$ )  $\delta$  23.8 ( $\text{CH}_2$ ); 26.3 ( $\text{CH}_2$ ); 40.8 (C-2); 43.6 ( $\text{CH}_2$ ); 55.2 ( $\text{CH}_2$ ); 62.5 ( $\text{CH}_2$ ); 74.2 (C-3); 126.9; 127.2; 129.1; 129.2; 132.4; 133.4; 133.6; 133.7; 134.8; 136.0; 136.5 (Aryl); 160.3, 169.4, 173.2, 179.8 (C=O). ESI-MS  $m/z$  calcd for  $\text{C}_{27}\text{H}_{26}\text{ClN}_3\text{O}_4\text{S}$  523,13, found 523.20.

## ***12.2 Biology***

### ***12.2.1 Cell cultures***

Human hepatocarcinoma cell line HuH7, human glioblastoma cell line LN299, human cardiac derived myocytes H9C2, human pancreatic adenocarcinoma cell line BxPC-3 and human breast adenocarcinoma cell line MCF7 were obtained from the American Type Culture Collection (Manassas, VA, USA) and cultured in DMEM medium (Dulbecco's modified Eagle's medium for HUH7, LN229 e H9C2 cells) and in RPMI-1640 medium (for BxPC-3 and MCF7 cells) supplemented with 10% (v/v) fetal bovine serum (Invitrogen<sup>TM</sup> Life Technologies, Carlsbad, CA, USA),  $100 \text{ U} \cdot \text{mL}^{-1}$  of penicillin and  $100 \mu\text{g} \cdot \text{mL}^{-1}$  of streptomycin at  $37^\circ\text{C}$  in a humidified atmosphere of 5%  $\text{CO}_2$  in air.

### **12.2.2 Cell viability assay**

Cell viability for all cell lines was determined using the 3-[4,5-dimethylthiazol-2,5-diphenyl-2H-tetrazolium bromide (MTT) colorimetric assay. The test is based on the ability of mitochondrial dehydrogenase to convert, in viable cells, the yellow MTT reagent (Sigma Chemical Co., St. Louis, MO) into a soluble blue formazan dye. Cells were seeded into 96-well plates to a density of 105 cells/100  $\mu$ L well. After 24 h of growth to allow attachment to the wells, compounds were added at various concentrations (from 0.1 to 25 mM). After 24 or 48 h of growth and after removal of the culture medium, 100  $\mu$ L/well medium containing 1 mg/mL MTT was added. Cell cultures were further incubated at 37 °C for 2 h in the dark. The solution was then gently aspirated from each well, and the formazan crystals within the cells were dissolved with 100  $\mu$ L of DMSO. Optical densities were read at 570 nm using a Multiskan Spectrum Thermo Electron Corporation reader. Results were expressed as percentage relative to vehicle-treated control (0.5% DMSO was added to untreated cells). IC<sub>50</sub> (concentration eliciting 50% inhibition) values were determined by linear and polynomial regression. Experiments were performed in triplicate.

### **12.2.3 Thiobarbituric acid-reactive species (TBARS) levels**

Lipid peroxidation was evaluated using an analytical quantitative methodology. It relies upon the formation of a colored adduct produced by the stoichiometric reaction of aldehydes with thiobarbituric acid (TBA). The TBARS assay was performed on membranes extracted from cells treated with 8, 12, 14, and doxorubicin, and from untreated, control cells, using an ice-cold lysis buffer (50 mM Tris, 150 mM NaCl, 10 mM EDTA, 1% Triton) supplemented with a mixture of protease inhibitors. The homogenate was centrifuged at 1200 g for 10 min in order to separate cytosol (supernatants) from membranes (pellet). The pellet was dissolved in 50 mM Tris, 150 mM NaCl and 10 mM EDTA, and the

protein content of the samples was determined by Bio-Rad assay (Bio-Rad Laboratories, San Diego, CA, USA). Aliquots (10 mL) of the membrane preparation were added to 2 mL of TBA–trichloroacetic acid (TCA) (15% TCA, 0.3% TBA in 0.12 N HCl) solution at 100°C for 30 min. The reaction was stopped by cooling the sample in cold water, and, after a centrifugation at 15 000 g for 10 min, the chromogen (TBARs) was quantified by spectrophotometry at a wavelength of 532 nm. The amount of TBARs was expressed as  $\mu\text{M}\cdot\mu\text{g}^{-1}$  proteins. All data are the mean $\pm$  SEM of three experiments.

#### ***12.2.4 Glucose uptake***

Cells were washed twice with 2 ml of HEPES buffer solution A (HEPES, 20 mM; NaCl, 137 mM; KCl, 4.7 mM; MgSO<sub>4</sub>, 1.2 mM; CaCl<sub>2</sub>, 1.8 mM; pH 7.4) in both upper and lower compartments. After washing, 1 ml of HEPES buffer containing D-[U-<sup>14</sup>C] glucose 0.5 mCi/ml and 1 mM total glucose (solution B) was added to the upper compartment. Cells were then incubated for 30 min at 37 C, the electrical resistance measured, and buffer from the upper and lower compartments removed. Glucose uptake was stopped by washing each membrane twice with ice-cold PBS. After that, 1 ml of NaOH solution (0.1 mol/l) was added to lyse the cells, and aliquots were removed for scintillation counting and protein measurement. Scintillation solution (5 ml, Ecoscint XR scintillation solution, National Diagnostics) and 0.5 ml of the different test solutions were mixed and analysed by scintillation counting using a Packard Liquid Scintillation Analyzer 1600TR.

#### ***12.2.5 Immunostaining and confocal microscopy***

LN299 cells grown were fixed in PBS 4% paraformaldehyde then permeabilized 5 min with PBS 1% Triton. Immunostaining was carried out by incubation with anti-vimentin antibodies 1:1000 followed by revelation using Cy3-conjugated anti-rabbit immunoglobulin (Ig) G antibodies (Jackson Immunoresearch

Laboratories, West Grove, PA) at a dilution of 1/200 for 45 minutes. The cells were analyzed by an LSM-410 Zeiss confocal microscope.

#### ***12.2.6 Western Blot analysis***

The effects of **14** on expression of AKT and caspase-9, were determined by Western blots. For cell extract preparation, cells were washed twice with ice-cold PBS/BSA, scraped and centrifuged for 30 min at 4°C in 1 ml of lysis buffer (1% Triton, 0.5% sodium deoxycholate, 0.1 M NaCl, 1 mM EDTA, pH 7.5, 10 mM Na<sub>2</sub>HPO<sub>4</sub>, pH 7.4, 10 mM PMSF, 25 mM benzamidin, 1 mM leupeptin, 0.025 U/ml aprotinin). Equal amounts of cell proteins were separated by SDS-PAGE. The proteins on the gels were electrotransferred to nitrocellulose membranes. The membranes were incubated over night with primary antibodies (anti-AKT, anti-caspase 9, anti-tubulin antibodies) in 1% buffer solution (Tris buffered saline solution containing 1% nonfat dry milk and 0.05% Tween 20), washed 3 times with 1% buffer solution and incubated with a horseradish peroxidase-labeled secondary antibody for 1 hr at room temperature. The immune complexes were visualized using the ECL system.

#### ***12.4 Statistical analysis***

All analyses were conducted using Graph-Pad Prism (GraphPad Software Inc., San Diego, CA). The significance of differences between groups was determined by Student t-test. Difference with P<0.05 (\*) was considered statistically significant.

---

**CHAPTER XIII**  
**CONCLUSIONS**

The ability of p53 to respond to stress signals by triggering cell-cycle arrest and cell death by apoptosis is crucial to inhibit tumor development and for the response to anticancer therapy. Inactivation of p53 by mutation occurs in about half of all human tumors. Tumors that retain wild-type p53 often acquire an alternative mechanism for its inactivation, largely through deregulation of MDM2 (murin double minute-2) protein. Negative regulation of p53 activity and stability is enhanced in many human tumors and effectively impairs the activities of the p53 pathway. Therefore, recovery of p53 activity in cancer cells by antagonizing MDM2 has been proposed as a novel approach for treating cancer and validated in vitro by macromolecular studies. More recently, genetic and biochemical analysis of the p53-MDM2 interaction have revealed structural features suggesting that it might be targetable by small molecules. The interaction of MDM2 and p53 was shown to be mediated by a deep well-defined hydrophobic cavity on the surface of MDM2. This cleft is filled only by three side chains of the helical region of p53, making this site an attractive target to design a small molecule able to mimic the contacts and the orientations of these key amino acids, thereby disrupting p53-MDM2 interaction. Several low molecular weight inhibitors, including bicyclic derivatives sulfonamides, oxindole and benzodiazepinediones have been identified and reported.

This PhD thesis presents the results obtained in the searching for small-molecules able to “reactive” the p53 transcriptional activity. The research was based on the identification of both DNA-damaging agents and p53-MDM2 interaction modulating compounds. Initially, the synthesis of a new 2-oxospiro [indoline-3,2'-thiazolidine] derivatives, designed as cellular cycle modulators and p53-MDM2 interaction inhibitors, was carried on, followed by in depth characterization of the biochemical events at the basis of their pharmacological activities. A second part of this PhD research project was dedicated to the design and synthesis of DTNQ derivatives as DNA- damaging

agents and then, to assess their involvement in the p53-MDM2 interaction. The first part of project led to design, synthesis and biological evaluation of a four series of new 2-oxospiro [indoline-3,2'-thiazolidine] derivatives, as inhibitors of p53-MDM2 protein-protein interaction. In particular, compound **13n (SM13)** was identified as a high efficacy compound in several tumour cell lines with great selectivity against the normal cell line. The well-known p53-MDM2 inhibitor, nutlin-3, was considerably less efficient in all tested cell lines and also in the in vitro p53-MDM2 binding inhibition assay. **SM13** reduces cell proliferation and induces apoptosis in vitro in cells carrying either p53 WT or mutated gene, suggesting that its effect is independent from p53 transcriptional activity. On the contrary, **SM13** has no effect in a p53 null cell line. In vivo, **SM13** induces cancer cell death in a dose-dependent manner through the activation of the mitochondrial-dependent death signalling in p53-mutated cells, also reducing tumour growth. Thus, **SM13** can be considered as a potential anticancer agents to be used for the treatment of p53-dependent tumours, even in the absence of p53 transcriptional activity.

In the second part of this PhD research project the synthetic procedures to obtain new highly functionalized DTNQ derivatives were provided. The derivatives thus obtained were biologically evaluated, These compounds exhibit cytotoxic activity against various solid tumour cell lines. In particular, compound **14** is more effective than doxorubicin against the LN229 (glioblastoma), and BxPC3 (pancreas) human cell lines, and is significantly less cytotoxic in the H9C2 cardiomyocytes. In LN299 cells, compound **14** strongly inhibits glucose uptake in LN229 cells, in comparison with doxorubicin. Concomitantly, compound **14** decreases serine/ threonine kinase AKT expression, which confirms the modulatory activity of this kinase on cellular glucose uptake. The results obtained confirm once again that chemical modifications of the DTNQ system

are able in provide potent pharmacological tools for the study of antitumor agents.

## **REFERENCES**

## References

---

1. Hanahan, D.; Weinberg, R. A., The hallmarks of cancer. *Cell* **2000**, *100* (1), 57-70.
2. Sonnenschein, C.; Soto, A. M., Somatic mutation theory of carcinogenesis: why it should be dropped and replaced. *Mol Carcinog* **2000**, *29* (4), 205-11.
3. Baker, S. G., TOFT better explains experimental results in cancer research than SMT (comment on DOI 10.1002/bies.201100025 and DOI 10.1002/bies.201100022). *Bioessays* **2011**, *33* (12), 919-21.
4. Soto, A. M.; Sonnenschein, C., Emergentism as a default: cancer as a problem of tissue organization. *J Biosci* **2005**, *30* (1), 103-18.
5. Rosenfeld, S., Are the somatic mutation and tissue organization field theories of carcinogenesis incompatible? *Cancer Inform* **2013**, *12*, 221-9.
6. Yarosh, D. B., Why is DNA damage signaling so complicated? Chaos and molecular signaling. *Environ Mol Mutagen* **2001**, *38* (2-3), 132-4.
7. Nowell, P. C., The clonal evolution of tumor cell populations. *Science* **1976**, *194* (4260), 23-8.
8. Stephens, P. J.; Greenman, C. D.; Fu, B.; Yang, F.; Bignell, G. R.; Mudie, L. J.; Pleasance, E. D.; Lau, K. W.; Beare, D.; Stebbings, L. A.; McLaren, S.; Lin, M. L.; McBride, D. J.; Varela, I.; Nik-Zainal, S.; Leroy, C.; Jia, M.; Menzies, A.; Butler, A. P.; Teague, J. W.; Quail, M. A.; Burton, J.; Swerdlow, H.; Carter, N. P.; Morsberger, L. A.; Iacobuzio-Donahue, C.; Follows, G. A.; Green, A. R.; Flanagan, A. M.; Stratton, M. R.; Futreal, P. A.; Campbell, P. J., Massive genomic rearrangement acquired in a single catastrophic event during cancer development. *Cell* **2011**, *144* (1), 27-40.
9. Coussens, L. M.; Werb, Z., Inflammation and cancer. *Nature* **2002**, *420* (6917), 860-7.
10. Lee, H. N.; Na, H. K.; Surh, Y. J., Resolution of inflammation as a novel chemopreventive strategy. *Semin Immunopathol* **2013**, *35* (2), 151-61.

## References

---

11. Dunn, J. H.; Ellis, L. Z.; Fujita, M., Inflammasomes as molecular mediators of inflammation and cancer: potential role in melanoma. *Cancer Lett* **2012**, *314* (1), 24-33.
12. Chen, R. Z.; Pettersson, U.; Beard, C.; Jackson-Grusby, L.; Jaenisch, R., DNA hypomethylation leads to elevated mutation rates. *Nature* **1998**, *395* (6697), 89-93.
13. Laird, P. W.; Jaenisch, R., The role of DNA methylation in cancer genetic and epigenetics. *Annu Rev Genet* **1996**, *30*, 441-64.
14. Vendramini-Costa, D. B.; Carvalho, J. E., Molecular link mechanisms between inflammation and cancer. *Curr Pharm Des* **2012**, *18* (26), 3831-52.
15. Radisky, D.; Hagios, C.; Bissell, M. J., Tumors are unique organs defined by abnormal signaling and context. *Semin Cancer Biol* **2001**, *11* (2), 87-95.
16. de Visser, K. E.; Eichten, A.; Coussens, L. M., Paradoxical roles of the immune system during cancer development. *Nat Rev Cancer* **2006**, *6* (1), 24-37.
17. Schwartz, G. K.; Shah, M. A., Targeting the cell cycle: a new approach to cancer therapy. *J Clin Oncol* **2005**, *23* (36), 9408-21.
18. Wuarin, J.; Nurse, P., Regulating S phase: CDKs, licensing and proteolysis. *Cell* **1996**, *85* (6), 785-7.
19. Hunter, T.; Pines, J., Cyclins and cancer. II: Cyclin D and CDK inhibitors come of age. *Cell* **1994**, *79* (4), 573-82.
20. Pardee, A. B., G1 events and regulation of cell proliferation. *Science* **1989**, *246* (4930), 603-8.
21. Hall, M.; Peters, G., Genetic alterations of cyclins, cyclin-dependent kinases, and Cdk inhibitors in human cancer. *Adv Cancer Res* **1996**, *68*, 67-108.
22. Sherr, C. J.; Roberts, J. M., CDK inhibitors: positive and negative regulators of G1-phase progression. *Genes Dev* **1999**, *13* (12), 1501-12.

## References

---

23. Grana, X.; Reddy, E. P., Cell cycle control in mammalian cells: role of cyclins, cyclin dependent kinases (CDKs), growth suppressor genes and cyclin-dependent kinase inhibitors (CKIs). *Oncogene* **1995**, *11* (2), 211-9.
24. Kaldis, P.; Russo, A. A.; Chou, H. S.; Pavletich, N. P.; Solomon, M. J., Human and yeast cdk-activating kinases (CAKs) display distinct substrate specificities. *Mol Biol Cell* **1998**, *9* (9), 2545-60.
25. Hunter, T., Signaling--2000 and beyond. *Cell* **2000**, *100* (1), 113-27.
26. Harbour, J. W.; Dean, D. C., The Rb/E2F pathway: expanding roles and emerging paradigms. *Genes Dev* **2000**, *14* (19), 2393-409.
27. Musgrove, E. A.; Caldon, C. E.; Barraclough, J.; Stone, A.; Sutherland, R. L., Cyclin D as a therapeutic target in cancer. *Nat Rev Cancer* **2011**, *11* (8), 558-72.
28. Sherr, C. J., Cancer cell cycles. *Science* **1996**, *274* (5293), 1672-7.
29. Baudino, T. A.; Cleveland, J. L., The Max network gone mad. *Mol Cell Biol* **2001**, *21* (3), 691-702.
30. Stocker, H.; Hafen, E., Genetic control of cell size. *Curr Opin Genet Dev* **2000**, *10* (5), 529-35.
31. Johnston, L. A.; Prober, D. A.; Edgar, B. A.; Eisenman, R. N.; Gallant, P., *Drosophila* myc regulates cellular growth during development. *Cell* **1999**, *98* (6), 779-90.
32. Elend, M.; Eilers, M., Cell growth: downstream of Myc - to grow or to cycle? *Curr Biol* **1999**, *9* (24), R936-8.
33. Gu, W.; Schneider, J. W.; Condorelli, G.; Kaushal, S.; Mahdavi, V.; Nadal-Ginard, B., Interaction of myogenic factors and the retinoblastoma protein mediates muscle cell commitment and differentiation. *Cell* **1993**, *72* (3), 309-24.

## References

---

34. Lasorella, A.; Nosedà, M.; Beyna, M.; Yokota, Y.; Iavarone, A., Id2 is a retinoblastoma protein target and mediates signalling by Myc oncoproteins. *Nature* **2000**, *407* (6804), 592-8.
35. Walczak, H.; Krammer, P. H., The CD95 (APO-1/Fas) and the TRAIL (APO-2L) apoptosis systems. *Exp Cell Res* **2000**, *256* (1), 58-66.
36. Vander Heiden, M. G.; Chandel, N. S.; Li, X. X.; Schumacker, P. T.; Colombini, M.; Thompson, C. B., Outer mitochondrial membrane permeability can regulate coupled respiration and cell survival. *Proc Natl Acad Sci U S A* **2000**, *97* (9), 4666-71.
37. Hengartner, M. O., The biochemistry of apoptosis. *Nature* **2000**, *407* (6805), 770-6.
38. Soengas, M. S.; Capodici, P.; Polsky, D.; Mora, J.; Esteller, M.; Opitz-Araya, X.; McCombie, R.; Herman, J. G.; Gerald, W. L.; Lazebnik, Y. A.; Cordon-Cardo, C.; Lowe, S. W., Inactivation of the apoptosis effector Apaf-1 in malignant melanoma. *Nature* **2001**, *409* (6817), 207-11.
39. Evan, G. I.; Wyllie, A. H.; Gilbert, C. S.; Littlewood, T. D.; Land, H.; Brooks, M.; Waters, C. M.; Penn, L. Z.; Hancock, D. C., Induction of apoptosis in fibroblasts by c-myc protein. *Cell* **1992**, *69* (1), 119-28.
40. Sherr, C. J.; Weber, J. D., The ARF/p53 pathway. *Curr Opin Genet Dev* **2000**, *10* (1), 94-9.
41. Woods, D. B.; Vousden, K. H., Regulation of p53 function. *Exp Cell Res* **2001**, *264* (1), 56-66.
42. Gibbs, J. B., Mechanism-based target identification and drug discovery in cancer research. *Science* **2000**, *287* (5460), 1969-73.
43. Felsher, D. W.; Bishop, J. M., Reversible tumorigenesis by MYC in hematopoietic lineages. *Mol Cell* **1999**, *4* (2), 199-207.
44. Joerger, A. C.; Fersht, A. R., The tumor suppressor p53: from structures to drug discovery. *Cold Spring Harb Perspect Biol* **2010**, *2* (6), a000919.

## References

---

45. Petitjean, A.; Mathe, E.; Kato, S.; Ishioka, C.; Tavtigian, S. V.; Hainaut, P.; Olivier, M., Impact of mutant p53 functional properties on TP53 mutation patterns and tumor phenotype: lessons from recent developments in the IARC TP53 database. *Hum Mutat* **2007**, *28* (6), 622-9.
46. Giaccia, A. J.; Kastan, M. B., The complexity of p53 modulation: emerging patterns from divergent signals. *Genes Dev* **1998**, *12* (19), 2973-83.
47. Jin, S.; Levine, A. J., The p53 functional circuit. *J Cell Sci* **2001**, *114* (Pt 23), 4139-40.
48. Royds, J. A.; Iacopetta, B., p53 and disease: when the guardian angel fails. *Cell Death Differ* **2006**, *13* (6), 1017-26.
49. Vogelstein, B.; Lane, D.; Levine, A. J., Surfing the p53 network. *Nature* **2000**, *408* (6810), 307-10.
50. Donehower, L. A., The p53-deficient mouse: a model for basic and applied cancer studies. *Semin Cancer Biol* **1996**, *7* (5), 269-78.
51. Pietsch, E. C.; Humbey, O.; Murphy, M. E., Polymorphisms in the p53 pathway. *Oncogene* **2006**, *25* (11), 1602-11.
52. Laptenko, O.; Prives, C., Transcriptional regulation by p53: one protein, many possibilities. *Cell Death Differ* **2006**, *13* (6), 951-61.
53. Matoba, S.; Kang, J. G.; Patino, W. D.; Wragg, A.; Boehm, M.; Gavrilova, O.; Hurley, P. J.; Bunz, F.; Hwang, P. M., p53 regulates mitochondrial respiration. *Science* **2006**, *312* (5780), 1650-3.
54. Bensaad, K.; Tsuruta, A.; Selak, M. A.; Vidal, M. N.; Nakano, K.; Bartrons, R.; Gottlieb, E.; Vousden, K. H., TIGAR, a p53-inducible regulator of glycolysis and apoptosis. *Cell* **2006**, *126* (1), 107-20.
55. Crighton, D.; Wilkinson, S.; O'Prey, J.; Syed, N.; Smith, P.; Harrison, P. R.; Gasco, M.; Garrone, O.; Crook, T.; Ryan, K. M., DRAM, a p53-induced modulator of autophagy, is critical for apoptosis. *Cell* **2006**, *126* (1), 121-34.

## References

---

56. Gatz, S. A.; Wiesmuller, L., p53 in recombination and repair. *Cell Death Differ* **2006**, *13* (6), 1003-16.
57. Bensaad, K.; Vousden, K. H., Savior and slayer: the two faces of p53. *Nat Med* **2005**, *11* (12), 1278-9.
58. Roger, L.; Gadea, G.; Roux, P., Control of cell migration: a tumour suppressor function for p53? *Biol Cell* **2006**, *98* (3), 141-52.
59. Kortlever, R. M.; Higgins, P. J.; Bernards, R., Plasminogen activator inhibitor-1 is a critical downstream target of p53 in the induction of replicative senescence. *Nat Cell Biol* **2006**, *8* (8), 877-84.
60. Teodoro, J. G.; Parker, A. E.; Zhu, X.; Green, M. R., p53-mediated inhibition of angiogenesis through up-regulation of a collagen prolyl hydroxylase. *Science* **2006**, *313* (5789), 968-71.
61. Murray-Zmijewski, F.; Lane, D. P.; Bourdon, J. C., p53/p63/p73 isoforms: an orchestra of isoforms to harmonise cell differentiation and response to stress. *Cell Death Differ* **2006**, *13* (6), 962-72.
62. Wang, X.; Kua, H. Y.; Hu, Y.; Guo, K.; Zeng, Q.; Wu, Q.; Ng, H. H.; Karsenty, G.; de Crombrughe, B.; Yeh, J.; Li, B., p53 functions as a negative regulator of osteoblastogenesis, osteoblast-dependent osteoclastogenesis, and bone remodeling. *J Cell Biol* **2006**, *172* (1), 115-25.
63. Lane, D. P., Cancer. p53, guardian of the genome. *Nature* **1992**, *358* (6381), 15-6.
64. Siliciano, J. D.; Canman, C. E.; Taya, Y.; Sakaguchi, K.; Appella, E.; Kastan, M. B., DNA damage induces phosphorylation of the amino terminus of p53. *Genes Dev* **1997**, *11* (24), 3471-81.
65. Kurz, E. U.; Lees-Miller, S. P., DNA damage-induced activation of ATM and ATM-dependent signaling pathways. *DNA Repair (Amst)* **2004**, *3* (8-9), 889-900.

## References

---

66. Gorgoulis, V. G.; Vassiliou, L. V.; Karakaidos, P.; Zacharatos, P.; Kotsinas, A.; Liloglou, T.; Venere, M.; Ditullio, R. A., Jr.; Kastriakis, N. G.; Levy, B.; Kletsas, D.; Yoneta, A.; Herlyn, M.; Kittas, C.; Halazonetis, T. D., Activation of the DNA damage checkpoint and genomic instability in human precancerous lesions. *Nature* **2005**, *434* (7035), 907-13.
67. Bartkova, J.; Horejsi, Z.; Koed, K.; Kramer, A.; Tort, F.; Zieger, K.; Guldborg, P.; Sehested, M.; Nesland, J. M.; Lukas, C.; Orntoft, T.; Lukas, J.; Bartek, J., DNA damage response as a candidate anti-cancer barrier in early human tumorigenesis. *Nature* **2005**, *434* (7035), 864-70.
68. Jackson, A. L.; Loeb, L. A., The contribution of endogenous sources of DNA damage to the multiple mutations in cancer. *Mutat Res* **2001**, *477* (1-2), 7-21.
69. Bartkova, J.; Rezaei, N.; Liontos, M.; Karakaidos, P.; Kletsas, D.; Issaeva, N.; Vassiliou, L. V.; Kolettas, E.; Niforou, K.; Zoumpourlis, V. C.; Takaoka, M.; Nakagawa, H.; Tort, F.; Fugger, K.; Johansson, F.; Sehested, M.; Andersen, C. L.; Dyrskjot, L.; Orntoft, T.; Lukas, J.; Kittas, C.; Helleday, T.; Halazonetis, T. D.; Bartek, J.; Gorgoulis, V. G., Oncogene-induced senescence is part of the tumorigenesis barrier imposed by DNA damage checkpoints. *Nature* **2006**, *444* (7119), 633-7.
70. Chao, C.; Herr, D.; Chun, J.; Xu, Y., Ser18 and 23 phosphorylation is required for p53-dependent apoptosis and tumor suppression. *EMBO J* **2006**, *25* (11), 2615-22.
71. Donehower, L. A., Effects of p53 mutation on tumor progression: recent insights from mouse tumor models. *Biochim Biophys Acta* **1996**, *1242* (3), 171-6.
72. Milne, D. M.; Campbell, L. E.; Campbell, D. G.; Meek, D. W., p53 is phosphorylated in vitro and in vivo by an ultraviolet radiation-induced protein

## References

---

kinase characteristic of the c-Jun kinase, JNK1. *J Biol Chem* **1995**, *270* (10), 5511-8.

73. Feng, J.; Yan, J.; Chen, J.; Schlake, G.; Jiang, Z.; Buzin, C. H.; Sommer, S. S.; Ditschilo, A., Absence of somatic ATM missense mutations in 58 mammary carcinomas. *Cancer Genet Cytogenet* **2003**, *145* (2), 179-82.

74. Gumy-Pause, F.; Wacker, P.; Sappino, A. P., ATM gene and lymphoid malignancies. *Leukemia* **2004**, *18* (2), 238-42.

75. Greenman, C.; Stephens, P.; Smith, R.; Dalgliesh, G. L.; Hunter, C.; Bignell, G.; Davies, H.; Teague, J.; Butler, A.; Stevens, C.; Edkins, S.; O'Meara, S.; Vastrik, I.; Schmidt, E. E.; Avis, T.; Barthorpe, S.; Bhamra, G.; Buck, G.; Choudhury, B.; Clements, J.; Cole, J.; Dicks, E.; Forbes, S.; Gray, K.; Halliday, K.; Harrison, R.; Hills, K.; Hinton, J.; Jenkinson, A.; Jones, D.; Menzies, A.; Mironenko, T.; Perry, J.; Raine, K.; Richardson, D.; Shepherd, R.; Small, A.; Tofts, C.; Varian, J.; Webb, T.; West, S.; Widaa, S.; Yates, A.; Cahill, D. P.; Louis, D. N.; Goldstraw, P.; Nicholson, A. G.; Brasseur, F.; Looijenga, L.; Weber, B. L.; Chiew, Y. E.; DeFazio, A.; Greaves, M. F.; Green, A. R.; Campbell, P.; Birney, E.; Easton, D. F.; Chenevix-Trench, G.; Tan, M. H.; Khoo, S. K.; Teh, B. T.; Yuen, S. T.; Leung, S. Y.; Wooster, R.; Futreal, P. A.; Stratton, M. R., Patterns of somatic mutation in human cancer genomes. *Nature* **2007**, *446* (7132), 153-8.

76. Rozenfeld-Granot, G.; Krishnamurthy, J.; Kannan, K.; Toren, A.; Amariglio, N.; Givol, D.; Rechavi, G., A positive feedback mechanism in the transcriptional activation of Apaf-1 by p53 and the coactivator Zac-1. *Oncogene* **2002**, *21* (10), 1469-76.

77. Bourdon, J. C.; Deguin-Chambon, V.; Lelong, J. C.; Dessen, P.; May, P.; Debuire, B.; May, E., Further characterisation of the p53 responsive element-identification of new candidate genes for trans-activation by p53. *Oncogene* **1997**, *14* (1), 85-94.

## References

---

78. Hoh, J.; Jin, S.; Parrado, T.; Edington, J.; Levine, A. J.; Ott, J., The p53MH algorithm and its application in detecting p53-responsive genes. *Proc Natl Acad Sci U S A* **2002**, *99* (13), 8467-72.
79. Hollstein, M.; Sidransky, D.; Vogelstein, B.; Harris, C. C., p53 mutations in human cancers. *Science* **1991**, *253* (5015), 49-53.
80. Vaziri, H.; West, M. D.; Allsopp, R. C.; Davison, T. S.; Wu, Y. S.; Arrowsmith, C. H.; Poirier, G. G.; Benchimol, S., ATM-dependent telomere loss in aging human diploid fibroblasts and DNA damage lead to the post-translational activation of p53 protein involving poly(ADP-ribose) polymerase. *EMBO J* **1997**, *16* (19), 6018-33.
81. Dudenhoffer, C.; Rohaly, G.; Will, K.; Deppert, W.; Wiesmuller, L., Specific mismatch recognition in heteroduplex intermediates by p53 suggests a role in fidelity control of homologous recombination. *Mol Cell Biol* **1998**, *18* (9), 5332-42.
82. Janus, F.; Albrechtsen, N.; Knippschild, U.; Wiesmuller, L.; Grosse, F.; Deppert, W., Different regulation of the p53 core domain activities 3'-to-5' exonuclease and sequence-specific DNA binding. *Mol Cell Biol* **1999**, *19* (3), 2155-68.
83. Albrechtsen, N.; Dornreiter, I.; Grosse, F.; Kim, E.; Wiesmuller, L.; Deppert, W., Maintenance of genomic integrity by p53: complementary roles for activated and non-activated p53. *Oncogene* **1999**, *18* (53), 7706-17.
84. Kim, Y. T.; Zhao, M., Aberrant cell cycle regulation in cervical carcinoma. *Yonsei Med J* **2005**, *46* (5), 597-613.
85. Fridman, J. S.; Lowe, S. W., Control of apoptosis by p53. *Oncogene* **2003**, *22* (56), 9030-40.
86. Moll, U. M.; Wolff, S.; Speidel, D.; Deppert, W., Transcription-independent pro-apoptotic functions of p53. *Curr Opin Cell Biol* **2005**, *17* (6), 631-6.

## References

---

87. Yonish-Rouach, E.; Resnitzky, D.; Lotem, J.; Sachs, L.; Kimchi, A.; Oren, M., Wild-type p53 induces apoptosis of myeloid leukaemic cells that is inhibited by interleukin-6. *Nature* **1991**, *352* (6333), 345-7.
88. Miyashita, T.; Krajewski, S.; Krajewska, M.; Wang, H. G.; Lin, H. K.; Liebermann, D. A.; Hoffman, B.; Reed, J. C., Tumor suppressor p53 is a regulator of bcl-2 and bax gene expression in vitro and in vivo. *Oncogene* **1994**, *9* (6), 1799-805.
89. Bennett, M. R.; Macdonald, K.; Chan, S. W.; Boyle, J. J.; Weissberg, P. L., Cooperative interactions between RB and p53 regulate cell proliferation, cell senescence, and apoptosis in human vascular smooth muscle cells from atherosclerotic plaques. *Circ Res* **1998**, *82* (6), 704-12.
90. Buckbinder, L.; Talbott, R.; Velasco-Miguel, S.; Takenaka, I.; Faha, B.; Seizinger, B. R.; Kley, N., Induction of the growth inhibitor IGF-binding protein 3 by p53. *Nature* **1995**, *377* (6550), 646-9.
91. Faraonio, R.; Vergara, P.; Di Marzo, D.; Pierantoni, M. G.; Napolitano, M.; Russo, T.; Cimino, F., p53 suppresses the Nrf2-dependent transcription of antioxidant response genes. *J Biol Chem* **2006**, *281* (52), 39776-84.
92. Chen, X.; Ko, L. J.; Jayaraman, L.; Prives, C., p53 levels, functional domains, and DNA damage determine the extent of the apoptotic response of tumor cells. *Genes Dev* **1996**, *10* (19), 2438-51.
93. Haupt, Y.; Rowan, S.; Shaulian, E.; Vousden, K. H.; Oren, M., Induction of apoptosis in HeLa cells by trans-activation-deficient p53. *Genes Dev* **1995**, *9* (17), 2170-83.
94. Korgaonkar, C.; Zhao, L.; Modestou, M.; Quelle, D. E., ARF function does not require p53 stabilization or Mdm2 relocalization. *Mol Cell Biol* **2002**, *22* (1), 196-206.

## References

---

95. Dumont, P.; Leu, J. I.; Della Pietra, A. C., 3rd; George, D. L.; Murphy, M., The codon 72 polymorphic variants of p53 have markedly different apoptotic potential. *Nat Genet* **2003**, *33* (3), 357-65.
96. Mihara, M.; Erster, S.; Zaika, A.; Petrenko, O.; Chittenden, T.; Pancoska, P.; Moll, U. M., p53 has a direct apoptogenic role at the mitochondria. *Mol Cell* **2003**, *11* (3), 577-90.
97. Vousden, K. H.; Lu, X., Live or let die: the cell's response to p53. *Nat Rev Cancer* **2002**, *2* (8), 594-604.
98. Levine, A. J., p53, the cellular gatekeeper for growth and division. *Cell* **1997**, *88* (3), 323-31.
99. Picksley, S. M.; Lane, D. P., The p53-mdm2 autoregulatory feedback loop: a paradigm for the regulation of growth control by p53? *Bioessays* **1993**, *15* (10), 689-90.
100. Wu, X.; Bayle, J. H.; Olson, D.; Levine, A. J., The p53-mdm-2 autoregulatory feedback loop. *Genes Dev* **1993**, *7* (7A), 1126-32.
101. Eischen, C. M.; Weber, J. D.; Roussel, M. F.; Sherr, C. J.; Cleveland, J. L., Disruption of the ARF-Mdm2-p53 tumor suppressor pathway in Myc-induced lymphomagenesis. *Genes Dev* **1999**, *13* (20), 2658-69.
102. Palmero, I.; Pantoja, C.; Serrano, M., p19ARF links the tumour suppressor p53 to Ras. *Nature* **1998**, *395* (6698), 125-6.
103. Momand, J.; Jung, D.; Wilczynski, S.; Niland, J., The MDM2 gene amplification database. *Nucleic Acids Res* **1998**, *26* (15), 3453-9.
104. Eymin, B.; Gazzeri, S.; Brambilla, C.; Brambilla, E., Mdm2 overexpression and p14(ARF) inactivation are two mutually exclusive events in primary human lung tumors. *Oncogene* **2002**, *21* (17), 2750-61.
105. (a) Polsky, D.; Bastian, B. C.; Hazan, C.; Melzer, K.; Pack, J.; Houghton, A.; Busam, K.; Cordon-Cardo, C.; Osman, I., HDM2 protein overexpression, but not gene amplification, is related to tumorigenesis of cutaneous melanoma.

## References

---

- Cancer Res* **2001**, *61* (20), 7642-6; (b) Leite, K. R.; Franco, M. F.; Srougi, M.; Nesrallah, L. J.; Nesrallah, A.; Bevilacqua, R. G.; Darini, E.; Carvalho, C. M.; Meirelles, M. I.; Santana, I.; Camara-Lopes, L. H., Abnormal expression of MDM2 in prostate carcinoma. *Mod Pathol* **2001**, *14* (5), 428-36.
106. Kussie, P. H.; Gorina, S.; Marechal, V.; Elenbaas, B.; Moreau, J.; Levine, A. J.; Pavletich, N. P., Structure of the MDM2 oncoprotein bound to the p53 tumor suppressor transactivation domain. *Science* **1996**, *274* (5289), 948-53.
107. Zhao, J.; Wang, M.; Chen, J.; Luo, A.; Wang, X.; Wu, M.; Yin, D.; Liu, Z., The initial evaluation of non-peptidic small-molecule HDM2 inhibitors based on p53-HDM2 complex structure. *Cancer Lett* **2002**, *183* (1), 69-77.
108. Chene, P., Inhibiting the p53-MDM2 interaction: an important target for cancer therapy. *Nat Rev Cancer* **2003**, *3* (2), 102-9.
109. Vassilev, L. T.; Vu, B. T.; Graves, B.; Carvajal, D.; Podlaski, F.; Filipovic, Z.; Kong, N.; Kammlott, U.; Lukacs, C.; Klein, C.; Fotouhi, N.; Liu, E. A., In vivo activation of the p53 pathway by small-molecule antagonists of MDM2. *Science* **2004**, *303* (5659), 844-8.
110. Grasberger, B. L.; Lu, T.; Schubert, C.; Parks, D. J.; Carver, T. E.; Koblisch, H. K.; Cummings, M. D.; LaFrance, L. V.; Milkiewicz, K. L.; Calvo, R. R.; Maguire, D.; Lattanze, J.; Franks, C. F.; Zhao, S.; Ramachandren, K.; Bylebyl, G. R.; Zhang, M.; Manthey, C. L.; Petrella, E. C.; Pantoliano, M. W.; Deckman, I. C.; Spurlino, J. C.; Maroney, A. C.; Tomczuk, B. E.; Molloy, C. J.; Bone, R. F., Discovery and cocrystal structure of benzodiazepinedione HDM2 antagonists that activate p53 in cells. *J Med Chem* **2005**, *48* (4), 909-12.
111. Ding, K.; Lu, Y.; Nikolovska-Coleska, Z.; Qiu, S.; Ding, Y.; Gao, W.; Stuckey, J.; Krajewski, K.; Roller, P. P.; Tomita, Y.; Parrish, D. A.; Deschamps, J. R.; Wang, S., Structure-based design of potent non-peptide MDM2 inhibitors. *J Am Chem Soc* **2005**, *127* (29), 10130-1.

## References

---

112. Allen, J. G.; Bourbeau, M. P.; Wohlhieter, G. E.; Bartberger, M. D.; Michelsen, K.; Hungate, R.; Gadwood, R. C.; Gaston, R. D.; Evans, B.; Mann, L. W.; Matison, M. E.; Schneider, S.; Huang, X.; Yu, D.; Andrews, P. S.; Reichelt, A.; Long, A. M.; Yakowec, P.; Yang, E. Y.; Lee, T. A.; Oliner, J. D., Discovery and optimization of chromenotriazolopyrimidines as potent inhibitors of the mouse double minute 2-tumor protein 53 protein-protein interaction. *J Med Chem* **2009**, *52* (22), 7044-53.
113. Hardcastle, I. R.; Ahmed, S. U.; Atkins, H.; Farnie, G.; Golding, B. T.; Griffin, R. J.; Guyenne, S.; Hutton, C.; Kallblad, P.; Kemp, S. J.; Kitching, M. S.; Newell, D. R.; Norbedo, S.; Northen, J. S.; Reid, R. J.; Saravanan, K.; Willems, H. M.; Lunec, J., Small-molecule inhibitors of the MDM2-p53 protein-protein interaction based on an isoindolinone scaffold. *J Med Chem* **2006**, *49* (21), 6209-21.
114. Gomez-Monterrey, I.; Bertamino, A.; Porta, A.; Carotenuto, A.; Musella, S.; Aquino, C.; Granata, I.; Sala, M.; Brancaccio, D.; Picone, D.; Ercole, C.; Stiuso, P.; Campiglia, P.; Grieco, P.; Iannelli, P.; Maresca, B.; Novellino, E., Identification of the spiro(oxindole-3,3'-thiazolidine)-based derivatives as potential p53 activity modulators. *J Med Chem* **2010**, *53* (23), 8319-29.
115. Bertamino, A.; Soprano, M.; Musella, S.; Rusciano, M. R.; Sala, M.; Vernieri, E.; Di Sarno, V.; Limatola, A.; Carotenuto, A.; Cosconati, S.; Grieco, P.; Novellino, E.; Illario, M.; Campiglia, P.; Gomez-Monterrey, I., Synthesis, in vitro, and in cell studies of a new series of [indoline-3,2'-thiazolidine]-based p53 modulators. *J Med Chem* **2013**, *56* (13), 5407-21.
116. Bertamino, A.; Aquino, C.; Sala, M.; Simone, N.; Mattia, C. A.; Erra, L.; Musella, S.; Iannelli, P.; Carotenuto, A.; Grieco, P.; Novellino, E.; Campiglia, P.; Gomez-Monterrey, I., Design and synthesis of spirotryprostatin-

## References

---

inspired diketopiperazine systems from prolyl spirooxoindolethiazolidine derivatives. *Bioorg Med Chem* **2010**, *18* (12), 4328-37.

117. (a) Szilagyi, L.; Gyorgydeak, Z., Comments on the putative stereoselectivity in cysteine-aldehyde reactions. Selective C(2) inversion and C(4) epimerization in thiazolidine-4-carboxylic acids. *Journal of the American Chemical Society* **1979**, *101* (2), 427-432; (b) Deroose, F. D.; De Clercq, P. J., A novel enantioselective synthesis of (+)-biotin. *Tetrahedron Letters* **1994**, *35* (16), 2615-2618.

118. Radeaglia, R., Neuhaus, D.; Williamson, M.: The nuclear overhauser effect in structural and conformational analysis. XXII, 522 S., 200 Abb., 80 Tab., 16 × 24 cm. New York: VCH Publishers, Inc. 1989. Pappereinband, 194,-DM. *Journal für Praktische Chemie* **1990**, *332* (5), 658-658.

119. Arva, N. C.; Talbott, K. E.; Okoro, D. R.; Brekman, A.; Qiu, W. G.; Bargonetti, J., Disruption of the p53-Mdm2 complex by Nutlin-3 reveals different cancer cell phenotypes. *Ethn Dis* **2008**, *18* (2 Suppl 2), S2-1-8.

120. Gonzalez-Lopez de Turiso, F.; Sun, D.; Rew, Y.; Bartberger, M. D.; Beck, H. P.; Canon, J.; Chen, A.; Chow, D.; Correll, T. L.; Huang, X.; Julian, L. D.; Kayser, F.; Lo, M. C.; Long, A. M.; McMinn, D.; Oliner, J. D.; Osgood, T.; Powers, J. P.; Saiki, A. Y.; Schneider, S.; Shaffer, P.; Xiao, S. H.; Yakowec, P.; Yan, X.; Ye, Q.; Yu, D.; Zhao, X.; Zhou, J.; Medina, J. C.; Olson, S. H., Rational design and binding mode duality of MDM2-p53 inhibitors. *J Med Chem* **2013**, *56* (10), 4053-70.

121. Sorriento, D.; Del Giudice, C.; Bertamino, A.; Ciccarelli, M.; Gomez-Monterrey, I.; Campiglia, P.; Novellino, E.; Illario, M.; Trimarco, B.; De Luca, N.; Iaccarino, G., New small molecules, ISA27 and SM13, inhibit tumour growth inducing mitochondrial effects of p53. *Br J Cancer* **2015**, *112* (1), 77-85.

## References

---

122. Speidel, D., Transcription-independent p53 apoptosis: an alternative route to death. *Trends Cell Biol* **2010**, *20* (1), 14-24.
123. Wolf, D.; Rotter, V., Major deletions in the gene encoding the p53 tumor antigen cause lack of p53 expression in HL-60 cells. *Proc Natl Acad Sci U S A* **1985**, *82* (3), 790-4.
124. Sorriento, D.; Campanile, A.; Santulli, G.; Leggiero, E.; Pastore, L.; Trimarco, B.; Iaccarino, G., A new synthetic protein, TAT-RH, inhibits tumor growth through the regulation of NFkappaB activity. *Mol Cancer* **2009**, *8*, 97.
125. Arima, Y.; Nitta, M.; Kuninaka, S.; Zhang, D.; Fujiwara, T.; Taya, Y.; Nakao, M.; Saya, H., Transcriptional blockade induces p53-dependent apoptosis associated with translocation of p53 to mitochondria. *J Biol Chem* **2005**, *280* (19), 19166-76.
126. Zhao, Y.; Chaiswing, L.; Velez, J. M.; Batinic-Haberle, I.; Colburn, N. H.; Oberley, T. D.; St Clair, D. K., p53 translocation to mitochondria precedes its nuclear translocation and targets mitochondrial oxidative defense protein-manganese superoxide dismutase. *Cancer Res* **2005**, *65* (9), 3745-50.
127. Colucci, M. A.; Moody, C. J.; Couch, G. D., Natural and synthetic quinones and their reduction by the quinone reductase enzyme NQO1: from synthetic organic chemistry to compounds with anticancer potential. *Org Biomol Chem* **2008**, *6* (4), 637-56.
128. Binaschi, M.; Bigioni, M.; Cipollone, A.; Rossi, C.; Goso, C.; Maggi, C. A.; Capranico, G.; Animati, F., Anthracyclines: selected new developments. *Curr Med Chem Anticancer Agents* **2001**, *1* (2), 113-30.
129. Lown, J. W., Anthracycline and anthraquinone anticancer agents: current status and recent developments. *Pharmacol Ther* **1993**, *60* (2), 185-214.
130. Baird, R. D.; Kaye, S. B., Drug resistance reversal--are we getting closer? *Eur J Cancer* **2003**, *39* (17), 2450-61.

## References

---

131. Krishna, R.; Mayer, L. D., Multidrug resistance (MDR) in cancer. Mechanisms, reversal using modulators of MDR and the role of MDR modulators in influencing the pharmacokinetics of anticancer drugs. *Eur J Pharm Sci* **2000**, *11* (4), 265-83.
132. Minotti, G.; Menna, P.; Salvatorelli, E.; Cairo, G.; Gianni, L., Anthracyclines: molecular advances and pharmacologic developments in antitumor activity and cardiotoxicity. *Pharmacol Rev* **2004**, *56* (2), 185-229.
133. Serrano, J.; Palmeira, C. M.; Kuehl, D. W.; Wallace, K. B., Cardioselective and cumulative oxidation of mitochondrial DNA following subchronic doxorubicin administration. *Biochim Biophys Acta* **1999**, *1411* (1), 201-5.
134. Burstein, H. J.; Piccart-Gebhart, M. J.; Perez, E. A.; Hortobagyi, G. N.; Wolmark, N.; Albain, K. S.; Norton, L.; Winer, E. P.; Hudis, C. A., Choosing the best trastuzumab-based adjuvant chemotherapy regimen: should we abandon anthracyclines? *J Clin Oncol* **2012**, *30* (18), 2179-82.
135. Harris, M., Monoclonal antibodies as therapeutic agents for cancer. *Lancet Oncol* **2004**, *5* (5), 292-302.
136. Baqi, Y.; Lee, S. Y.; Iqbal, J.; Ripphausen, P.; Lehr, A.; Scheiff, A. B.; Zimmermann, H.; Bajorath, J.; Muller, C. E., Development of potent and selective inhibitors of ecto-5'-nucleotidase based on an anthraquinone scaffold. *J Med Chem* **2010**, *53* (5), 2076-86.
137. Coelho-Cerqueira, E.; Netz, P. A.; do Canto, V. P.; Pinto, A. C.; Follmer, C., Beyond topoisomerase inhibition: antitumor 1,4-naphthoquinones as potential inhibitors of human monoamine oxidase. *Chem Biol Drug Des* **2014**, *83* (4), 401-10.
138. Clark, G. R.; Pytel, P. D.; Squire, C. J.; Neidle, S., Structure of the first parallel DNA quadruplex-drug complex. *J Am Chem Soc* **2003**, *125* (14), 4066-7.

## References

---

139. Lee, J. A.; Jung, S. H.; Bae, M. K.; Ryu, C. K.; Lee, J. Y.; Chung, J. H.; Kim, H. J., Pharmacological effects of novel quinone compounds, 6-(fluorinated-phenyl)amino-5,8-quinolinediones, on inhibition of drug-induced relaxation of rat aorta and their putative action mechanism. *Gen Pharmacol* **2000**, *34* (1), 33-42.
140. (a) Gomez-Monterrey, I.; Campiglia, P.; Aquino, C.; Bertamino, A.; Granata, I.; Carotenuto, A.; Brancaccio, D.; Stiuso, P.; Scognamiglio, I.; Rusciano, M. R.; Maione, A. S.; Illario, M.; Grieco, P.; Maresca, B.; Novellino, E., Design, synthesis, and cytotoxic evaluation of acyl derivatives of 3-aminonaphtho[2,3-b]thiophene-4,9-dione, a quinone-based system. *J Med Chem* **2011**, *54* (12), 4077-91; (b) Gomez-Monterrey, I.; Campiglia, P.; Bertamino, A.; Aquino, C.; Sala, M.; Grieco, P.; Dicitore, A.; Vanacore, D.; Porta, A.; Maresca, B.; Novellino, E.; Stiuso, P., A novel quinone-based derivative (DTNQ-Pro) induces apoptotic death via modulation of heat shock protein expression in Caco-2 cells. *Br J Pharmacol* **2010**, *160* (4), 931-40; (c) Gomez-Monterrey, I.; Campiglia, P.; Carotenuto, A.; Califano, D.; Pisano, C.; Vesci, L.; Lama, T.; Bertamino, A.; Sala, M.; di Bosco, A. M.; Grieco, P.; Novellino, E., Design, synthesis, and cytotoxic evaluation of a new series of 3-substituted spiro[(dihydropyrazine-2,5-dione)-6,3'-(2',3'-dihydrothieno[2,3-b]naphtho-4',9'-dione)] derivatives. *J Med Chem* **2007**, *50* (8), 1787-98; (d) Gomez-Monterrey, I.; Campiglia, P.; Carotenuto, A.; Stiuso, P.; Bertamino, A.; Sala, M.; Aquino, C.; Grieco, P.; Morello, S.; Pinto, A.; Ianelli, P.; Novellino, E., Spiro[(dihydropyrazin-2,5-dione)-6,3'-(2',3'-dihydrothieno[2,3-b]naphtho-4',9'-dione)]-based cytotoxic agents: structure-activity relationship studies on the substituent at N4-position of the diketopiperazine domain. *J Med Chem* **2008**, *51* (10), 2924-32; (e) Gomez-Monterrey, I.; Campiglia, P.; Grieco, P.; Diurno, M. V.; Bolognese, A.; La Colla, P.; Novellino, E., New benzo[g]isoquinoline-5,10-diones and dihydrothieno [2,3-b]naphtho-4,9-dione

- derivatives: synthesis and biological evaluation as potential antitumoral agents. *Bioorg Med Chem* **2003**, *11* (17), 3769-75; (f) Gomez-Monterrey, I.; Campiglia, P.; Scognamiglio, I.; Vanacore, D.; Dicitore, A.; Lombardi, A.; Caraglia, M.; Novellino, E.; Stiuso, P., DTNQ-Pro, a Mimetic Dipeptide, Sensitizes Human Colon Cancer Cells to 5-Fluorouracil Treatment. *J Amino Acids* **2013**, *2013*, 509056; (g) Gomez-Monterrey, I.; Santelli, G.; Campiglia, P.; Califano, D.; Falasconi, F.; Pisano, C.; Vesci, L.; Lama, T.; Grieco, P.; Novellino, E., Synthesis and cytotoxic evaluation of novel spirohydantoin derivatives of the dihydrothieno[2,3-b]naphtho-4,9-dione system. *J Med Chem* **2005**, *48* (4), 1152-7.
141. Bertamino, A.; Musella, S.; Di Sarno, V.; Ostacolo, C.; Manfra, M.; Vanacore, D.; Stiuso, P.; Novellino, E.; Campiglia, P.; Gomez-Monterrey, I. M., Dihydrithieno[2,3-b]naphto-4,9-dione analogues as anticancer agents: Synthesis and in cell pharmacological studies. *Eur J Med Chem* **2015**, *102*, 106-14.
142. Ohshima, T.; Hayashi, Y.; Agura, K.; Fujii, Y.; Yoshiyama, A.; Mashima, K., Sodium methoxide: a simple but highly efficient catalyst for the direct amidation of esters. *Chem Commun (Camb)* **2012**, *48* (44), 5434-6.
143. Campiglia, P.; Aquino, C.; Bertamino, A.; De Simone, N.; Sala, M.; Castellano, S.; Santoriello, M.; Grieco, P.; Novellino, E.; Gomez-Monterrey, I. M., Unprecedented synthesis of a novel amino quinone ring system via oxidative decarboxylation of quinone-based alpha,alpha-amino esters. *Org Biomol Chem* **2010**, *8* (3), 622-7.
144. Castellano, S.; Bertamino, A.; Gomez-Monterrey, I.; Santoriello, M.; Grieco, P.; Campiglia, P.; Sbardella, G.; Novellino, E., A practical, green, and selective approach toward the synthesis of pharmacologically important quinone-containing heterocyclic systems using alumina-catalyzed Michael addition reaction. *Tetrahedron Letters* **2008**, *49* (4), 583-585.

## References

---

145. Minniti, G.; Muni, R.; Lanzetta, G.; Marchetti, P.; Enrici, R. M., Chemotherapy for glioblastoma: current treatment and future perspectives for cytotoxic and targeted agents. *Anticancer Res* **2009**, *29* (12), 5171-84.
146. Rius, C.; Aller, P., Vimentin expression as a late event in the in vitro differentiation of human promonocytic cells. *J Cell Sci* **1992**, *101* ( Pt 2), 395-401.
147. Zhou, Y.; Zhou, Y.; Shingu, T.; Feng, L.; Chen, Z.; Ogasawara, M.; Keating, M. J.; Kondo, S.; Huang, P., Metabolic alterations in highly tumorigenic glioblastoma cells: preference for hypoxia and high dependency on glycolysis. *J Biol Chem* **2011**, *286* (37), 32843-53.
148. (a) Elstrom, R. L.; Bauer, D. E.; Buzzai, M.; Karnauskas, R.; Harris, M. H.; Plas, D. R.; Zhuang, H.; Cinalli, R. M.; Alavi, A.; Rudin, C. M.; Thompson, C. B., Akt stimulates aerobic glycolysis in cancer cells. *Cancer Res* **2004**, *64* (11), 3892-9; (b) Yang, C.; Sudderth, J.; Dang, T.; Bachoo, R. M.; McDonald, J. G.; DeBerardinis, R. J., Glioblastoma cells require glutamate dehydrogenase to survive impairments of glucose metabolism or Akt signaling. *Cancer Res* **2009**, *69* (20), 7986-93.
149. Cardone, M. H.; Roy, N.; Stennicke, H. R.; Salvesen, G. S.; Franke, T. F.; Stanbridge, E.; Frisch, S.; Reed, J. C., Regulation of cell death protease caspase-9 by phosphorylation. *Science* **1998**, *282* (5392), 1318-21.
150. (a) Buzzai, M.; Bauer, D. E.; Jones, R. G.; Deberardinis, R. J.; Hatzivassiliou, G.; Elstrom, R. L.; Thompson, C. B., The glucose dependence of Akt-transformed cells can be reversed by pharmacologic activation of fatty acid beta-oxidation. *Oncogene* **2005**, *24* (26), 4165-73; (b) Grabacka, M.; Reiss, K., Anticancer Properties of PPARalpha-Effects on Cellular Metabolism and Inflammation. *PPAR Res* **2008**, *2008*, 930705.

*References*

---

151. Janicke, R. U.; Sprengart, M. L.; Wati, M. R.; Porter, A. G., Caspase-3 is required for DNA fragmentation and morphological changes associated with apoptosis. *J Biol Chem* **1998**, *273* (16), 9357-60.